

Dissertation for Doctor of Philosophy

Cooperation and Decision-making Strategies for
Harsh Communication Environments

Zafar Iqbal

School of Electrical Engineering and Computer Science

Gwangju Institute of Science and Technology

2017

박사 학위 논문

극한 통신 환경을 위한 협력 및 의사결정 전략

자파 이크발

전기전자컴퓨터공학부

광주과학기술원

2017

Cooperation and Decision-making Strategies for Harsh Communication Environments

Advisor: Heung-No Lee

by

Zafar Iqbal

School of Electrical Engineering and Computer Science

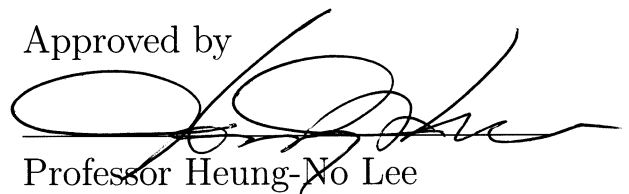
Gwangju Institute of Science and Technology

A thesis submitted to the faculty of the Gwangju Institute of Science and Technology in partial fulfillment of the requirements for the degree of Doctor of Philosophy in the School of Electrical Engineering and Computer Science

Gwangju, Korea

May 19, 2017

Approved by



Professor Heung-No Lee

Thesis Advisor

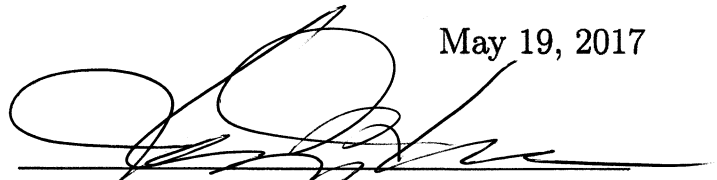
Cooperation and Decision-making Strategies for Harsh Communication Environments

Zafar Iqbal

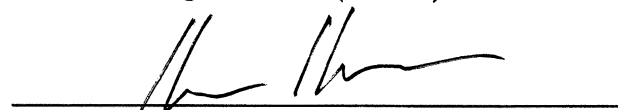
Accepted in partial fulfillment of the requirements for the
degree of Doctor of Philosophy

May 19, 2017


Thesis Advisor


Prof. Heung-No Lee (GIST)

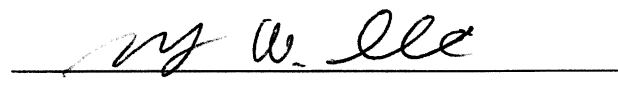
Committee Member


Prof. Kiseon Kim (GIST)

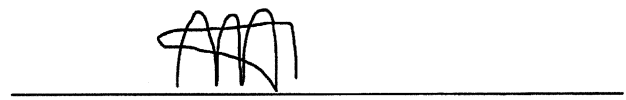
Committee Member


Prof. Hyuk Lim (GIST)

Committee Member


Prof. Jungwoo Lee (SNU)

Committee Member


Prof. Jalel Ben-Othman (Uni. Paris 13)

To my parents, my lovely wife, and the little superstar

Abstract

This dissertation discusses and analyzes the cooperation and decision-making strategies being used in the harsh communication environments. It proposes strategies for cooperation and decision-making among wireless sensors in the underwater and indoor industrial communication environments by utilizing network and channel coding, relaying, and majority-voting criteria. The purpose is to reduce energy consumption and improve error-rate performance in order to extend the lifetime of the deployed sensors and achieve accurate monitoring results.

In the first part, it explains the use of network coding and message-passing decoding algorithm for cooperation among sensors deployed underwater. The purpose is to design a message-passing decoding algorithm for a concatenated channel and network code, used to improve the reliability of the data received from sensor nodes, and reduce the energy consumption, in an underwater wireless communication environment. The second part deals with the cooperation among wireless sensors deployed in an indoor industrial environment. It focuses on decision-making strategy of the wireless sensor network at the base station, by using the cooperative information received from the sensors, to achieve a highly accurate decision. Later, the technique is further modified to reduce the latency in data communication to the base station and also reduce the energy consumption as compared to the original method.

©2017

Zafar Iqbal

ALL RIGHTS RESERVED

Contents

Abstract	i
List of Contents	ii
List of Tables	v
List of Figures	vi
1 Introduction	1
1.1 Harsh Communication Environment	2
1.2 User Cooperation and Relaying for Reliable Communication	4
1.3 Reliable Decision-making using Sensor Data Fusion	5
1.4 Contributions of this Thesis	7
2 Cooperation among Nodes Using Network Coding	11
2.1 Background and Contributions of this work	12
2.2 Deployment of Sensor Nodes	16
2.3 The Underwater Acoustic Communication Channel	19
2.3.1 Doppler Spread	19
2.3.2 Multipath Frequency Response	20
2.3.3 Underwater Acoustic Signal Fading	26
2.3.4 Ambient Noise	27
2.3.5 Simulation of the Channel Model	27
2.3.6 Received SNR	28
2.4 Cooperative Network-Coded Communication	29
2.4.1 LDPC-COFDM System	30
2.4.2 Limitations in LDPC-COFDM System	33
2.4.3 Design of the SCCNC Scheme	35
2.4.4 SCCNC Decoding Algorithm	40
2.4.5 EXIT Chart Analysis of the SCCNC Decoder	45
2.5 Performance Analysis	48
2.5.1 Energy Consumption of Cooperative and Non-Cooperative Schemes	49
2.5.2 Network Coding Gain	50
2.5.3 Comparison of Random and Grid Deployment	55

2.5.4	Delay and Extended Battery Life	55
2.6	Conclusion	56
3	Cooperative Relaying and Fusion of Sensor Data	58
3.1	Background and Contributions of this Work	59
3.2	Network Design	61
3.2.1	Sensor Deployment	62
3.2.2	Sensor Localization	64
3.2.3	Time Synchronization	64
3.2.4	The Indoor Wireless Channel Characteristics	66
3.3	Cross Layer Design	69
3.3.1	Design of the Data Packet	70
3.3.2	Design of the Schedule Packet	71
3.3.3	Organize and Operate Protocol (OOP)	72
3.3.4	Cooperative Communication	75
3.3.5	Fusion at the Base Station	78
3.4	Performance Analysis	80
3.4.1	Symbol Error Rate	80
3.4.2	Latency and Energy Consumption	83
3.4.3	Comparison with Related Works	86
3.5	Simulation Results	87
3.6	Conclusion	89
4	Cooperative Relaying Using Cluster Heads	91
4.1	Background and Contributions of this Work	91
4.2	Network Design	93
4.2.1	Organize and Operate Protocol with Cluster Heads (OOP-CH)	93
4.2.2	Cooperative Communication	95
4.2.3	Fusion at the Base Station	96
4.3	Performance Analysis	97
4.3.1	Symbol Error Rate	97
4.3.2	Latency and Energy Consumption	101
4.3.3	Comparison with Related Works	104

4.4	Simulation Results	106
4.5	Conclusion	108
5	Conclusions and Future Research Directions	109
5.1	Summary of Contributions	109
5.2	Future Research Directions	110
5.2.1	Adaptive SCCNC	110
5.2.2	Development of MAC Protocol for Industrial Communication	111
	Bibliography	112
	Acknowledgements	127

List of Tables

2.1	Underwater Acoustic Channel Parameters	28
2.2	OFDM System Parameters	32
3.1	Data Fusion at the Base Station	79
3.2	FAR and PDR Comparison	86
3.3	Simulation Parameters	87
4.1	Data Fusion at the Base Station	98
4.2	FAR and PDR Comparison	105
5.1	Summary of Contributions	110

List of Figures

2.1	2D triangular grid deployment of sensors in an $l \times h$ area.	17
2.2	Doppler spread caused by reflection on the sea surface.	20
2.3	Classification of multipath: (a) acoustic rays reflected odd number of times. (b) acoustic rays reflected even number of times.	22
2.4	(a) Geometrical representation of the multipath propagation in the UAC. (b) Example of calculating the reflection-path distance.	23
2.5	The normalized impulse response of the modeled UAC.	28
2.6	Received SNR at varying distance from the transmitter.	30
2.7	LDPC-COFDM system block diagram.	31
2.8	Performance comparison between LDPC-CODFM and uncoded OFDM systems.	34
2.9	Effects of lognormal shadowing on uncoded and coded OFDM systems.	35
2.10	(a) Spatial representation of the network-cooperation scenario; (b) transmission sequence and time slots for each sensor node.	37
2.11	Example of the SCCNC scheme: each sensor sends an LDPC codeword in the first phase. The spatial-domain checksums are computed and sent during the second phase, which are the LDPC coded symbols received during the first phase.	40
2.12	Iterative decoding procedure for the proposed SCCNC scheme.	46
2.13	EXIT chart for the SCCNC decoder for a UAC with SNRs ranging from 1–7 dB.	48

2.14	Power-consumption comparison between cooperation and non-cooperation networks.	51
2.15	Underwater WSN scenario (Not to scale).	52
2.16	Performance of the proposed SCCNC scheme compared with the LDPC-COFDM and uncoded OFDM schemes for the UAC.	53
2.17	Performance comparison of random and grid deployment by using the proposed SCCNC scheme for the UAC.	54
3.1	Cooperative wireless sensor network.	62
3.2	Sensor nodes deployed in a rectangular area. (a) Triangular-grid, ensuring the coverage of the whole area with minimal overlap. (b) Indoor communication scenario showing a floor layout.	63
3.3	Information transmission to the base station.	65
3.4	Calculation of the time-of-arrival (TOA) at BS.	66
3.5	Calculation of the received signal strength.	67
3.6	(a) Data packet structure of each node in Phase 1. (b) Schedule packet structure used for organization of the network. (c) Data packet structure of each node in Phase 2 for cooperative data transmission.	71
3.7	The proposed Organize and Operate Protocol (OOP) for WSN.	75

3.8	The proposed two-phase communication system. In Phase 1, sensor s_1 in the cooperation group sends its information to all other sensors during its time slot. Similarly, all the other sensors send their information to s_1 during their allocated time slots. In Phase 2, the sensors then make a cooperative packet and send it to the destination, D	80
3.9	Results of (3.28), (3.29), and (3.30). (a) Time delay for packet delivery. (b) Energy consumption of the network.	85
3.10	Simulation results for 12-node cooperation group, showing the probability of error in different parts of the received packet at the BS.	88
3.11	Comparison of simulation result after fusion at the BS and the approximated SER given in (3.26).	89
4.1	The proposed organize and operate protocol with cluster heads (OOP-CH) for WSN.	95
4.2	The proposed two-phase communication system. In Phase 1, sensor s_1 in the cooperation group sends its information to all CH sensors during its time slot. Similarly, all the other sensors send their information to CH sensors during their allocated time slots. In Phase 2, only the CH sensors then make a cooperative packet and send it to the destination, D	99
4.3	Comparison of CH simulation and the approximated result given in (4.9). In this experiment, 5 CH nodes were chosen from a cooperation group of 12.	102

4.4	Comparison of non-cooperative and cooperative schemes in terms of power consumption and latency.	105
4.5	Comparison of the probability of error in the received information, between direct, relayed, F-Rep., and CH cooperation transmission.	106
4.6	Comparison of simulated results of the proposed CH scheme, F-Rep. scheme, relayed transmission, and no cooperation scheme.	107

Chapter 1

Introduction

We are living in the age of information overload and it has become increasingly important to use the available information effectively, and to make correct and timely decisions by using the available information. In the past two decades, the field of digital communications, both wired and wireless, has seen tremendous growth and has affected people's lives in a positive way. With the introduction of broadband wireless communication technologies, such as WiFi, WiMAX, LTE, and 5G, and smart devices, such as smart phone and tablet PCs, users are able to communicate effortlessly and seamlessly over the wireless network. Similarly, wireless sensor network (WSN) and internet-of-things (IoT) are also becoming increasingly important in our daily lives. The applications include access, control, and monitoring of remotely located equipment, devices, as well as environment.

However, despite all the advancement in communication technology, the wireless communication channel still faces a lot of challenges in order to achieve the goal of efficient and reliable communication between two entities. The traditional wireless channel has been successful in achieving this goal. But the indoor building area, factory area, and underwater communication channels still pose many challenges in achieving the above-mentioned goal. Also, the current wave of intelligent decision-making in information systems has brought out new challenges of effective utilization of the generated

information from sensors and IoT devices. In the following subsections, we briefly discuss these research issues and finally we present contributions of this work to overcome these problems.

1.1 Harsh Communication Environment

The environment in which the wireless communication channel suffers from severe degradation due to time-varying channel conditions, propagation loss, and multipath fading can be referred to as harsh communication environment. Examples of such environments include but not limited to, industrial communication, bad urban, hilly terrain communication, underwater communication, power line communication, and satellite communication. A bad wireless channel may result in repeated transmissions of the data towards the destination, and/or use of higher transmit power. This leads to higher energy consumption and reduced overall throughput of the network. In this thesis, we will limit our discussion to indoor industrial communication and underwater acoustic communication. Nonetheless, these results and insights provided in this dissertation can be generalized to other extreme communication environments.

The underwater acoustic channel (UAC) is time-varying because of the spatial position changes caused by sea currents, roughness of the sea surface, changes in temperature, and geometry of the channel. Because of its low-attenuation characteristics [1], the acoustic wave is being considered the major carrier in underwater communication. But the limited bandwidth and time-varying response of the UAC leads to difficulties in obtaining an accurate channel state information (CSI) at the transmitter and/or

receiver. Also, the reflections at the sea surface and bottom causes multipath delay spread, which leads to inter-symbol interference (ISI) and frequency-selective fading. These factors degrade the reliable communication capability of the underwater acoustic communication system [2], [3]. The applications of underwater acoustic communications include underwater environment monitoring, military/oceanic surveillance, underwater navigation, radiation leaks monitoring, and resource exploration. These applications require advanced underwater sensor networks, for which, researchers have attempted to design reliable and robust systems [4],[5].

The indoor industrial communication channel also suffers from propagation loss, time-variation, and multipath fading. In an indoor industrial environment, the quality of a wireless channel is vital to the reliable transmission of the data collected by sensors or distributed nodes to a central processing unit in order to make effective and timely decisions. A lot of work has been done on multipath fading and channel characterization for industrial environments, including [6] and a work that deals with underground link quality characteristics [7]. A recent work and the references therein, provide suitable channel models for indoor industrial environments [8]. The applications of indoor industrial communications include, machine condition monitoring (MCM) and maintenance, especially the machines located in harsh areas such as nuclear plants or large factories, environmental monitoring, surveillance, healthcare, and security services [9]. In order to deal with the issues in industrial communication, researchers have proposed solutions based on WSNs, such as [10], [11], [12], and [13].

1.2 User Cooperation and Relaying for Reliable Communication

User (node) cooperation and relaying techniques have been introduced by the wireless communication community in order to overcome the signal fading due to multipath propagation in the wireless channel. Cooperation between multiple users (nodes) is achieved by allowing multiple users to transmit their information to the destination by using all or a subset of the available single-antenna nodes. The cooperation and relaying techniques help users to exploit the spatial diversity available in the wireless network, which results in an improved link reliability. The basic methods for a node to cooperate with its partners is to first listen to the transmission from its partners and then transmit a cooperative version of the received signal towards the destination in an orthogonal manner (a different time or frequency slot) by using either, an amplify-and-forward (AF), a decode-and-forward (DF) [14], or a compress-and-forward (CF) scheme [15].

To overcome the problems we face in underwater acoustic communication, mentioned in Section 1.1, coded orthogonal frequency division multiplexing (COFDM) systems have been proposed that employ low-density parity-check (LDPC) codes [16]-[18], Reed-Solomon codes [19], and adaptive modulation and coding (AMC) [20] in OFDM systems for UACs. LDPC-coded and OFDM-based underwater acoustic communication has been well investigated in [16]-[18], and [21]-[23], respectively. However, we observe that a non-cooperative LDPC-COFDM system exhibits significant performance degradation in the presence of random fading. Also, because point-to-point systems are vulnerable to long-term deep fading, Doppler spread, and shadow zones [4],

[24], [25], the interest in designing cooperative communication systems with network coding, has recently increased.

In the case of industrial WSN (IWSN), various techniques have been proposed to deal with the issues mentioned in Section 1.1. These techniques include, user cooperation in communication [14], [26], and [27] for improved spatial diversity, time-slot reassignment [11], and sleep scheduling [12] strategies used to improve the energy efficiency of the WSN. In the case of cooperation among sensor nodes, data aggregation at the intermediate nodes is an important factor of multi-hop communication. Since the size of data packets is usually small and are addressed to a single destination, therefore, reducing the number of transmissions and the size of control packet overhead, improves the energy efficiency and throughput of the system [13].

1.3 Reliable Decision-making using Sensor Data Fusion

In a WSN, the sensors sense the surrounding environment and then share the observed information with a central fusion center (FC), with or without local processing or decision-making at the sensor. Energy consumption and bandwidth are the two main concerns in the performance of a WSN. Therefore, several architectures have been developed for reporting the sensed data to the FC to reduce energy consumption, maximize the efficiency of bandwidth usage, and provide a reliable decision from the observed information. These architectures include, centralized (each node sends the observed information as measurement to the FC, and the FC makes a reliable global decision based on the received information) [28], decentralized (each sensor collects

information from its neighboring sensors and makes an autonomous decision) [29], and distributed (each sensor makes a local decision on its observed information and transmits it to the FC, the FC then makes a more reliable global decision by considering the decisions of all other sensors) [30].

Due to the recent interest in intelligent decision-making, autonomous systems, and IoT applications, sensor data fusion has attracted substantial attention from the research community. Some of the notable works dealing with sensor data fusion techniques are as follows. Sensor data fusion has been used to understand human behaviors in a smart city [31]. A method for fusion of sensor data, which optimizes the detection performance while considering the resource limitations in WSNs has been presented in [32]. A distributed estimation (DES) algorithm for joint successive interference cancellation (SIC) and minimum mean square error (MMSE) estimation for correlated data in a WSN was presented in [33]. A sensor localization method based on artificial neural network (ANN) in a WSN was presented in [34]. A biosensor data collection and fusion framework, which proposes a data fusion model using decision matrix and fuzzy set theory, has been proposed for health monitoring [35]. A decision-fusion method, for WSN operating in Rician-mixture fading channels in a virtual MIMO environment where the FC is equipped with multiple antennas, has been proposed in [36]. An optimal distributed federated Kalman filter fusion (DFKFF) algorithm for multisensory unreliable networked systems was proposed in [37] and a Dempster-Shafer Theory (DST) based MCM system was proposed in [38].

1.4 Contributions of this Thesis

After briefly pointing out the issues faced by WSN and IoT applications in harsh communication environments such as underwater acoustic communication and indoor industrial communication, we introduce the contributions made by this work to overcome these issues. The solutions provided in this thesis help improve the performance of the wireless network and reduce overall energy consumption by using and proposing novel techniques in node cooperation, network coding, and sensor data fusion.

In the first part of this thesis, our aim is to develop a cooperative network communication scheme for underwater WSNs that resolves the aforementioned challenges of the UAC and reduces the power consumption in order to enhance the lifetime of the overall network. The envisioned network is a WSN wherein multiple sensors inside a shallow body of water cooperate while transmitting to a buoy on the water surface. To resolve the aforementioned problems, we propose a cooperation scheme that enables a group of transmitting sensors to form a network code over the spatial domain and is suitable for time- and frequency-selective UACs. The proposed cooperation scheme provides a considerable transmit power saving compared with the conventional non-cooperative scheme. Our study shows that the network coding benefit is sufficiently large to offset the increase in the power consumption due to the cooperation among the sensors in the network and yields an overall benefit of ~ 11 dB.

This work will be explained in detail in Chapter 1. The achievements of this research have been published as follows:

[39]. Zafar Iqbal and Heung-No Lee, "Spatially concatenated channel-network code for

underwater wireless sensor networks,” *IEEE Transactions on Communications*, vol. 64, no. 9, pp. 3901-3914, Sep. 2016.

- [40]. Heung-No Lee, and Zafar Iqbal, “Sensing data processing apparatus and data processing method,” *Korean Patent*, Application number: 10-2016-0066621, May 30, 2016.
- [41]. Zafar Iqbal and Heung-No Lee, “Deployment strategy analysis for underwater cooperative wireless sensor networks,” *6th Int. Conf. on ICT Convergence (ICTC)*, South Korea, Oct. 2015.
- [42]. Zafar Iqbal and Heung-No Lee, “Underwater acoustic channel model and variations due to changes in node and buoy positions,” *5th Pacific Rim Underwater Acoustics Conference*, Russia, Sep. 2015.
- [43]. Zafar Iqbal, Hyeonh-Won Jeon, and Heung-No Lee, “A realistic channel model for OFDM based underwater acoustic communications,” *2012 Korea Inf. and Commun. Society Summer Conference*, South Korea, Jun. 2012.

In the second part of this thesis, we propose a cooperation scheme for IWSNs, in which the network consists of small cooperation groups of sensors. Each node in the cooperation group shares its information with all others in the first phase. In the second phase each node forms a cooperative data packet and sends it to the base station (BS). A sensor data fusion technique is adopted at the BS to combine the information received from the sensors and make a final optimized decision. In this way, the nodes help relay information for its neighbor nodes to the BS reliably and with a significant

reduction in energy consumption of ~ 18 dB, at the cost of an acceptable reduced throughput compared to the conventional non-cooperative schemes. Our proposed also provides improved packet delivery ratio and reduced false alarm rate as compared to the state-of-the-art related works.

This work will be explained in detail in Chapter 2. The achievements of this research have been published as follows:

- [44]. Zafar Iqbal, Kiseon Kim, and Heung-No Lee, “A cooperative wireless sensor network for indoor industrial monitoring,” *IEEE Transactions on Industrial Informatics*, vol. 13, no. 2, pp. 482-491, Apr. 2017.
- [45]. Heung-No Lee, and Zafar Iqbal, “Data processing apparatus and method for wireless sensor network,” *Korean Patent*, Application number: 10-2016-0066625, May 30, 2016.
- [46]. Zafar Iqbal and Heung-No Lee, “A self-organizing wireless sensor network for industrial monitoring,” *31st Int. Conf. on Circuits/Systems, Computers, and Commun. (ITC-CSCC 2016)*, Okinawa, Japan, pp. 351-354, Jul. 2016.

In the third part of this thesis, we propose an improvement to our own proposed cooperation scheme for IWSNs in Chapter 2. In this work, we use cluster heads for cooperation instead of full repetition, which helps in reducing the amount of transmissions required to transmit the same information to the BS and also reduces the latency at the expense of some reduction in performance. All the sensors in a cooperation group share their information with each other in the first phase. In the second

phase, the cooperative information is sent to the BS by a selected number of cluster head (CH) nodes. This work combines the data aggregation and cooperation mechanism to improve the reliability of the received information at the BS as well as keep the redundancy overhead to a certain limit in order to perform at a low-latency.

This work will be explained in detail in Chapter 3. The achievements of this research have been published as follows:

- [47]. Zafar Iqbal and Heung-No Lee, "Performance analysis of a clustered cooperative WSN for indoor communication," *Submitted to IEEE Access*, Apr. 2017.
- [48]. Zafar Iqbal and Heung-No Lee, "Low-latency and high-reliability cooperative WSN for indoor industrial monitoring," *IEEE 85th Vehicular Tech. Conf.*, Sydney, Australia, Jun. 4-7, 2017.

Chapter 2

Cooperation among Nodes Using Network Coding

In this chapter, we discuss our proposed cooperation scheme and the associated network coding scheme for underwater acoustic communication. Underwater environment monitoring is an important application of underwater WSNs. But the underwater WSNs face challenges of shorter lifetime, robustness of the network, harsh UAC, and cost constraints. Thus, it becomes a challenging task to design a cooperative coded orthogonal frequency division multiplexing (COFDM) system, which can operate robustly in the doubly-selective (time- and frequency-selective) UAC, with an acceptable power consumption.

In this chapter, we propose a cooperative spatial-domain coding scheme combined with the COFDM system, called spatially concatenated channel-network code (SC-CNC), for underwater acoustic WSNs. Our scheme exhibits a significant advantage over the non-cooperative COFDM system in terms of the required number of sensors, bit error rate (BER), and power consumption. We also analyze sensor deployment schemes to show the applicability of our proposed scheme in a certain area.

2.1 Background and Contributions of this work

After the idea of network coding was proposed in [49] and its application to linear network coding in [50], different strategies for cooperation, using network coding, have been proposed. These schemes may be classified based on the network types assumed, such as the single-source single-relay network [51]-[55], single-source multiple-relay network [15], [56]-[61], multiple-source single-relay network [62], [63], and multiple-source multiple-relay network [15], [64]-[67].

For multiple-source multiple-relay networks with a single destination where CSI is not readily available for relay assignment, adaptive network coded cooperation (ANCC) was proposed in [64]. In this scheme, each relay randomly selects a small number of correctly decoded messages from all the source nodes to generate a parity-check message in the cooperation phase. This leads to the formation of a graph code at the destination and a belief propagation decoding algorithm is used for decoding. However, for the decode-and-forward relaying scheme, detection errors at the relays should be taken into consideration for performance analysis and code design. While [64] assumes a set of relays that can successfully decode the received messages, [67] considers the possibility of unsuccessful decoding at the relays, making the scheme more realistic. In addition, [67] also assigns fixed relays to each source node and therefore, the relays do not have the overhead of sending an extra bit-map field to the destination to inform it about the underlying connections in the graph code.

More recently, [63] proposed a two-user and single-relay bilayer spatially-coupled LDPC (SC-LDPC) scheme for correlated sources. The system uses joint source-channel

coding to transmit to the relay as well as to the destination. Correct decoding of the received signal is assumed at the relay and the relay then uses network coding to combine the received data before forwarding it to the destination. The scheme uses a factor-graph-based design of joint source-channel-network decoder at the destination when the sources are correlated. Also, an OFDM-based dynamic coded cooperation (DCC) for underwater acoustic channels is presented in [55]. The relay listens until correct decoding of the received signal and then generates either an identical or a different OFDM block from the source and superimposes it on the transmission from the source in the cooperation phase. A delay control mechanism is used at the relay to achieve block-level synchronization between the source and the relay. This scheme requires a powerful relay node with abundant resources, such as a surface buoy, to assist the communication between the source and the destination.

Compared to the above-mentioned works, our design is based on multiple sources with multiple relays that transmit to a single destination. Because practical networks suffer from link failures and topology changes due to randomly fading channels, fixed relay assignment, as proposed in [67], is subject to failure in certain situations. Therefore, instead of the fixed relay assignment, we use random relay selection mechanism. In this scheme, a relay receives data from the neighboring source nodes. Some of these data are selected at random, encoded and transmitted in the relay phase. Our scheme of random relay selection thus, provides more robustness against link/node failures and outages in the underwater sensor network, without the need for a very powerful relay node as is the case in [55]. In our proposed cooperation mechanism, the relay randomly

selects a small number of symbols from the data received from its neighbor nodes, without decoding it. It then re-encodes the symbols using an LDGM code, resulting in a concatenated channel-network code. For this channel-network code a joint iterative decoder is designed and its performance is evaluated using extrinsic information transfer (EXIT) charts and BER simulations. The above-mentioned schemes either use repetition codes, convolutional codes, or some form of block codes in a distributed way, but in our scheme, each node independently encodes the data with an LDPC code and then in the cooperation phase, the nodes concatenate the received LDPC-coded symbols with an LDGM code in a distributed manner. Thus, our scheme combines the power of concatenated coding with adaptive network coding for underwater acoustic communication where CSI is not readily available. It also uses the random relay selection mechanism, resulting in a more practical cooperation scheme.

The contributions of this chapter are summarized as follows:

- We consider a doubly-selective channel which was not considered in [64]. The work in [64] does not consider the effects of time- and frequency-selectivity, while our work takes care of time- and frequency-selectivity by using OFDM modulation and the scheme has been applied to underwater acoustic communication, for the first time. In the proposed scheme, the underwater acoustic sensors should take the role of relays for cooperation, but the sensors are limited in power, computational resources, and the challenge of underwater acoustic communication is great. Therefore, investigating the effectiveness of the cooperative coding scheme for underwater communication is very important and has not been addressed in

the works discussed above.

- We have removed some unrealistic assumptions considered in [64]. The work in [64] considers network coding part only while assuming that a perfect channel coding has been performed. Our work removes this assumption as we have extended the network code by concatenating it with a channel code and included the effect of propagated error from the channel code to the network code part. The proposed scheme is termed as a spatially concatenated channel-network code (SCCNC) for underwater acoustic communication.
- Our relaying mechanism is different from [64] and other previous works. In the previous works, in the event of unsuccessful decoding, the relay either remains silent or sends its own data to the destination. In our proposed scheme, the relays do not need to decode the received codewords; they only detect the binary symbols. The relays then re-encode randomly selected symbols received from a number of sources and send it to the destination in the second phase. Therefore, the relays do not need to spend power on decoding the received codewords, thus saving time, energy, and hardware resources. This is very critical for underwater acoustic sensor networks, keeping in mind the limited power and computational resources of the sensors.
- In underwater acoustic communications, the sensor nodes require a particularly high power for the transmission and reception. Thus, the power consumption of the overall network is expected to increase, as each node must listen to the

neighboring nodes' transmissions in order to realize the cooperation. In Section 2.5.1, we present an analysis indicating that the cooperation among sensor nodes significantly increases the power consumption of the network. Energy consumption analysis of both the cooperative and non-cooperative schemes is performed to observe the effects on the battery life of the sensor nodes.

- Random and grid-deployment schemes are considered, and the performance of these schemes is compared based on the BER and cost of network deployment and operation.

2.2 Deployment of Sensor Nodes

In this section, we discuss the sensor deployment method used in our work. Sensor deployment is an important issue, especially in underwater WSNs, because the harsh underwater environments pose various challenges for the effective operation and robustness of the network. Sensor deployment addresses the problem of the coverage and connectivity of the network by targeting the minimized power consumption for a prolonged network lifetime.

The underwater WSN can be deployed in two types of communication architectures: two-dimensional (2D), where the sensors are deployed at the bottom of the sea, and three-dimensional (3D), where the sensors float at different depths to cover the entire volume of water [4]. Herein, we consider a static and 2D grid deployment for our WSN, which is relatively easy to deploy and operate. We use the k -coverage parameter to ensure that the target area is almost fully covered. A region is said to be k -covered

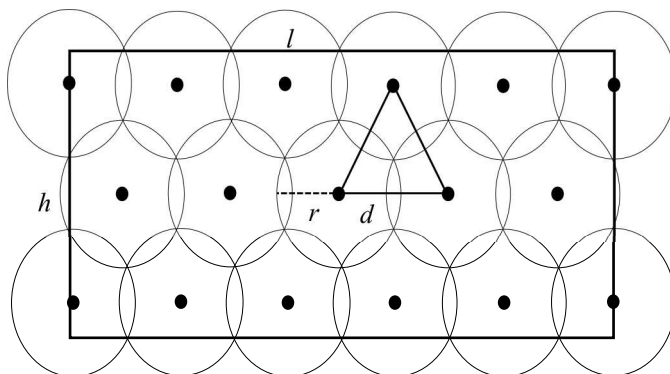


Figure 2.1: 2D triangular grid deployment of sensors in an $l \times h$ area.

if every point inside it falls within the sensing range r of at least k sensors. Our deployment target is to achieve 1 -coverage, as the underwater acoustic sensors are expensive devices, and we wish to minimize the power consumption and the associated cost of operation.

The optimal deployment strategy to cover a 2D rectangular area using the minimum number of sensors involves placing each sensor at a vertex on a grid of equilateral triangles [68], as shown in Fig. 2.1. To obtain the full coverage, the coverage ratio η (covered area/target area) should be 1, which can be achieved by adjusting the distance d among the sensors, such that $d = \sqrt{3}r$. This makes the uncovered areas shown in Fig. 2.1 zero, and the overlapping areas are minimized. Using ([68], eq. (3)), we can compute the minimum number of sensors U required to cover a target area $l \times h$ to satisfy a given coverage ratio η as $U(l, h, d, r) = \lceil \frac{l-d}{d} + 1 \rceil \times \lceil \frac{2\sqrt{3}h-6d+4\sqrt{3}r}{3d} + 1 \rceil$. Thus, the minimum number of sensors necessary to provide 1 -coverage in an area of $100\text{ m} \times 100\text{ m}$ for $r = 20\text{ m}$ is 12.

The next step is to estimate the number of redundant sensors required to ensure the

robustness of the network to node failures within a pre-determined observation period. We assume that all the nodes have the same failure rate and that the node failures occur according to a Poisson distribution and are independent of each other. Therefore, the number of redundant sensors required to compensate for the Poisson-distributed node failures is given in ([68], eq. (18)) as $\sum_{u=0}^{\Delta U} \frac{(\lambda T)^u e^{-\lambda T}}{u!} \geq \Gamma$, where λ is the sensor failure rate, T is the observation time in days, u is the number of sensors that may fail during the time T , and Γ is the probability that no more than ΔU failures occur in the observation time T . For example, with an average of one sensor failure every month ($\lambda = 1/(365/12)$) and a success probability of $\Gamma = 0.95$, there are approximately six sensor failures during a period of three months [68]. Thus, to ensure network connectivity and provide 1-coverage in an area of $100\text{ m} \times 100\text{ m}$ for $r = 20\text{ m}$ and an observation period of three months we must deploy 18 sensors rather than 12.

Finally, to ensure the connectivity of the network, we use the argument given in [69]: $\Theta(\log U)$ neighbors are necessary and sufficient for a sensor network to be asymptotically connected. This number is proven to be between $0.074 \log U$ and $5.1774 \log U$. Therefore, for a network of 12 or 18 nodes, we select the minimum required number of neighbors as 5.

Although the triangular-grid deployment appears to be a cost-effective solution regarding the number of sensors needed to provide the coverage and connectivity in a given area of interest, it may not be an effective solution for underwater area monitoring when cooperative communication is used to enhance the performance of the network. Moreover, compared with a randomly deployed network, a triangular-grid structure

may be expensive to deploy and maintain for a long period of time in an underwater environment. Herein, we compare the effects of random and triangular-grid 2D static deployment strategies employing cooperation among sensor nodes that communicate to a buoy on the sea surface.

2.3 The Underwater Acoustic Communication Channel

Here, we explain the channel model used for the simulating the acoustic communication phenomenon in the underwater environment. We use the geometrical ray-tracing model [3], [70], [71]-[73], to investigate the underwater sound propagation and aim to describe the modeling procedure step-by-step, along with the channel characteristics.

2.3.1 Doppler Spread

The surface scattering of UAC depends on the sea surface condition. Under an ideally flat surface condition, incident waves are almost perfectly reflected with a phase shift of π . However, under practical conditions, swells lead to movement of the reflection point and create energy dispersion. The Doppler spread with a carrier frequency f kHz [74] is represented as follows,

$$f_D = (0.0175/c) f \cdot w^{3/2} \cdot \cos \theta \quad (2.1)$$

where c , w , and θ are sound speed, sea surface wind speed, and grazing angle, respectively. Sound speed is affected by salinity, water temperature, pressure, etc., but it is 1500 m/s under normal conditions. Fig. 2.2 shows the Doppler spread against the carrier frequency and sea surface wind speed when we assume $\cos \theta = 1$ in (2.1) at both the

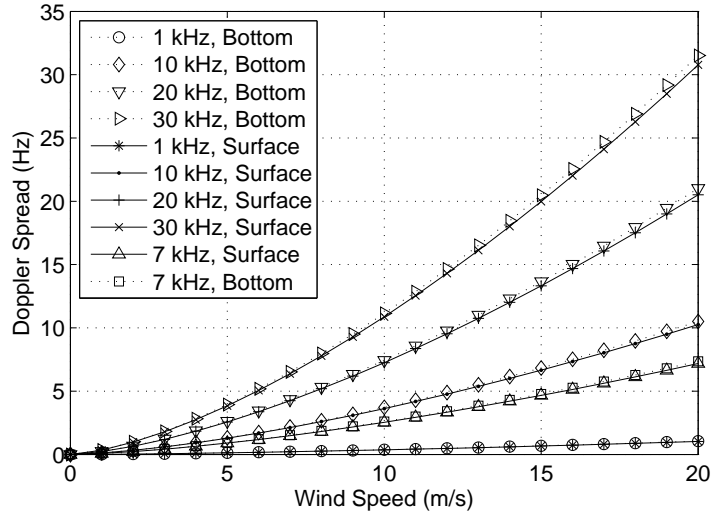


Figure 2.2: Doppler spread caused by reflection on the sea surface.

sea surface and bottom. This result depicts a geometric Doppler spread increase using a higher carrier frequency. Although using a higher carrier frequency has an advantage in the form of increased available transmission bandwidth, it also has a disadvantage of geometric increase in the Doppler spread. Thus, this trade-off relationship should be considered while designing the communication system for underwater communication.

2.3.2 Multipath Frequency Response

In a UAC, the acoustic waves are reflected at the sea surface and bottom and form a multipath [3], [24]. The reflection paths are classified into four types according to the total number of reflections (odd or even) and the first reflection point (surface or bottom).

Fig. 2.3 (a) and (b) show such classification in terms of total number of reflections. Fig. 2.3(a) shows the acoustic waves reflected odd number of times. The dashed rays

is a case where the first reflection occurred on the sea surface and the dotted rays is a case where the first reflection occurred on the bottom. Similarly, Fig. 2.3(b) shows the acoustic waves reflected even number of times. The dashed rays and dotted rays show the first reflection occurred on the sea surface and sea bottom, respectively.

The channel transfer function is a superposition of the transfer functions of each propagation path from the transmitter to the receiver. It is given as

$$H(f, t) = \sum_p H_p(f, t) e^{-j2\pi f \tau_p(t)}, \quad (2.2)$$

where $H_p(f, t)$ and $\tau_p(t)$ represent the transfer function of the p^{th} path at frequency f and the corresponding delay at time t , respectively. The transfer function of each reflection path is represented as a function of the frequency, number of reflections, and path length. The transfer function of the p^{th} path is given as

$$H_p(f, t) = \frac{V_p}{\sqrt{\mathcal{C}(\mathcal{L}_p(t), f)}}, \quad (2.3)$$

where $\mathcal{C}(\mathcal{L}_p(t), f)$ is the single path attenuation with distance \mathcal{L}_p m and carrier frequency f Hz, $V_p = v_s^{n_{sp}} v_b^{n_{bp}}(\theta_p)$ is the reflection coefficient, which is the number of times a ray is reflected from the sea surface (n_{sp}) and bottom (n_{bp}), where v_s and v_b are the reflection coefficients at the sea surface and bottom, respectively [25]. In addition, θ_p is the grazing angle. Under flat sea surface condition, v_s is approximated as -1 and v_b is calculated as follows,

$$v_b(\theta) = \begin{cases} \frac{\rho_b \sin \theta - \rho \sqrt{(c/c_b)^2 - \cos^2 \theta}}{\rho_b \sin \theta + \rho \sqrt{(c/c_b)^2 - \cos^2 \theta}}, & \cos \theta \leq c/c_b \\ 1, & otherwise \end{cases} \quad (2.4)$$

where ρ and c are the sea surface layer water density and sound speed; and, ρ_b and c_b are the water density and sound speed at the sea bottom. We chose the values for

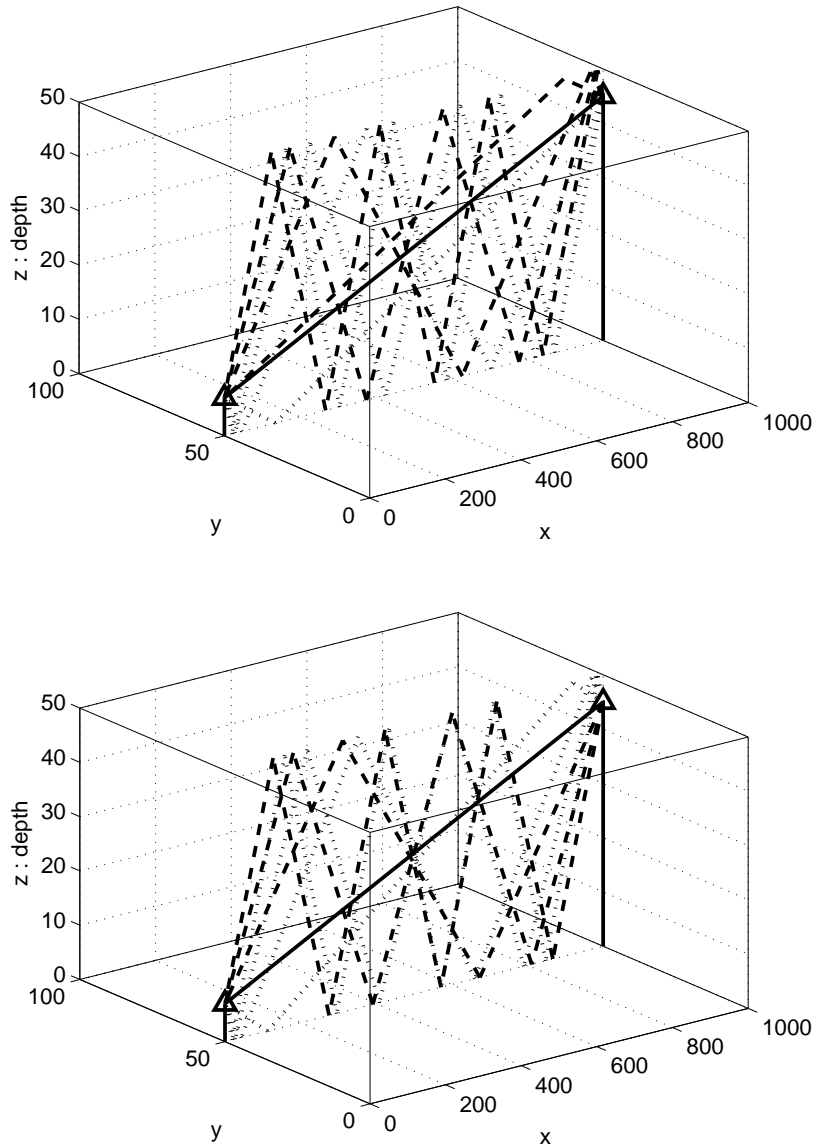


Figure 2.3: Classification of multipath: (a) acoustic rays reflected odd number of times.
 (b) acoustic rays reflected even number of times.

these parameters as 1022 kg/m^3 , 1526 m/s , 1027 kg/m^3 , and 1490 m/s , respectively [75], [76].

Because the single-path loss is a function of the carrier frequency and path length, it

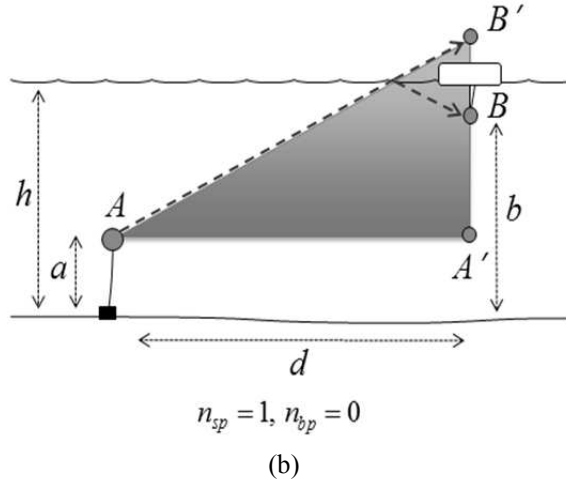
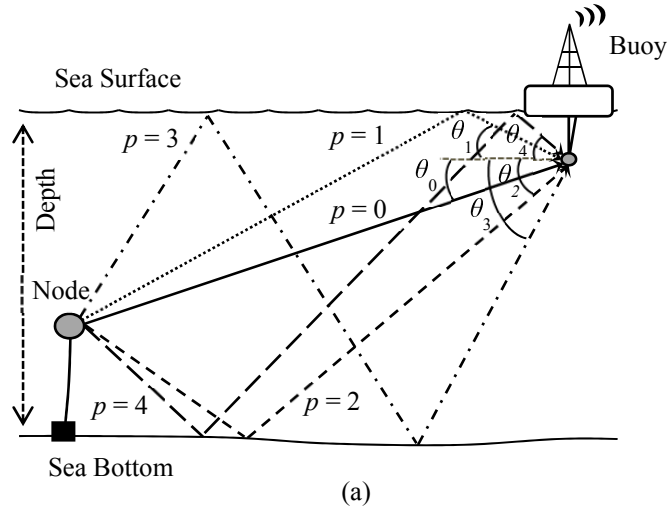


Figure 2.4: (a) Geometrical representation of the multipath propagation in the UAC.
 (b) Example of calculating the reflection-path distance.

is necessary to calculate the length of the reflection path. Similarly, the grazing angle θ_p is an essential factor for calculating the reflection coefficient. We illustrate the proposed method using Fig. 2.4(b). To calculate the length of the reflection path from A to B , (i) move B to B' against the sea surface; (ii) calculate the length of the baseline d ; (iii) calculate the height of the triangle, which is given by $2h - a - b$, as the distance from the

sea surface to point A' is $h-a$ and the distance from the sea surface to B' is $h-b$; and
 (iv) calculate the distance using the Pythagorean Theorem: $\mathcal{L}_p^2 = d^2 + (2h - a - b)^2$.

This approach is used to obtain a general equation for the length of the reflection path, which is given as follows:

$$\mathcal{L}_p = \sqrt{d^2 + (2h \cdot n_{sp} + \alpha a + \beta b)^2}, \quad (2.5)$$

where α and β are classification values in accordance with the first reflection point (surface or bottom) and the total number of reflections (odd or even). Specifically, $(\alpha, \beta) = (-1, -1), (+1, +1), (-1, +1),$ and $(+1, -1)$ for the paths having the first reflection on the surface with an odd number of reflections ($p = 1$), the first reflection on the bottom with an odd number of reflections ($p = 2$), the first reflection on the surface with an even number of reflections ($p = 3$); and the first reflection on the bottom with an even number of reflections ($p = 4$), respectively, as shown in Fig. 2.4(a).

Using the parameters $d, h, n_{sp}, a, b, \alpha,$ and β (distance, depth, number of reflections on sea surface, distance from the bottom to the node, distance from the bottom to the buoy, and classification factors) in (2.5), the lengths of all possible reflection paths can be calculated easily. After calculating the lengths of all possible reflection paths, the grazing angle can then be calculated as $\theta_p = \cos^{-1}(d/\mathcal{L}_p)$.

In (2.3), the single-path loss with the distance \mathcal{L}_p m and carrier frequency f Hz is $\mathcal{C}(\mathcal{L}_p(t), f) = \mathcal{C}_0 \mathcal{L}_p^\psi(t) \chi(f)^{\mathcal{L}_p(t)}$, where \mathcal{C}_0 is a constant scaling factor, and ψ is the spreading factor, which ranges between 1 and 2, according to the type of spreading. We set \mathcal{C}_0 as 1 and ψ as 1.5, considering practical spreading. $\chi(f)$ is the absorption coefficient, expressed in dB/km, which is defined by Thorp's empirical formula at fre-

quencies above a few hundred Hz as $\chi(f) = \frac{0.11f^2}{1+f^2} + \frac{40f^2}{4100+f^2} + 2.75 \times 10^{-4}f^2 + 0.003$ [25]. The acoustic path loss is then expressed in dB as $10 \log \mathcal{C}(\mathcal{L}_p(t), f)/\mathcal{C}_0 = \psi \cdot 10 \log \mathcal{L}_p(t) + \mathcal{L}_p(t) \cdot 10 \log \chi(f)$.

We assume that the length of the p^{th} propagation path is

$$\mathcal{L}_p(t) = \bar{\mathcal{L}}_p + \Delta\mathcal{L}_p(t), \quad (2.6)$$

where $\bar{\mathcal{L}}_p$ is the nominal length, and $\Delta\mathcal{L}_p(t)$ is the variation in the length $\mathcal{L}_p(t)$. The nominal path transfer function for the reference path ($p = 0$) can be written as

$$Q(f) = \frac{1}{\sqrt{\mathcal{C}(\bar{\mathcal{L}}_0, f)}}. \quad (2.7)$$

Therefore,

$$H_p(f, t) = \frac{V_p}{\sqrt{\left((\mathcal{L}_p(t)/\bar{\mathcal{L}}_0)^\psi \chi(f)^{\mathcal{L}_p(t)-\bar{\mathcal{L}}_0}\right)}} Q(f). \quad (2.8)$$

According to the analysis presented in [77], Eq. (2.8) is approximated as $H_p(f, t) \approx h_p(t) \cdot Q(f)$, and the path gain is expressed as follows:

$$h_p(t) \approx \bar{h}_p e^{-\zeta_p \Delta\mathcal{L}_p(t)/2}, \quad (2.9)$$

where $\bar{h}_p = \frac{V_p}{\sqrt{(\mathcal{L}_p/\bar{\mathcal{L}}_0)^\psi \chi_0^{\mathcal{L}_p-\bar{\mathcal{L}}_0}}}$, $\chi_0 \approx 1$, and $\zeta_p = \chi_0 - 1 + \psi/\bar{\mathcal{L}}_p$.

Therefore, using the above discussion, a channel model that decouples the effects of time-varying multipath and the path filtering, can be used. The overall transfer function for the UAC is thus given as,

$$H(f, t) = Q(f) \cdot \sum_p h_p(t) e^{-j2\pi f \tau_p(t)}, \quad (2.10)$$

and taking the inverse Fourier transform of (2.10), we obtain the following channel impulse response:

$$h(\tau, t) = \sum_p h_p(t) q(\tau - \tau_p(t)). \quad (2.11)$$

where $h_p(t)$ is the time-varying gain of the p -th path, and $\tau_p(t) = \mathcal{L}_p(t)/c$ is the delay in p -th path. The filtering effect remains the same for all paths statistically, which is given by the time-invariant transfer function $Q(f)$, having the inverse Fourier transform $q(\tau)$.

2.3.3 Underwater Acoustic Signal Fading

The presence of large rocks, coral reefs, and uneven surfaces causes signal fading in UACs. The signal-strength fading or gain $g(t)$ is a random process in UACs that has been approximated using numerous distribution models, including Ricean, Rayleigh, and lognormal distributions [77]-[79]. We use the lognormal distribution [80] to model the fading effects and thereby make our channel model more realistic, as this distribution is well-known to yield a good fit for the long-term, large-scale fading phenomenon in UACs for shallow water [77]-[79]. The channel gain from a sensor to the buoy is modeled as $g(t) \sim \ln \mathcal{N}(\mu, \sigma^2)$, with a mean of 1 and variance of 2, and used to include the fading effect. Here, $g(t)$ is assumed to be independent from one sensor to another. For simplicity, it is assumed to be fixed during each OFDM symbol transmission from a sensor i .

2.3.4 Ambient Noise

The noise in underwater communication is classified as ambient noise and site-specific noise. Site-specific noise exists only in certain areas while ambient noise is always present and can be modelled as Gaussian. It consists of four major factors including turbulence, shipping, waves, and thermal noise. The power spectral density (PSD) of the ambient noise is given as follows,

$$\begin{aligned}10 \log N_t(f) &= 17 - 30 \log f \\10 \log N_s(f) &= 40 + 20(s - 0.5) + 26 \log f - 60 \log(f + 0.03) \\10 \log N_w(f) &= 50 + 7.5w^{1/2} + 20 \log f - 40 \log(f + 0.4) \\10 \log N_{th}(f) &= -15 + 20 \log f\end{aligned}\tag{2.12}$$

where f is the carrier frequency in kHz, s is the shipping activity factor ranging from 0 to 1 for low and high activity, respectively, and w is the wind speed in m/s [81]. The overall PSD of the ambient noise in dB re μ Pa per Hz, as a function of frequency in kHz is given as,

$$N(f) = N_t(f) + N_s(f) + N_w(f) + N_{th}(f).\tag{2.13}$$

2.3.5 Simulation of the Channel Model

As discussed in the above subsections, the parameters used for modeling the underwater acoustic channel are given in Table 2.1. Using these parameters, the impulse response of the UAC is obtained as given in Fig. 2.5.

Table 2.1: Underwater Acoustic Channel Parameters

Parameter	Value
Sea surface wind speed: w	15 m/s
Maximum Doppler spread: $B\tau_{max}$	4.744 Hz
Sea surface water density: ρ	1022 kg/m ³
Sea bottom water density: ρ_b	1027 kg/m ³
Sea surface sound speed: c	1526 m/s
Sea bottom sound speed: c_b	1490 m/s
Shipping activity factor (moderate activity): s	0.5
Constant scaling factor: \mathcal{C}_0	1
Spreading factor (practical spreading): ψ	1.5

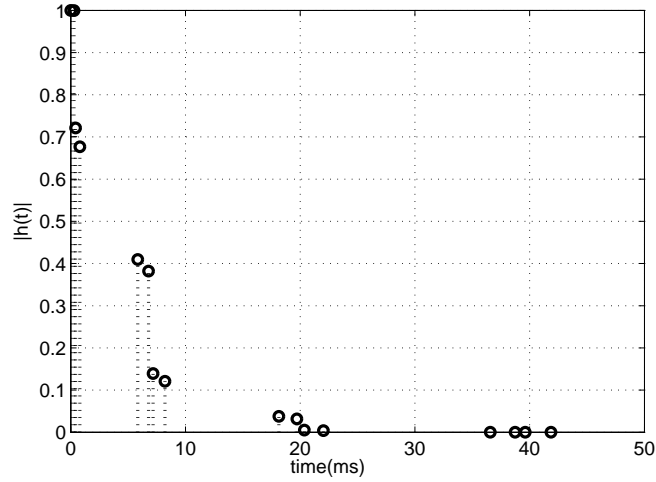


Figure 2.5: The normalized impulse response of the modeled UAC.

2.3.6 Received SNR

The SNR observed over a distance \mathcal{L} with a transmitted signal power P and carrier frequency f can be evaluated by using the noise PSD $N(f)$ and the signal attenuation

$\mathcal{C}(\mathcal{L}, f)$. The narrow-band SNR is thus given by,

$$SNR(\mathcal{L}, f) = \frac{P/\mathcal{C}(\mathcal{L}, f)}{N(f)\Delta f} \quad (2.14)$$

where Δf is the receiver noise bandwidth. The frequency-dependent received SNR is plotted in Fig. 2.6 for a varying transmission distance \mathcal{L} , a wind speed $w = 15 \text{ m/s}$, and shipping activity factor $s = 0.5$, considering moderate shipping activity. From Fig. 2.6, we can observe that with the relays located within 100 m distance from the transmitter, the received SNR is ~ 15 dB higher than that of the destination which is at 1000 m distance from the transmitter at a carrier frequency of 7 kHz. This observation is used as a basis for the simulation of our proposed SCCNC scheme. According to our deployment scheme discussed in Section 2.2, the minimum distance between two sensor nodes is 35 m and the maximum distance could be up to 141.5 m in a 100 $m \times 100 m$ area. Looking at Fig. 2.6, the received SNR difference between a relay at $\sim 200 m$ and destination at $\sim 900 m$ is almost 10 dB. Therefore, considering the worst case scenario, we will use a 10 dB inter-sensor channel SNR, which in ideal case would be up to 15 dB.

2.4 Cooperative Network-Coded Communication

The point-to-point LDPC-COFDM communication system for the UAC has been thoroughly investigated [18], [21], [22], [70]. The results show that COFDM systems perform robustly in UACs designed with simplified channel conditions. Here, we show that a point-to-point COFDM system may encounter problems under the realistic fading conditions that exist in UACs. Moreover, the variations in the positions of the

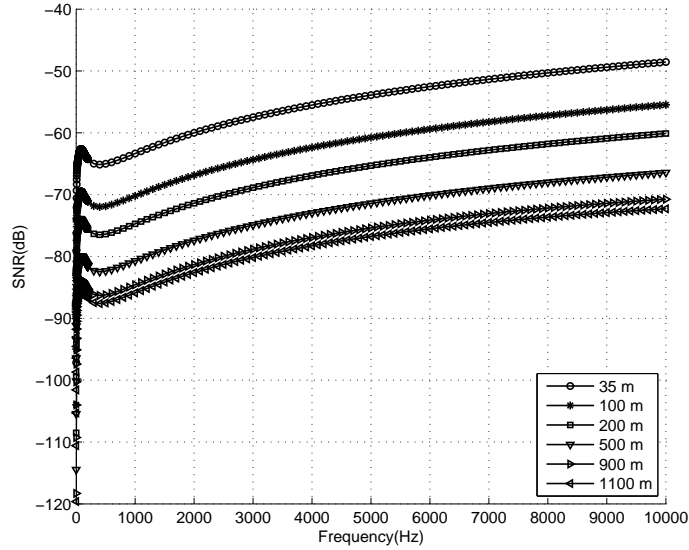


Figure 2.6: Received SNR at varying distance from the transmitter.

sensors and buoy can significantly change the impulse response of the UAC, yielding a performance variation.

2.4.1 LDPC-COFDM System

Fig. 2.7 shows a block diagram of the suggested COFDM system employing the regular LDPC code [82]. The OFDM system parameters are summarized in Table 2.2. The block size N is kept the same as the number of sub-carriers in the designed OFDM system. It is essential to choose a number of subcarriers that satisfies the conditions to overcome both frequency-selective fading ($\Delta f \leq B_C$) and time-selective fading ($T_S \ll T_C$). Because the Doppler spread increases geometrically as the carrier frequency increases [74], to overcome the time-selective fading, a suitable carrier frequency should be selected for the UAC. Based on our distance assumption of 1000 m , a

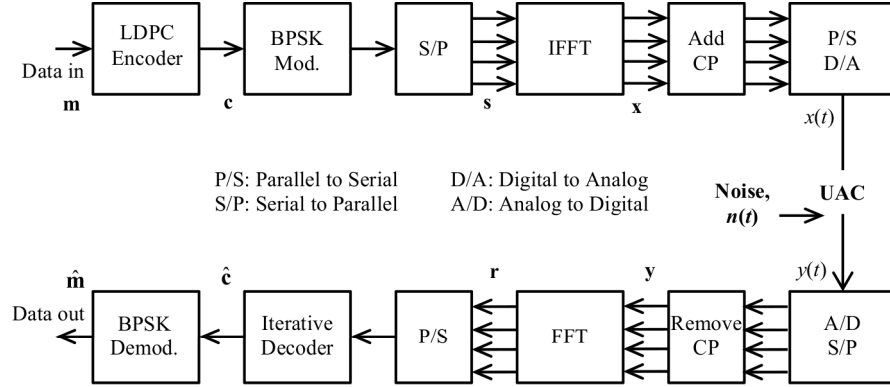


Figure 2.7: LDPC-COFDM system block diagram.

bandwidth of 10 kHz is chosen, along with a carrier frequency of 7 kHz [2]. To overcome the ISI problem, the cyclic prefix (CP) period is set as 25 ms via an analysis of the impulse response of the modeled channel. Under this setting, the maximum delay spread and coherent time of the channel are approximately 25 ms and 210 ms, respectively [83]. The designed OFDM system can overcome not only frequency-selective fading, $\Delta f < B_C$, but also ISI, $T_{CP} \geq \tau_{max}$, as well as time-selective fading, $T_S \ll T_C$.

An OFDM block of size N is generated by splitting the incoming information into N subcarriers. Therefore, the input data sequence \mathbf{m} is encoded using a regular LDPC ($N = 256, j = 4, k = 8$) code-generator matrix \mathbf{G}_{LDPC} to generate $\mathbf{c} = \mathbf{m}\mathbf{G}_{LDPC}$, where $\mathbf{c} = [c_1, c_2, c_3, \dots, c_N]$, and the subscripts represent the k^{th} bit of the codeword mapped to the k^{th} subcarrier, i.e., $k = 1, 2, 3, \dots, N$. After the binary phase-shift keying (BPSK) modulation of \mathbf{c} , the resulting sequence, $\mathbf{s} = 2\mathbf{c} - 1$, is converted from serial to parallel form, where $\mathbf{s} = [s_1, s_2, s_3, \dots, s_N]^T$. Then, taking the inverse fast Fourier transform of \mathbf{s} yields $\mathbf{x} = \text{IFFT}_N \{\mathbf{s}\}$, which is transmitted through the UAC in the

Table 2.2: OFDM System Parameters

Parameter	Value
Carrier frequency: f	7 kHz
Transmission bandwidth: BW	10 kHz
Maximum Doppler spread: $B\tau_{max}$	4.744 Hz
Coherent time: $T_C = 1/B\tau_{max}$	210 ms
Maximum delay spread: τ_{max}	25 ms
Coherent bandwidth: $B_C = 1/\tau_{max}$	40 Hz
Number of sub-carriers: N	256
Sub-carrier bandwidth: $\Delta f = BW/N$	39.0625 Hz
Valid symbol duration: $T_D = 1/\Delta f$	25.6 ms
CP period: $T_{CP} \geq \tau_{max}$	25 ms
OFDM symbol duration: $T_S = T_D + T_{CP}$	50.6 ms

form of $x(t)$ after the CP is added and a digital-to-analog conversion is performed.

At the receiver, a discrete-time signal $\mathbf{y} = [y_1, y_2, y_3, \dots, y_N]^T$ is obtained by sampling the received signal $y(t)$ after removing the CP. This is then transformed into \mathbf{r} by taking its Fourier transform, i.e., $\mathbf{r} = \text{FFT}_N \{\mathbf{y}\}$, and represented as

$$\mathbf{r} = \sqrt{E_s} \mathbf{H} \mathbf{s} + \mathbf{n}, \quad (2.15)$$

where \mathbf{n} is an i.i.d. Gaussian noise vector; $\mathbf{n} \sim \mathcal{N}^{N \times 1}(0, \sigma^2)$, \mathbf{r} , \mathbf{s} , and \mathbf{n} are each an $N \times 1$ vector, E_s is the symbol energy, and \mathbf{H} is an $N \times N$ diagonal matrix whose diagonal entries are the transfer-function coefficients $(H_1, H_2, H_3, \dots, H_N)$ of the UAC multiplied by the lognormal gain g , as discussed in Section 2.3.

Let E_b represent the energy per bit in the transmitted codeword in joules, and

N_0 is the noise power spectral density of the AWGN given in (2.15). To observe the performance of the COFDM system in UACs, we simulated the designed system by setting average random heights of the transmitting sensor (s_H) and receiver (D_H) from the sea bottom. The result is shown in Fig. 2.8, which compares the BER performance of the LDPC-COFDM system with that of an uncoded OFDM system. The COFDM system may overcome the severe frequency-selective performance falloff observed in the uncoded OFDM system, via the LDPC code. The coded system not only achieves a benefit of ~ 18 dB in E_b/N_0 but also reduces the performance variation due to the channel conditions. We observe a performance variation of ~ 3 dB when the positions of the sensor node and buoy change with respect to the sea bottom. This indicates the randomly changing nature of the UAC in shallow waters, which introduces the need for a more effective communication strategy that considers both the time- and frequency-selective fading, along with the other factors described in Section 2.3.

2.4.2 Limitations in LDPC-COFDM System

We showed that the LDPC-COFDM system is suitable for time- and frequency-selective channels such as UACs, exhibiting a reasonably robust performance. However, as UACs suffer from long-term large-scale fading, we must observe the performance of the designed system under lognormal fading. Fig. 2.9 shows the performance of the LDPC-COFDM system under the lognormal shadowing channel model. The results show that although the LDPC code can mitigate the deep frequency-selective fading effect at certain specific subcarriers, it cannot effectively resolve the problem of large-

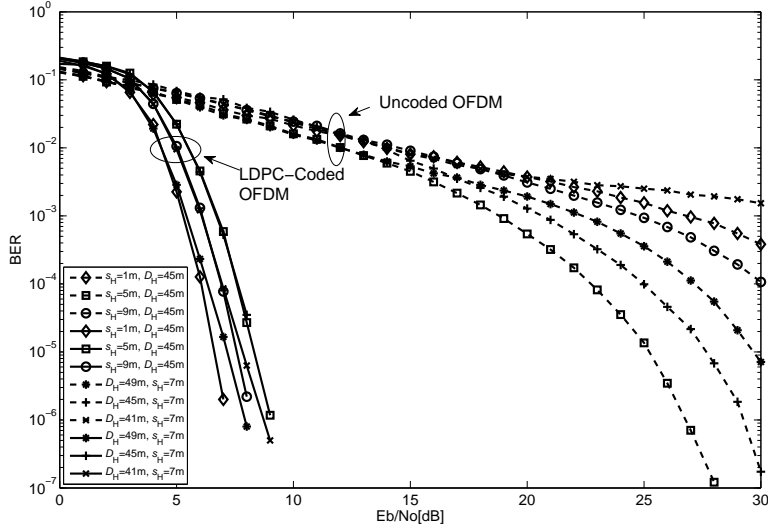


Figure 2.8: Performance comparison between LDPC-CODFM and uncoded OFDM systems.

scale fading, exhibiting a degradation of ~ 13 dB in E_b/N_0 at 10^{-4} BER. This effect is so detrimental that the sensors equipped with the LDPC-CODFM system spend on average ~ 13 dB more transmit power to obtain a BER of 10^{-4} than the amount needed with no shadowing.

User cooperation has been particularly beneficial for wireless systems that are subject to independent spatial fading. Thus, we are interested in the possibility of employing a user-cooperation scheme to resolve the detrimental effects of the fading in UACs. We propose the SCCNC scheme, as follows.

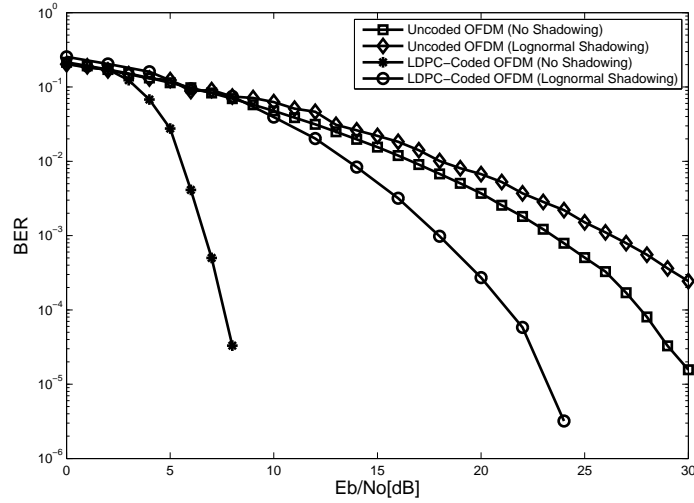


Figure 2.9: Effects of lognormal shadowing on uncoded and coded OFDM systems.

2.4.3 Design of the SCCNC Scheme

The famous two-phase user-cooperation scheme, which is common in wireless-network coding, [51]-[67], is utilized for our design of the underwater acoustic WSN. This approach is unique in that it aims to simultaneously exploit the diversity benefit from the frequency and spatial domains. The LDPC-coded and OFDM-modulated symbols transmitted by each sensor are relayed by the neighboring sensors, which helps to overcome the frequency-selective fading. Although our proposed system employs the idea of two-phase user cooperation reported by [64], in our scheme, the relays do not need to decode the received symbols, rather the symbols are used in the relay phase without regard to being correct or not. In this scheme, the SCCNC is formed across the spatial and frequency domain. A joint iterative-decoding algorithm for this cooperative network code is then developed.

Fig. 2.10(a) depicts the assumed network-cooperation scenario. In this model, U nodes communicate wirelessly to a common destination D via two-phase user cooperation. In each phase, the U nodes transmit BPSK-modulated COFDM symbols using time division multiple access (TDMA). The solid lines in Fig. 2.10(a) represent the channels between the sensor nodes, and the dashed lines represent the channels between a sensor and the destination. Because of the changing channel conditions, some of the links shown here may be broken at a particular instant of time. The two-phase user cooperation strategy and the decoding algorithm are described as follows.

Broadcast Phase

Each sensor node transmits to the destination D an N -bit LDPC-COFDM symbol of duration T_S in its assigned time slot, as shown in Fig. 2.10(b). Let $\mathbf{r}_{1,i,D}$ be the received signal at the destination D , sent from the node i during the first phase. The received signal from the i^{th} node at the destination D is given as follows:

$$\mathbf{r}_{1,i,D} = \sqrt{E_{s1}} \mathbf{H}_{i,D} \mathbf{s}_{i,D} + \mathbf{n}_{i,D}, \quad (2.16)$$

where E_{s1} is the transmitted symbol energy in the first phase, the index i denotes the transmission from the i^{th} sensor node to the destination D , with $i = 1, 2, 3, \dots, U$. Because we use a TDMA transmission scheme, with the exception of the transmitting node, all of the $U - 1$ other nodes overhear the transmission, $x(t)$, and the received signal $\mathbf{z}_{i,j}$ at the node j is given as

$$\mathbf{z}_{i,j} = \sqrt{E_{s1}} \mathbf{H}_{i,j} \mathbf{s}_{i,j} + \mathbf{n}_{i,j} \quad j \neq i, \quad (2.17)$$

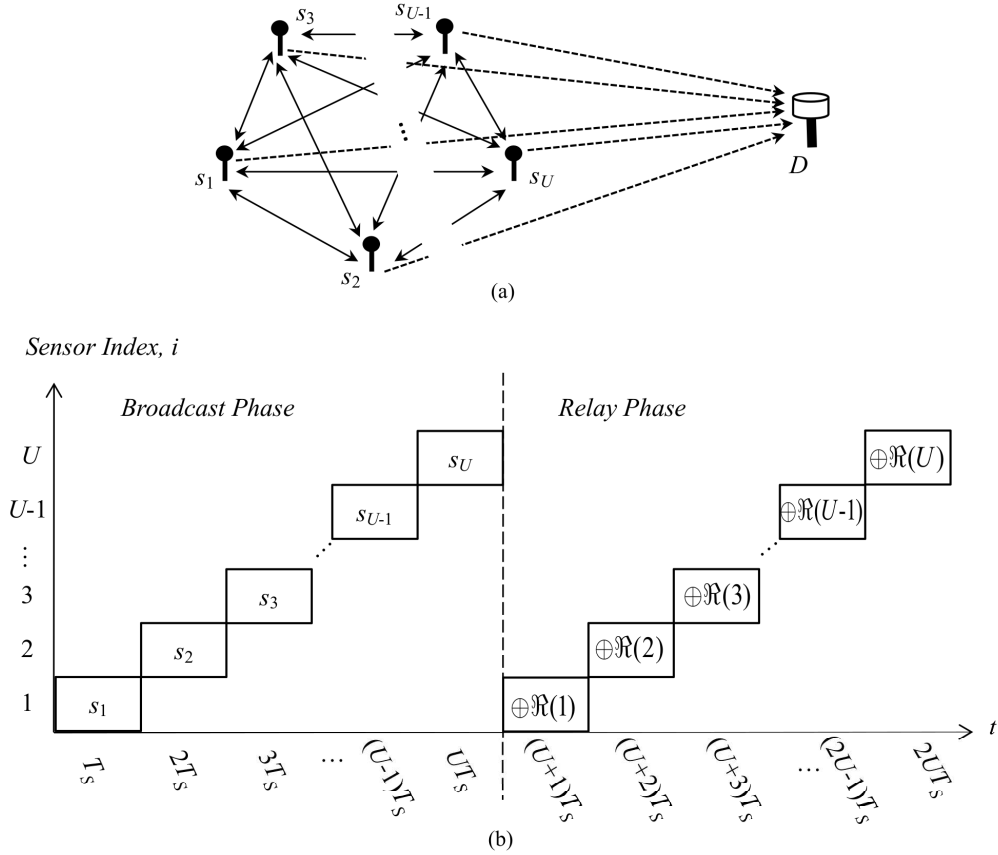


Figure 2.10: (a) Spatial representation of the network-cooperation scenario; (b) transmission sequence and time slots for each sensor node.

where j is the index of the receiving node, i is that of the transmitting node, and $j = 1, 2, 3, \dots, U$.

Because of the variation in the channel conditions, not all of the nodes can recover the transmitted codewords. We use a receive-set $\mathcal{R}(j) \subseteq \{1, 2, \dots, U\}$, which stores the indices of the sensors whose transmissions are received at the node j , where U is the total number of cooperating sensor nodes. The expression $i \in \mathcal{R}(j)$ indicates that node j has successfully received node i 's broadcasted symbol. Therefore, at the end of

this phase, the destination node D has received $\{\mathbf{r}_{1,1}, \mathbf{r}_{1,2}, \dots, \mathbf{r}_{1,U}\}$ symbols, and each sensor node j in the cooperating group has received $\{\mathbf{z}_{1,j}, \mathbf{z}_{2,j}, \dots, \mathbf{z}_{U-1,j}\}$ symbols, as given by (2.16) and (2.17), respectively. Assuming that the switching time from one transmitting node to another is negligible, the time taken by U nodes to complete a broadcast phase is UT_S , where T_S is the OFDM symbol duration given in Table 2.2. This phase is similar to that in the traditional COFDM communication system, except that the overhearing nodes in the cooperating group also store the recovered symbols for use in the relay phase. Note that the overhearing nodes do not decode the received symbols, but only store the received binary information.

Relay Phase

Each node randomly selects a small group of nodes from $\mathfrak{R}(j)$ (5 nodes), computes a checksum over their respective symbols, and forwards the checksum symbol $\oplus\mathfrak{R}(j)$, having length N , to the destination by using the same OFDM parameters in its assigned time slot, as shown in Fig. 2.10(b). Because the system operates using TDMA, the receive-set satisfies $\mathfrak{R}(j) \subseteq \{1, 2, \dots, U\}$. The spatial-domain code is formed using a code matrix similar to a randomly systematic low-density generator matrix (LDGM) code [84].

The codeword is formed using $\mathbf{G}_{\text{SCCNC}}$, which is the generator matrix for random-cooperation network coding, according to the procedure explained in Section 2.4.1. Because of the random nature of the network code, a small bit field is included in the relay packet so that the destination node knows how the checksum was computed

and can perform the message-passing decoding accordingly. Let $\mathbf{r}_{2,j,D}$ be the received SCCNC signal sent from the node j to the destination D during the relay phase. Then, the received signal at the destination D in the relay phase is given as

$$\mathbf{r}_{2,j,D} = \sqrt{E_{s2}} \mathbf{H}_{j,D} \mathbf{s}_{j,D} + \mathbf{n}_{j,D}, \quad (2.18)$$

where E_{s2} is the transmitted symbol energy in the relay phase, $\mathbf{s}_{j,D}$ is the SCCNC COFDM signal transmitted through the UAC from a sensor node j to the destination D , and $j = 1, 2, 3, \dots, U$. The source-symbols received in the first phase (2.16) constitute the systematic symbols of the network code, and the relay symbols received in the second phase (2.18) constitute the parity symbols. Hence, a set of U nodes completes the transmission of one SCCNC network codeword with length $2NU$ by the end of the second phase. The code rate at the destination is the combined code rate of the LDPC code and the network code, which is given as $R_{\text{SCCNC}} = R_{\text{LDPC}} \times R_{\text{LDGM}}$.

Assuming that the switching time from one transmitting node to another is negligible, the time taken by U nodes to complete a relay phase is UT_S . Therefore, the total time taken by U nodes to complete the transmission of an SCCNC symbol is $2UT_S$. The resulting SCCNC graph, as seen by the destination node, is shown in Fig. 2.11. The circles in Fig. 2.11 represent the bit nodes, and the squares represent the check nodes in the graph. The figure shows a U -node cooperation scheme, where each node uses a rate $1/4$ SCCNC. The broadcast phase bit nodes shown in Fig. 2.11 represent $\mathbf{r}_{1,i,D}$, and the relay phase bit nodes represent $\mathbf{r}_{2,j,D}$ as defined in (2.16) and (2.18), respectively.

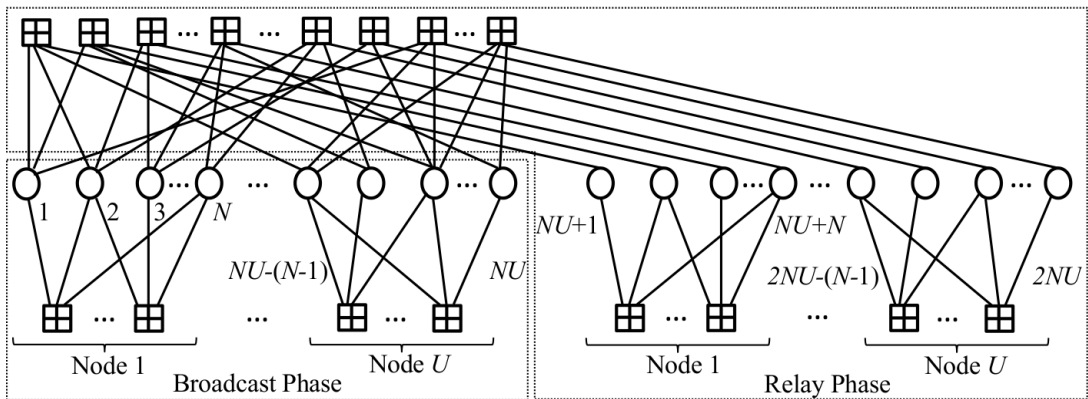


Figure 2.11: Example of the SCCNC scheme: each sensor sends an LDPC codeword in the first phase. The spatial-domain checksums are computed and sent during the second phase, which are the LDPC coded symbols received during the first phase.

2.4.4 SCCNC Decoding Algorithm

We propose a joint message-passing decoding algorithm at the destination, whereby extrinsic information is exchanged between the channel code (LDPC) and the spatial-code (LDGM) decoders in every iteration. In this section, we consider imperfect inter-sensor channel condition and try to develop an algorithm incorporating the inter-sensor channel error. For random selection at the relays, probabilistically, each of the links has equal channel condition and the average error probability for a single link is given as

$$\bar{p} = \frac{1}{2} \left(1 - \sqrt{\frac{E_{s1}\gamma}{E_{s1}\gamma + 1}} \right), \quad (2.19)$$

where $\gamma = \mathbb{E} \left[\frac{g_{i,j}^2}{N_0} \right]$ with $g_{i,j}^2$ as the magnitude square of the lognormal fading coefficients.

If each of the relay nodes chooses L_{deg} of its neighboring nodes' information to form a parity checksum, the corresponding probability of error for each link can be computed

as

$$p_e = \sum_{k=1, k \text{ is odd}}^{L_{\text{deg}}} \binom{L_{\text{deg}}}{k} \bar{p}^k (1 - \bar{p})^{L_{\text{deg}} - k} = \frac{1 - (1 - 2\bar{p})^{L_{\text{deg}}}}{2}. \quad (2.20)$$

The parity-check bits go through two serially concatenated channels; therefore, a modification is needed in the initialization part of the message-passing algorithm to incorporate the inter-sensor channel error in the decoding process. The channel log-likelihood ratio used to initialize the decoding iterations for the parity-check bits is given as

$$\text{LCr}_{j,D} = \frac{(1 - p_e) 4E_{s2} \mathbf{r}_{2,j,D} \left| \hat{\mathbf{H}}_{j,D} \right|^2 + (p_e) 4E_{s2} \mathbf{r}_{2,j,D} \left| \hat{\mathbf{H}}_{j,D} \right|^2}{N_0}. \quad (2.21)$$

The symbols received in the first phase go through one channel and the initialization for the decoding iterations is done as follows,

$$\text{LCr}_{i,D} = \frac{4E_{s1} \mathbf{r}_{1,i,D} \left| \hat{\mathbf{H}}_{i,D} \right|^2}{N_0}. \quad (2.22)$$

Let $\mathbf{R} = \{\mathbf{r}_{1,i,D}, \mathbf{r}_{2,j,D}\}$ be the received SCCNC signal matrix of size $N \times 2U$, $E_s(R_{\text{SCCNC}} \times E_b)$ be the received symbol energy, $\hat{\mathbf{H}}$ is the received estimated channel transfer function, and N_0 is the normalized noise power. Let N_{rs} and N_{cs} , be the number of rows and number of columns, respectively, of the parity-check matrix of the spatial code S. Let N_{rl} and N_{cl} , be the number of rows and number of columns, respectively, of the parity-check matrix of the LDPC code L. We define the messages from the check nodes to the bit nodes of the spatial code and LDPC code as LSr and LLr, respectively. Similarly, the messages from the bit nodes to the check nodes of the spatial code and LDPC code are defined as LSq and LLq, respectively. The number of 1s in each row of the spatial-code parity-check matrix S, called the degree of the code, is S_{deg} , and

the number of 1s in each row of the LDPC-code parity-check matrix L is called L_{deg} . Furthermore, we introduce a symmetric function $f(x) := -\log\left(\tanh\left(\frac{x}{2}\right)\right) = \log\left[\frac{e^x+1}{e^x-1}\right]$ satisfying $f^{-1}(x) = f(x)$. We also define the functions $\text{find}(\cdot)$, which selects all the non-zero indices from a matrix and stores them into another matrix, and $\text{sgn}(\cdot)$, which selects the sign of the argument.

The SCCNC decoding algorithm, which performs joint iterative decoding over the network code at the destination, is described here. LCr is the combined channel log-likelihood ratio for both phases, used to initialize the decoding iterations. The input data to this decoder is not a vector but a 2D matrix of size $N_{cl} \times N_{cs}$, as each cooperating node sends an LDPC-coded vector signal. The number of iterations (*max_iter*) can be set according to the desired decoding performance. During an iteration, the decoder calculates the bit-to-check node messages and then the check-to-bit node messages for all the nodes, first for the spatial code and then for the LDPC code.

Finally, the output values are calculated at each node, and a decision of 0 or 1 is made to obtain the SCCNC codeword. The codeword can then be decoded using the corresponding parity-check matrices of $\mathbf{G}_{\text{SCCNC}}$ and then \mathbf{G}_{LDPC} to obtain the message received from each node in the cooperating group. A pseudo-code for the proposed algorithm is given as follows. In the next subsection, we will present the EXIT chart analysis of the proposed algorithm to verify its functionality.

Algorithm 2.1: Message-passing decoding algorithm for SCCNC

Input

$$\mathbf{R}_{(N \times 2U)} = [\mathbf{r}_{1,u} : \mathbf{r}_{2,u}], \quad E_s/N_0$$

$$\hat{\mathbf{H}}_{(N \times 2U)} = [\hat{\mathbf{H}}_u : \hat{\mathbf{H}}_w]$$

$$v = 1, 2, \dots, N, \quad u = 1, 2, \dots, U, \quad w = U + 1, U + 2, \dots, 2U$$

Initialization

$$\text{LCr}_{v,u} = \left((1 - p_e) 4E_{s2} \hat{\mathbf{H}}_{v,u}^2 / N_0 \right) \mathbf{R}_{v,u} + \left((p_e) 4E_{s2} \hat{\mathbf{H}}_{v,u}^2 / N_0 \right) \mathbf{R}_{v,u}$$

$$\text{LCr}_{v,w} = \left(4E_{s1} \hat{\mathbf{H}}_{v,w}^2 / N_0 \right) \mathbf{R}_{v,w}$$

$$\text{Lp}_{v,p} = [0], \quad p = 1, 2, \dots, 2U$$

$$\text{LSr}(N_{cs}, N_{rs}, N_{cl}) = [0], \quad \text{LSq}(N_{cs}, N_{rs}, N_{cl}) = [0]$$

$$\text{LLr}(N_{cl}, N_{rl}, N_{cs}) = [0], \quad \text{LLq}(N_{cl}, N_{rl}, N_{cs}) = [0]$$

Iterations

While ($num_iter < max_iter$)

(i) Calculate the spatial code bit-to-check node messages.

For: $l = 1$ to N_{cl} , $m = 1$ to N_{cs}

$\text{Sc} = \text{find}(\text{S}_{\text{all rows}, m});$ $\text{Lc} = \text{find}(\text{L}_{\text{all rows}, l});$

$$\text{LSq}_{m, \text{Sc}, l} = \text{LCr}_{l, m} + \sum_{m' \neq m, \text{Sc}' \neq \text{Sc}, l' \neq l} \text{LSr}_{m', \text{Sc}', l'} + \sum \text{LLr}_{l, \text{Lc}, m}$$

End For

(ii) Calculate the spatial code check-to-bit node messages.

For: $l = 1$ to N_{cl} , $m = 1$ to N_{rs}

$Sc = \text{find}(S_{m, \text{all columns}})$;

$$LSr_{Sc,m,l} = \prod_{Sc' \neq Sc, m' \neq m, l' \neq l} \text{sgn}(LSq_{Sc',m',l'}) \times f \left(\sum_{Sc' \neq Sc, m' \neq m, l' \neq l} f(|LSq_{Sc',m',l'}|) \right) (-1)^{S_{\text{deg}}+1}$$

End For

(iii) Calculate the LDPC code bit-to-check node messages.

For: $l = 1$ to N_{cl} , $m = 1$ to N_{cs}

$Sc = \text{find}(S_{\text{all rows},m})$; $Lc = \text{find}(L_{\text{all rows},l})$;

$$LLq_{l,Lc,m} = LCr_{l,m} + \sum_{l' \neq l, Lc' \neq Lc, m' \neq m} LLr_{l',Lc',m'} + \sum LSr_{m,Sc,l}$$

End For

(iv) Calculate the LDPC code check-to-bit node messages.

For: $l = 1$ to N_{cs} , $m = 1$ to N_{rl}

$Lc = \text{find}(L_{m, \text{all columns}})$;

$$LLr_{Lc,m,l} = \prod_{Lc' \neq Lc, m' \neq m, l' \neq l} \text{sgn}(LLq_{Lc',m',l'}) \times f \left(\sum_{Lc' \neq Lc, m' \neq m, l' \neq l} f(|LLq_{Lc',m',l'}|) \right) (-1)^{L_{\text{deg}}}$$

End For

End While

Calculating the Result

Calculate the output value at the bit nodes.

For: $l = 1$ to N_{cl} , $m = 1$ to N_{cs}

$S_c = \text{find}(S_{\text{all rows},m});$ $L_c = \text{find}(L_{\text{all rows},l});$

$L_{p_{l,m}} = L_{C_{r_{l,m}}} + \sum L_{S_{r_{m,S_c,l}}} + \sum L_{L_{l,L_c,m}}$

End For

Making Combined Decision

Make a decision based on the values of L_p calculated in the previous step.

If $L_{p_{v,p}} > 0$, $\hat{c}_{v,p} = 1$; else $\hat{c}_{v,p} = 0$

Result

SCCNC codeword $\hat{\mathbf{c}}$ of size $N \times 2U$.

2.4.5 EXIT Chart Analysis of the SCCNC Decoder

To determine the characteristics and verify the performance of the joint iterative decoder for the SCCNC, an EXIT chart was used. EXIT charts are used to quantify the extrinsic information exchanged between the constituent decoders in an iterative decoding scheme. The EXIT chart plots two curves, showing the mutual information of the extrinsic log-likelihood ratios with respect to the mutual information of the *a priori* log-likelihood ratios, one for each decoder.

Fig. 2.12 shows the SCCNC decoding procedure using the LDGM decoder as the inner decoder and the LDPC decoder as the outer decoder. The *a priori* information about the source bits is not shown in the diagram because it is considered to be zero

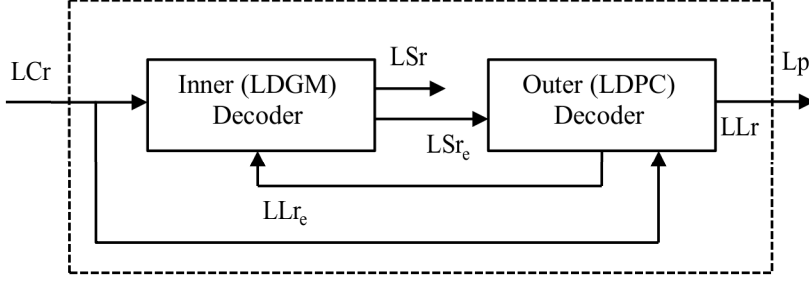


Figure 2.12: Iterative decoding procedure for the proposed SCCNC scheme.

for equiprobable source bits. The LCr , given as $LCr = \{LCr_{j,D}, LCr_{i,D}\}$, represents the channel log-likelihood ratios, and LSr_e and LLr_e represent the extrinsic information output from the inner and outer decoders, respectively:

$$LSr_e = LSr - LCr \tag{2.23}$$

$$LLr_e = LLr - (LCr + LSr_e).$$

The extrinsic information from the inner decoder LSr_e is used as an *a priori* input to the outer decoder to determine LLr_e . The new LLr_e is then used as an *a priori* input to the outer decoder in the next iteration.

The *a priori* input A to a constituent decoder is modeled using an independent Gaussian random variable n_A with a mean of zero and a variance of σ_A^2 . It is given as follows:

$$A = \mu_A \cdot m \cdot H_A + n_A, \tag{2.24}$$

where $\mu_A = \sigma_A^2/2$ is the mean of the Gaussian-distributed log-likelihood ratios of A , m is the transmitted systematic bit, and H_A is the corresponding frequency-response coefficient of the fading channel.

With the equiprobable source symbols input to the encoder at the transmitter, the

bitwise mutual information content of the *a priori* information $I_A = I(M; A)$ and the extrinsic information $I_E = I(M; E)$ are calculated as follows:

$$I_A = \frac{1}{2} \sum_{m=0}^1 \int_{-\infty}^{\infty} p_A(\xi | M = m) \times \log_2 \frac{2p_A(\xi | M = m)}{p_A(\xi | M = 0) + p_A(\xi | M = 1)} d\xi, \quad (2.25)$$

$$I_E = \frac{1}{2} \sum_{m=0}^1 \int_{-\infty}^{\infty} p_E(\xi | M = m) \times \log_2 \frac{2p_E(\xi | M = m)}{p_E(\xi | M = 0) + p_E(\xi | M = 1)} d\xi, \quad (2.26)$$

where M is a random variable representing the bits m of the input symbol \mathbf{m} ; and p_A and p_E are the conditional probability distributions for the *a priori* information and extrinsic information of each decoder, respectively, and are obtained by simulations using histogram measurements. For more details on the EXIT-chart procedure and analysis, the reader is referred to [85]. Fig. 2.13 shows the EXIT chart for our proposed SCCNC decoder for a network of randomly deployed 12 nodes. The bitwise mutual information is averaged over the symbols received from all the sensors. We show the proposed decoder's EXIT characteristics for a range of SNRs (1–7 dB) for the UAC. It is observed that the decoder converges at an SNR of ~ 7 dB for the UAC. The decoding trajectory shows that at least 10 iterations are needed for the decoder to converge. The convergence point is also verified by the simulation results in Fig. 2.16 and Fig. 2.17, which show a waterfall region starting near the SNR of 7 dB for a network of randomly deployed 12 nodes. The degradation in the performance of the decoder, compared with that in [85], arises from the harshness of the UAC.

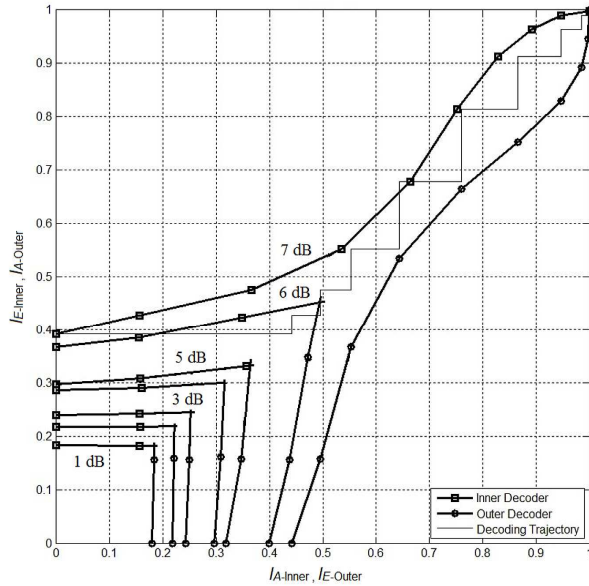


Figure 2.13: EXIT chart for the SCCNC decoder for a UAC with SNRs ranging from 1–7 dB.

2.5 Performance Analysis

In this section, we aim to analyze the energy consumption and network coding benefits of the designed network code. The coding gain obtained in the case of channel coding is obvious and well-understood, but in the case of the designed network code, we must consider other factors, such as the energy spent by sensors for receiving and decoding the overheard transmitted symbols, sending the parity check bits, and decoding the network-coded received signal at the destination. We aim to determine whether the network coding gain is sufficiently large to offset the increase in the power consumption for cooperative transmission and network (de)coding operations in the proposed scheme.

2.5.1 Energy Consumption of Cooperative and Non-Cooperative Schemes

With the current technology, an underwater acoustic modem uses an approximate transmit power of 2 W, a receiving power of 0.8 W, and an idle listening power of 0.2 W for communication over a distance of 1000 m [86], [87]. The message-passing decoder power dissipation is shown to be on the order of 500 mW for a throughput of 1 Gbps [88]-[90]. In the proposed cooperation scheme, the power consumption of the message-passing decoder increases by a factor greater than 2 as the length of the codeword doubles. Because the data rate of our proposed scheme is very low, therefore, for a throughput of 1 Mbps, we can safely assume the decoding power dissipation to be ~ 0.5 mW in the case of non-cooperation and 1 mW in case of cooperation schemes.

Let E_t , E_r , E_i , E_{dnc} , and E_{dc} , denote the energy consumed by the acoustic modem during the transmit operation by the sensors, receive operation at the sensor/buoy, idle listening by the sensors (no transmit/receive operation), decoding operations at the buoy in the non-cooperative case, and decoding operations at the buoy in the cooperative case, respectively. In the case of non-cooperation, the total energy consumed during one symbol period by the network of U nodes, $E_{s(non-coop)}$, is the sum of the following: the energy of a single transmission by U nodes, $U - 1$ multiplied by the idle listening energy of each node, the energy required for the receive operation, and the decoding energy consumption for U nodes at the destination D . It is given as

$$E_{s(non-coop)} = U (E_t + (U - 1) E_i + E_r + E_{dnc}). \quad (2.27)$$

In the case of node cooperation, the total energy consumed during one symbol period by the network of U nodes, $E_{s(coop)}$, is the sum of the following: twice the

energy of transmission for U nodes, $U - 1$ multiplied by the energies for the reception operations of each node, twice the energy of the receive operation, and the energy of the decoding operations for U nodes in the cooperative case at the destination D . It is given as

$$E_{s(coop)} = U (2E_t + (U - 1) E_r + 2E_r + E_{dc}). \quad (2.28)$$

Using the aforementioned values for E_t , E_r , E_i , E_{dnc} , and E_{dc} , the corresponding power consumption for Eqs. (2.27) and (2.28) is plotted in Fig. 2.14 for a varying number of sensor nodes in the network. The results indicate increases of approximately 1.58, 1.9, and 2.5 dB in the power consumption for $U = 12, 18,$ and 50 , respectively, in the cooperative network. The increase in the power consumption converges to ~ 3 dB for a cooperative network having up to 1000 nodes (not shown here). This shows that for cooperation among a reasonable number of nodes, i.e., $U < 50$, the increase in the power consumption is less than 3 dB.

2.5.2 Network Coding Gain

To analyze the BER, we assume that the underwater sensor nodes are distributed at the sea bottom as shown in Fig. 2.15. The numbers of sensor nodes considered are 12 and 18, according to the calculations done in Section 2.2. The nodes are placed at an average height of 7 m from the sea bottom within the 100 m \times 100 m range and the buoy is placed 5 m below the sea surface. In the case of random deployment, the position of each node is generated randomly uniform for every OFDM symbol transmission, as well as time-varying channel responses between the nodes and buoy. Similarly, for the

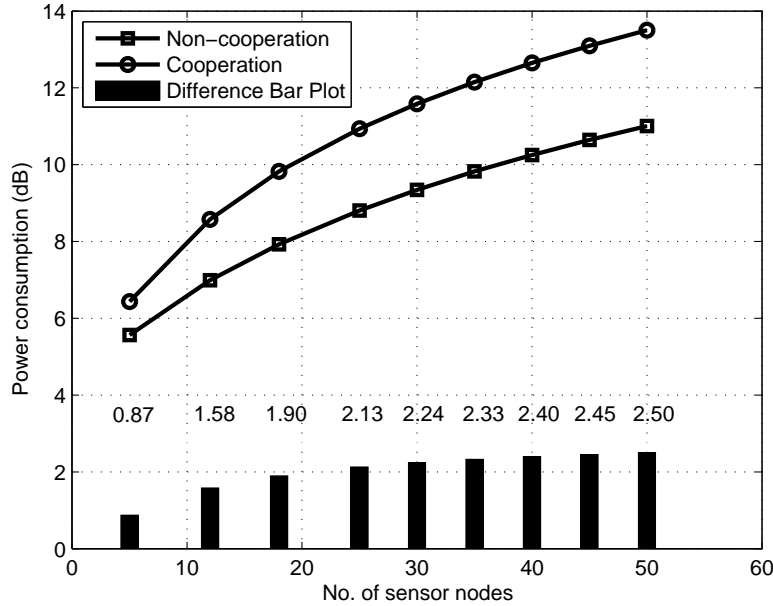


Figure 2.14: Power-consumption comparison between cooperation and non-cooperation networks.

case of triangular-grid deployment, the position of each node is generated in the form of a triangular grid. Other factors affecting the channel are a maximum sea-surface wind speed of 15 m/s , water depth of 50 m (considering the 44- m average depth of the Korean Western Sea), and distance of 1000 m between the node and buoy. Each node has a transmission range of 1000 m and a data rate of 2.5 kbps. The data-packet size is set as 32 bytes. Each node sends 1 packet of data in the broadcast phase and 1 packet of data in the relay phase towards the buoy.

Fig. 2.16 shows the performance of the proposed SCCNC scheme for the UAC with the lognormal shadowing model, using random deployment. Here, we simulate two different scenarios, one with a perfect inter-sensor channel (ISC) and another with

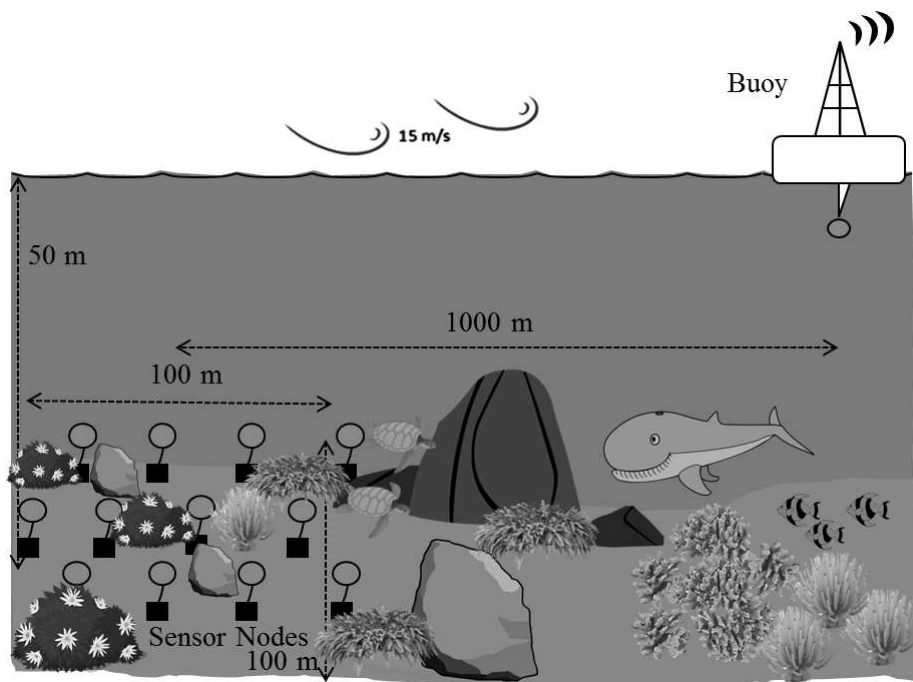


Figure 2.15: Underwater WSN scenario (Not to scale).

a realistic underwater channel including the errors induced by the inter-sensor communication in the first phase. The SNR for realistic scenario is chosen to be 10 dB higher than that at the destination, based on the argument given in Section 2.3.6. As shown, the proposed SCCNC scheme exhibits a significant improvement compared with the LDPC-COFDM system. For example, at the point where the BER is 10^{-4} , with 18-node cooperation, we obtain a 13-dB benefit compared with the LDPC-COFDM system. We also observe an improvement of ~ 11 dB at the point where the BER is 10^{-3} for a network comprising as few as 12 randomly deployed nodes.

When we compare the performance of the proposed scheme for a realistic channel with perfect ISC, a degradation of ~ 1.5 dB is observed in both the random and grid deployment (Fig. 2.17) for 12 and 18 nodes cooperation, which is negligible compared

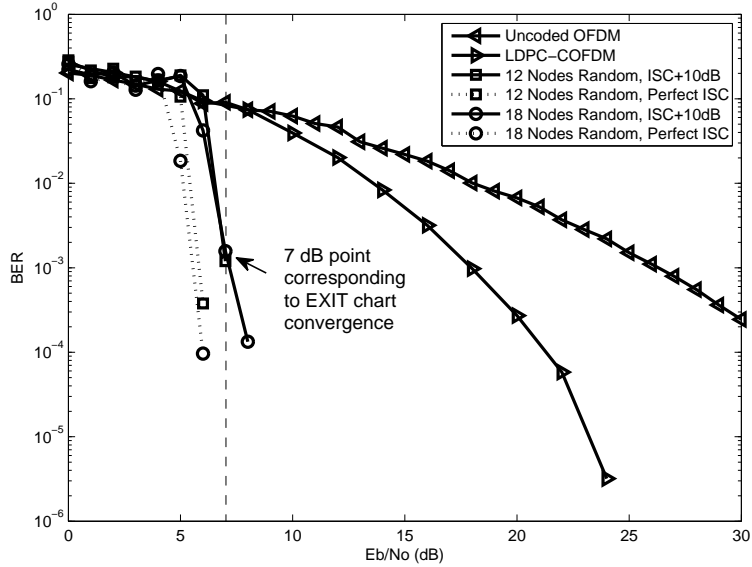


Figure 2.16: Performance of the proposed SCCNC scheme compared with the LDPC-COFDM and uncoded OFDM schemes for the UAC.

to the huge network coding gain of 13 dB. The perfect ISC assumption is equivalent to the scheme proposed in [64] combined with OFDM transmission, as all the symbols are assumed to be correctly received at the relays. Consequently, the codewords formed at the relays contain the information from correctly received symbols. Therefore, we can deduce that ideally, [64] will perform similar to the dotted lines shown in Fig. 2.16 and Fig. 2.17 on the underwater acoustic channel. However, in [64], the relay needs to decode the received symbol and decide whether it was correctly received or not, therefore, it spends more power and the hardware is more complex as compared to our proposed scheme. Our results show that without using this complex hardware and spending more power, we can achieve a similar performance by concatenating the

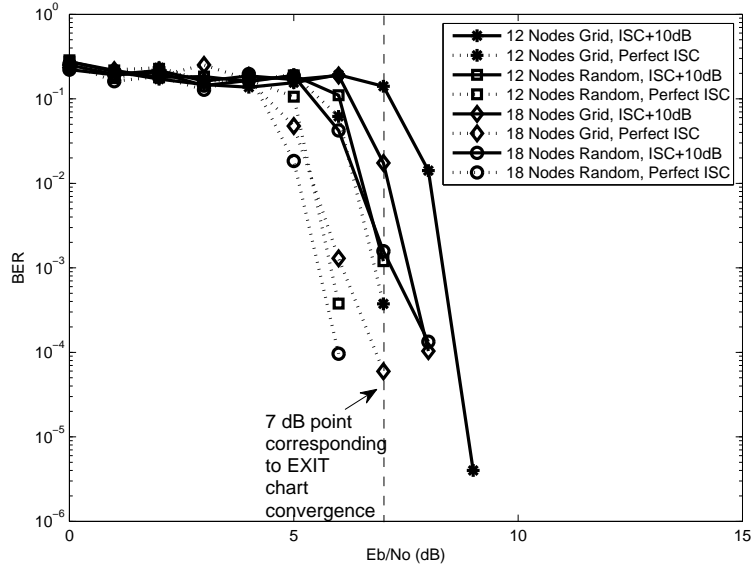


Figure 2.17: Performance comparison of random and grid deployment by using the proposed SCCNC scheme for the UAC.

channel and network codes.

The proposed SCCNC scheme for underwater acoustic communication benefits from the spatial diversity offered by the network, along with the frequency-diversity benefit, which is exploited by the LDPC-coded modulation with the OFDM transmission. Considering the additional 1.9 dB of power consumed by the cooperative network (Fig. 2.14), the designed cooperation scheme saves ~ 11 dB of the transmit-power consumption over the non-cooperative LDPC-COFDM system for a network comprising as few as 18 cooperating sensor nodes deployed within a $100\text{ m} \times 100\text{ m}$ area. Using the received SNR curves obtained in Section 2.3.6, the deployment area where our proposed scheme can be beneficial might extend up to $500\text{ m} \times 500\text{ m}$, intuitively, which can be

exactly determined in a future work.

2.5.3 Comparison of Random and Grid Deployment

Fig. 2.17 shows the BER performance of the random and fixed triangular-grid deployment of sensor nodes over an area of $100\text{ m} \times 100\text{ m}$. The grid deployments of both 12 and 18 nodes exhibit slightly higher BERs than the random deployment.

Therefore, we conclude that the random deployment is preferred over the triangular-grid deployment for an underwater acoustic WSN, as the random deployment is easier and cheaper to deploy and maintain over a period of time. Moreover, it exhibits a slightly better performance than the triangular-grid deployment with regard to the BER.

2.5.4 Delay and Extended Battery Life

In the case of the non-cooperative network, the throughput of the message-passing decoder at the destination D is $\frac{NU}{UT_s}$ bps (~ 6 kbps), whereas in the case of cooperation, it is $\frac{NU}{2UT_s}$ bps (~ 3 kbps). Thus, the throughput in the case of cooperation is reduced by half, which is expected because the destination must receive all the parity-check symbols from the cooperating sensor nodes before it can start decoding.

We wish to compute the effect on the battery life of the sensor in our proposed scheme. For a sensor battery life of h hours, the total power consumed by a network of U nodes is

$$P_{non-coop} = \frac{E_{s(non-coop)}}{h} = \mathcal{P} \text{ (dB)}, \quad (2.29)$$

and that for a cooperative network is

$$P_{coop} = \frac{E_{s(coop)}}{h} \cong (\mathcal{P} + 1.9 - 13) \cong (\mathcal{P} - 11) \text{ (dB)}. \quad (2.30)$$

Eq. (2.30) incorporates the 1.9-dB increase in the power consumption and the 13-dB network coding gain in our proposed scheme, showing that the scheme consumes ~ 13 times less power than the non-cooperation scheme as given in (2.29). However, because the time required to transmit the same amount of data is now $2h$ hours, the battery life improves by a factor of ~ 6.5 overall, increasing to $6.5h$ hours. Because the battery life is a very important factor in the operation/maintenance of underwater WSNs and the delay is not critically important, our proposed scheme is a very good option for low-energy consumption and improved-BER underwater communication networks.

2.6 Conclusion

We discussed the design of a network coding scheme for underwater acoustic communication and networking systems. We found that the non-cooperative LDPC-COFDM communication system mitigates deep frequency-selective fading effects but cannot effectively resolve the problem of shadowing in the UAC. On the other hand, cooperative communication enhanced the BER but significantly increased the power consumption of the network. To solve these problems, we propose a user-cooperation-based network coding scheme called the SCCNC. This scheme is applied to both randomly deployed and triangular-grid networks to facilitate cooperation among the sensors. It greatly enhanced the BER of the network, improving the SNR by ~ 11 dB overall, consuming ~ 13 times less power, and increasing the battery life by a factor of 6.5 compared

with the non-cooperative point-to-point LDPC-COFDM system. This benefit can be obtained when the cooperating sensor nodes are deployed within a $100\text{ m} \times 100\text{ m}$ area. Our results also show that a random deployment of the underwater acoustic WSN is superior to a triangular-grid deployment with regard to the BER and the deployment cost.

Chapter 3

Cooperative Relaying and Fusion of Sensor Data

In this chapter we discuss a cooperative relaying and in-network data aggregation scheme for industrial wireless networks (IWSNs). IWSNs are gaining importance for monitoring the indoor industrial area as well as machinery and equipment installed in hard-to-reach areas. It is important to monitor the condition of machines as well as environment in such industrial areas reliably in order to be able to activate response mechanisms on time. For example, evacuation in case of an accident, shutting down of machines in case of malfunctioning, and/or maintenance to keep a healthy and safe environment in the industrial area. However the indoor wireless communication channel is a very harsh channel and the information gathered by remote sensors cannot be sent to the BS reliably.

In this chapter, we propose a novel cooperation mechanism and a medium access control (MAC) protocol for cooperation among the sensors in an IWSN. A closed-form expression for the symbol error rate (SER) analysis has been derived, which confirms that the proposed scheme achieves the full diversity order offered by the cooperation mechanism. The proposed scheme increases the reliability of the data received at the BS, and reduces the overall energy consumption as compared to non-cooperative

schemes. The proposed scheme achieves a higher packet delivery ratio and lower false alarm rate as compared to the state-of-the-art related works.

3.1 Background and Contributions of this Work

Recently, network coding has become one of the most widely used techniques for cooperation among nodes in a wireless communication network. Some works that deal with improving the energy efficiency and packet delivery ratio include, a reliable reactive routing enhancement (R3E) algorithm for IWSN, which finds a guide path towards the sink and provides a reliable and energy-efficient packet delivery against the unreliable wireless links [10]. A physical-layer cooperative transceiver, which can use either amplify-and-forward (AF) or decode-and-forward (DF) relaying to improve the packet error rate, was proposed in [14]. The work in [26] presents an adaptive-gain M -relay AF cooperative system with conventional relay (CR) and best relay (BR) selection schemes and shows that the BR scheme provides higher asymptotic error limits than that of the CR scheme. A generalized dynamic-network code (GDNC) for a network of M users sending independent information to a common base station using independent block fading channels was proposed in [27]. The proposed scheme offers a much better tradeoff between rate and diversity as compared to the DNC. Similarly, [91] presents a selective cooperative relaying protocol with periodic, adaptive, and reactive relay selection mechanism. The scheme improves packet delivery ratio and reduces the number of retransmissions for successful delivery.

An adaptive and energy-efficient TDMA-based MAC protocol called receiver-driven

MAC (RMAC), which uses a timeslot stealing and timeslot reassignment mechanism, was proposed in [11]. RMAC performs better in terms of average packet delay and average power consumption per packet as compared to S-MAC. An energy-aware sleep scheduling mechanism for wireless sensor networks was presented in [12], which significantly reduces the variation in energy level among sensors and extends the lifetime of the network by around 18%. A practical wireless model-based predictive networked control system (W-MBPNCS) was proposed in [92], in order to achieve a decent control under severe impairments, such as unbounded delay, burst of packet loss, and ambient wireless traffic.

Another solution, used for MCM in large factories, distributes the signal processing operations among the central unit and the sensor nodes to reduce the energy consumption in data transmission and improve the network throughput, was proposed in [93]. Similarly, [38] presents an IWSN-based MCM system which overcomes false alarms caused by loss of data, interference, or invalid data. An improvement in the SNR and false alarm detection rate, after Dempster-Shafer Theory (DST)-based fusion method, was observed.

Most of the above-mentioned works use cooperative and selective relaying to improve packet delivery and energy consumption of the network. However, relay selection comes with an extra overhead of reduced network throughput and the problem becomes more evident in the case of multi-hop and multiple cluster sensor networks. We propose a method in which the cooperation groups are fixed in the organization stage of the network. A source node acts as a relay node in the cooperative phase of transmission.

A relay node uses data aggregation and AF relaying to send the cooperative packet to the BS.

The contributions of this work are as follows,

- We propose a novel two-phase cooperation scheme that works in a dual-hop manner.
- A closed-form expression has been derived for the symbol error rate analysis and it is shown that the proposed method achieves full diversity order.
- Our proposed scheme does not involve the extra overhead of relay selection and retransmission to ensure successful packet delivery, unlike [10], [26], and [91].
- The relay does not need to check whether the data was correctly received. It forwards the detected binary symbols without regard to the error induced in it in the first hop.
- We also propose a TDMA-based MAC protocol for the organization and operation of the sensor network.
- We have carried out the throughput and energy consumption analysis to show the effectiveness of the proposed scheme.

3.2 Network Design

Fig. 3.1 shows a cooperative WSN where the sensor nodes share their information with each other in the first phase and send the cooperative information to the base

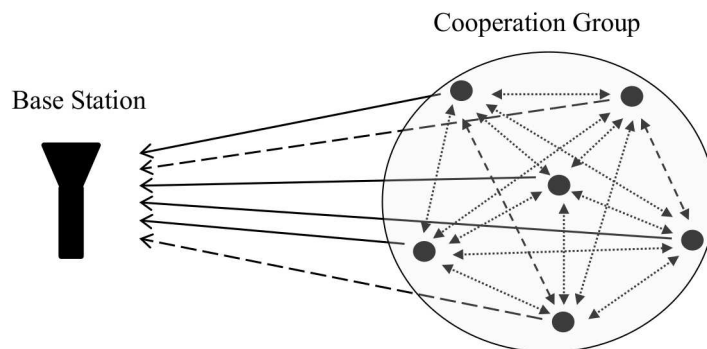


Figure 3.1: Cooperative wireless sensor network.

station in the second phase. Inter-sensor channels are shown by dotted lines while the channels from sensor to base station are shown by solid lines. We assume that some of the communication links between the sensors and from a sensor to the base station might be broken at a particular time instance, shown by long-dashed lines.

3.2.1 Sensor Deployment

Sensor deployment deals with the problem of coverage and connectivity of the sensor network while minimizing the power consumption for prolonged network lifetime and to transmit the sensed data timely and efficiently to the BS. In our case of indoor industrial area monitoring, the sensors could be deployed according to a pre-planned location map around huge machines in the factories. Considering these scenarios, our coverage problem becomes a static coverage problem, where the nodes do not change their positions. Assume that the sensing range of a sensor is r , the minimum number of sensors required to cover the area of interest [94], is given as,

$$\frac{N \times r^2 \pi}{P_{AREA}} = \frac{2\pi}{\sqrt{27}}, \quad (3.1)$$

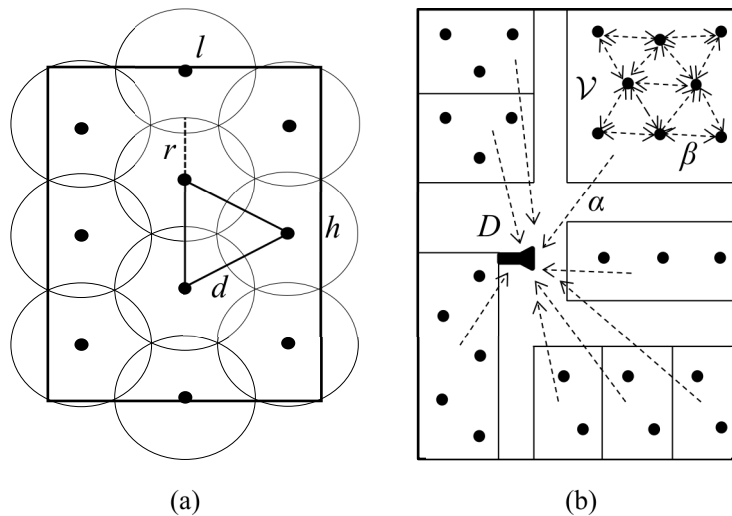


Figure 3.2: Sensor nodes deployed in a rectangular area. (a) Triangular-grid, ensuring the coverage of the whole area with minimal overlap. (b) Indoor communication scenario showing a floor layout.

where N is the minimal number of nodes needed to cover the area of interest, P_{AREA} . This kind of optimal regular deployment is shown in Fig. 3.2(a). Every three nodes, whose sensing ranges intersect, form an equilateral triangle with each side $d = r\sqrt{3}$.

In order to ensure connectivity, we use the argument in [69] for the minimum number of neighbor nodes, which says that for a network to be connected, $\Theta(\log N)$ ($0.074 \log N$ to $5.1774 \log N$) neighbors are necessary and sufficient. Therefore, we choose the minimum number of neighbors for a sensor to be equal to 6, with which it can communicate in a single-hop manner. This is used to enable cooperative transmission to the base station for a combined decision on the sensed data.

3.2.2 Sensor Localization

Sensor localization is used to locate the sensor positions and time of the observed information in the network. We consider a medium-sized fixed sensor network. Each sensor contains its local coordinate information, which is sent to the base station along with its observation. The local coordinate system (LCS) field in the transmitted packet contains geographic coordinates and floor number in case of multi-story buildings. The received signal strength (RSS) and angle-of-arrival (AOA) information could be used to find the sensors' distance and angular position, respectively, but the LCS field in the transmitted packet already contains the position information. Therefore, the only information that needs to be determined is the time of the event. Thus, along with the LCS, we use the time-of-arrival (TOA) information in order to locate the time of the event. This will help us localize the received information in both time and geographical location of the observation.

The transmitted packet structure and alarm information by each sensor is shown in Fig. 3.3. This information will be decoded at the base station by the fusion center to find out the nature of the observations at a particular location in the network and activate response mechanisms on time.

3.2.3 Time Synchronization

In our problem of a medium-sized network, most of the computations are done by the BS and the sensors are supposed to be in harsh environmental conditions which make it difficult for fine-grained synchronization algorithms to be used. Therefore, we

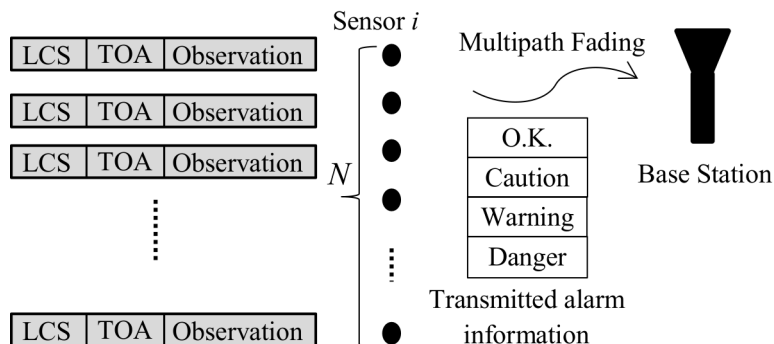


Figure 3.3: Information transmission to the base station.

adapt the Wisden system [95] of coarse-grained synchronization. In our synchronization technique, each sensor records the delay from the time of generation/reception of a sample to the time it is transmitted to the next hop or BS. Also, the cooperating node will record its own time delay for the packet that it processes before sending it to the base station. The TOA field in the transmitted packet contains this time delay information of all the nodes that the packet has traversed before reaching the BS.

Assume that the time spent by each packet k at the sensor node i is λ_i^k . Let the number of hops the packet traverses be n , and the time of arrival of the packet k , at the base station D , be T_D^k . Then, the start time of the packet at the origin node s , can be calculated as,

$$T_s^k = T_D^k - \sum_{i=1}^n \lambda_i^k. \quad (3.2)$$

The second term in (3.2) represents the time spent by the packet in the network. Thus, we can get the time of origination of the observation at the BS by subtracting the total time spent in the network from the current time at the BS. This process is shown in Fig. 3.4. The BS is assumed to have an accurate reference clock periodically

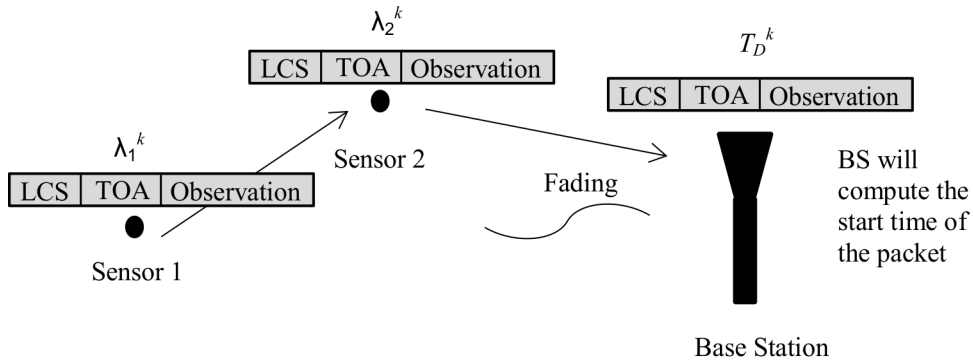


Figure 3.4: Calculation of the time-of-arrival (TOA) at BS.

synchronized with the GPS time reference while each sensor node has its own local clock. This method of achieving time synchronization is simple, cost-effective, and robust to many sources of latency that contribute to error but is vulnerable to varying clock drifts in the intermediate nodes. But we assume a well-maintained medium-sized network of nodes and a moderate accuracy requirement; therefore, clock drift is not a very critical issue and can be traded off with the simplicity of the approach.

3.2.4 The Indoor Wireless Channel Characteristics

We consider a medium-sized indoor industrial WSN with mixed line-of-sight (LOS) and non-line-of-sight (NLOS) configurations, therefore we will use the statistical one-slope radio propagation model for path-loss [8].

Received Signal Strength

In order to find the received signal strength at each sensor from all other sensors in the cooperation group, we use the log distance path loss or lognormal shadowing model,

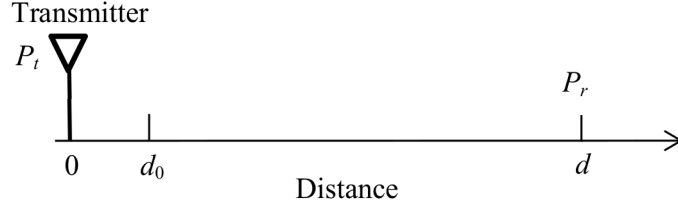


Figure 3.5: Calculation of the received signal strength.

as shown in Fig. 3.5. This is a generic model used to predict the propagation loss for a wide range of environments including free space and indoor factory environments.

The path loss measured in dB at a distance d from the transmitter is given by,

$$PL_{dB}(d) = PL_{dB}(d_0) + 10\eta \log_{10} \left(\frac{d}{d_0} \right) + X_{\sigma,dB}, \quad (3.3)$$

where PL_{dB} is the path-loss in dB, η is the path-loss exponent indicating the rate of decay of the mean signal with respect to distance, d_0 is a reference distance, and $X_{\sigma,dB}$ is a zero-mean Gaussian random variable with standard deviation σ . In (3.3), $PL_{dB}(d_0)$ is the path loss in dB at a reference distance d_0 , which is calculated using the Friis free-space propagation model. It is used to model the line-of-sight (LOS) path loss incurred in the channel, given as

$$P_r(d_0) = P_t \frac{G_t G_r \lambda^2}{(4\pi d_0)^2 L}, \quad (3.4)$$

where $P_r(d_0)$ is the received signal power in Watts, P_t is the transmitted signal power in Watts, G_t and G_r are the gains of transmitter and receiver, respectively. λ is the wavelength of the carrier in meters, and L is the system losses which are not associated with propagation loss. Generally, it is more convenient to work in log domain because

the transmit and receive power are usually available in dBm and the antenna gains in dBi. Therefore, the Friis free-space equation is given in log domain as,

$$\begin{aligned}
 PL_{dB}(d_0) &= P_{t,dB} + 10\log_{10}(G_t) + 10\log_{10}(G_r) \\
 &+ 20\log_{10}(\lambda) - 20\log_{10}(4\pi d_0) - 10\log_{10}(L).
 \end{aligned}
 \tag{3.5}$$

In (3.5), G_t , G_r , and L are taken equal to 1 as we consider unit gain antennas and the internal system losses are considered as 1, whereas the reference distance d_0 is taken as 1 m. Using (3.3) and (3.5), the received signal strength at a sensor is calculated as,

$$P_{r,dB}(d) = P_{t,dB} - PL_{dB}(d).
 \tag{3.6}$$

The model in (3.6) provides a very good approximation for the indoor industrial wireless channel by considering the multipath and shadowing effects present in the environment. However, the values of η and σ need to be carefully chosen according to the environment, as described in [8] and the references therein. We will use (3.6) to calculate the received signal strength by using the parameters which are suitable for indoor factory non-line-of-sight (NLOS) environments.

Cluster Organization

Fig. 3.2(b) shows a floor map of a building with sensors scattered all over the floor that communicate to a common BS. Each link in the network is modeled by using (3.6) and incorporating η and σ with respect to indoor communication scenario. The inter-node channels, β_i , and the node-destination channels, α_i , are modeled as lognormal distributed Rayleigh fading channels.

The wireless nodes are clustered into different cooperation groups by their geographic locations. The cooperative transmission is done within each cooperation group, $\mathcal{V} = \{V_i\}_{i=1}^{\mathcal{G}}$, where \mathcal{G} is the maximum number of nodes in a cooperation group. The wireless nodes V_i 's in a cooperation group are physically close to each other and the destination node is relatively far away from the group. Further assumptions are that the channels from each node V_i to the destination D is modeled as a lognormal fading channel with fading coefficient α_i , which is assumed to be fixed for a sufficiently longer period of time. As the group of wireless nodes is collocated and the destination is relatively far away, the fading coefficients α_i 's are assumed to have the same average magnitude determined by the path loss from V_i to D . Also, the fading channels from V_i to D , are independent, thus, the fading coefficients α_i 's, from V_i to D , are i.i.d. lognormal random variables. The channel from a transmitting node V_i to a node V_j within a group are also modeled as lognormal fading channels with fading coefficients $\beta_{i,j}$. To further simplify the analysis, it is assumed that the relative distance among these nodes is almost the same. Under this assumption, $\beta_{i,j}$'s are also i.i.d. lognormal random variables with the same average magnitude determined by the path loss among them.

3.3 Cross Layer Design

Some of the major sources of energy wastage in WSNs are packet collisions, overhearing, packet overhead, and idle listening [96]. In order to reduce the energy loss to collisions and overhearing, we will use a TDMA-based MAC scheme in a two-phase

communication model. Scheduling reduces packet collisions over the air, while the overheard information by each sensor is used to reduce the error rate and improve data transfer to the base station, which helps reduce the energy wastage in the network. For a medium-sized network of fixed sensors, we propose this protocol to meet our needs of scheduling, to reduce the header length and computation time.

3.3.1 Design of the Data Packet

As mentioned earlier, the data packet contains LCS, TOA, and Observation fields. The LCS contains the location information of the sensor which is embedded in it during the network deployment stage. It contains the following information fields:

- *Floor Number*: Although this parameter may vary according to the design under consideration, we choose this value to be 3 bit in order to cover up to 8-story buildings with our design.
- *Sensor ID*: Each sensor on a floor is assigned a unique identification number. We assign 7 bits to this field to allow up to 128 sensors on each floor of the building.
- *TOA*: This field is of 10 bits and contains the time duration between the time-of-arrival/observation of information on the current sensor and the time it was transmitted.
- *Observation*: The 2-bit observation field contains the alarm information, i.e., OK, Caution, Warning, and Danger.

The resulting data packet is a 22-bit packet as shown in Fig. 3.6(a). If Δ is the

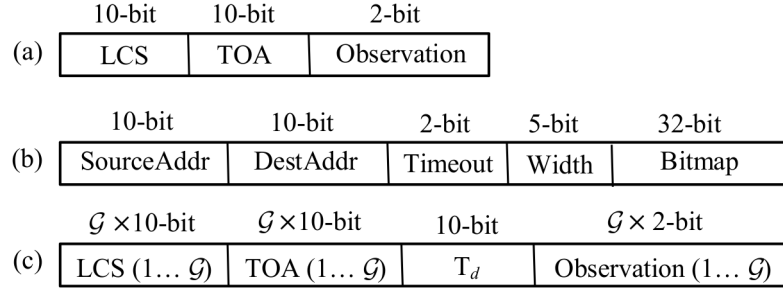


Figure 3.6: (a) Data packet structure of each node in Phase 1. (b) Schedule packet structure used for organization of the network. (c) Data packet structure of each node in Phase 2 for cooperative data transmission.

total time taken by the network to transmit one sensing event to the base station in a TDMA manner, then in the worst-case scenario, each sensor may have to wait for Δ seconds before it can send its data to the base station.

3.3.2 Design of the Schedule Packet

In our proposed scheme, each sensor transmits a schedule packet to select the winner of a given time slot, which is called Schedule, as shown in Fig. 3.6(b).

- The source and destination node addresses of the current schedule packet are called SourceAddr and DestAddr, respectively. These fields contain the LCS information of the corresponding nodes and are therefore 10 bits each.
- Timeout is used to resend the scheduling information to the next node in case it did not respond at the first time. The number of retries is limited to 4, after which the node is considered dead, its bitmap is set to 1, and the DestAddr is

changed to next node in the schedule.

- Width defines the number of nodes in a cooperation group and in turn the size of the data packet each node has to send to the BS. This value is set to 5 bit in our design for a maximum of 32 nodes in the cooperation group.
- Bitmap contains a bitmap of all the sensors in the network. A ‘0’ in the bitmap means the node is not organized and a ‘1’ means the node is organized in the network. A node ID corresponding to the bitmap is saved at each node in the network, so that it knows which bit represents which node in the network.

3.3.3 Organize and Operate Protocol (OOP)

Our proposed network consists of fixed nodes and therefore mobility issues are not considered. Further, the network is assumed to have local groups of nodes that communicate cooperatively with the destination in a dual-hop manner. There are no cluster-heads formed because all the nodes in a group will schedule their communication links independently and in collaboration with other nodes in their vicinity. As mentioned earlier, a node is able to communicate with a minimum number of neighboring nodes in the network. Each node keeps a list of 6 to 20 neighboring nodes by saving the source address of these nodes which will be broadcasted using a low-frequency control channel. A node will decode the received information only from the nodes within its neighbor list. The rest of the received information will be discarded. The cooperation group will be updated periodically depending upon the application and conditions of the sensor nodes.

Based on the above described scheme, we propose a TDMA-based protocol for the operation of the WSN. It consists of two main steps, organization of the nodes and operation of the network, and therefore referred to as Organize and Operate Protocol (OOP). The OOP is described as follows and shown graphically in Fig. 3.7.

Algorithm 3.1: Organize and Operate Protocol (OOP)

1. Organize

(a) BS sends Organize message to all the nodes in the network, using the Schedule packet described earlier.

- The Bitmap is set to all 0's, i.e., none of the nodes is organized as yet.
- It also contains the address of the first node to start the Organize process from. This address will be generated randomly on each Organize message.

(b) Upon receiving the Organize message, each node turns to Organize mode, i.e.,

- Stop all the current transmit/receive operations.
- Update its current list of neighbor nodes.
- Listen to the received Schedule packet from neighbor node.
- After receiving a Schedule packet, each node updates its information in the Schedule packet, sets its corresponding bit in the Bitmap field to '1' and passes the Schedule packet to the next node.

(c) When the bitmap becomes all 1's,

- The current node transmits this information to the BS, by setting the DestAddr to that of the BS.
- The BS, upon receiving this packet, sends a global message to all the nodes indicating to start normal sense and transmit operations mode, called Operate.

2. Operate

Upon receiving the Operate message from BS, each sensor then,

- (a) Senses the surrounding environment and wait for its turn to transmit.
- (b) Shares the data with the nodes in its neighbor list.
 - Each node in the neighbor list receives this data and stores it in its local memory.
- (c) Upon receiving the data from all the nodes in its neighbor list,
 - IF this was the first node in Organize stage ¹,
Transmit the cooperative data packet to the BS,
ELSE
Wait for its turn to transmit.
- (d) Go to (a)

¹Each node stores the bitmap and next node DestAddr information during the Organize stage, which is also used in the operation scheduling.

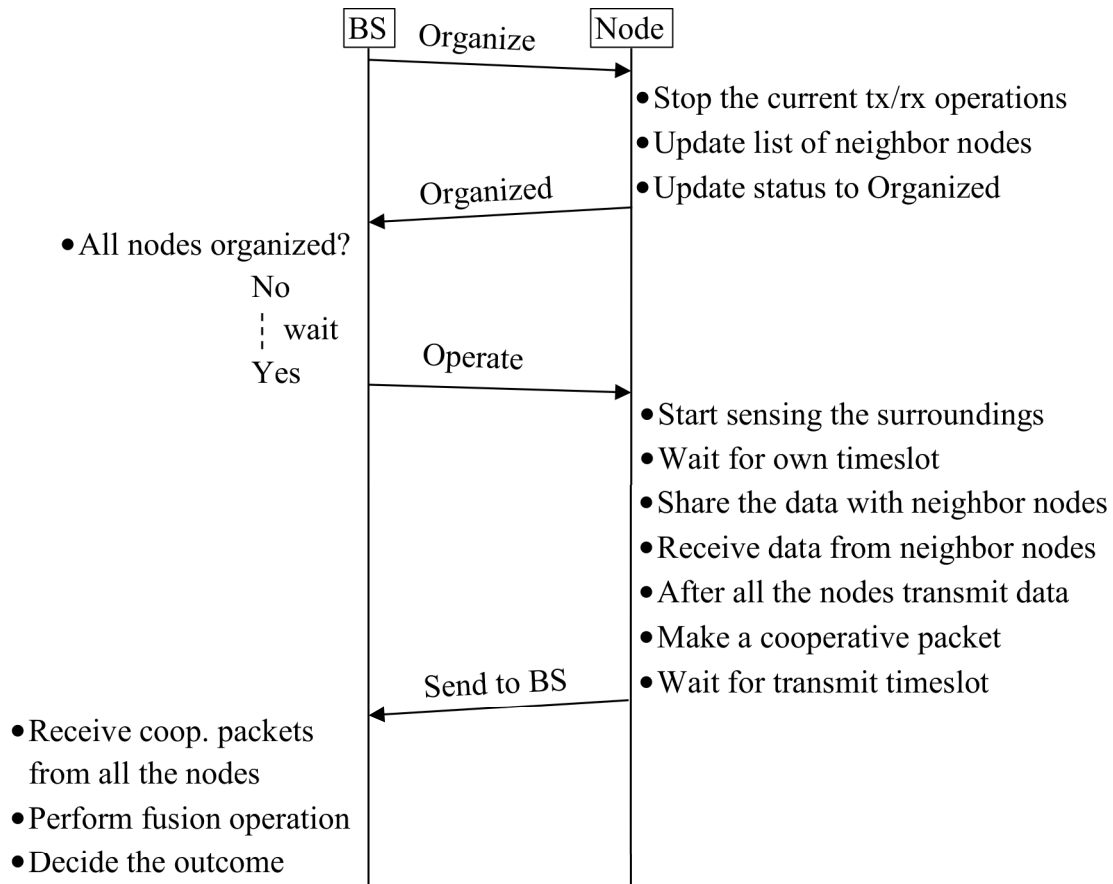


Figure 3.7: The proposed Organize and Operate Protocol (OOP) for WSN.

3.3.4 Cooperative Communication

Assume that the network is organized in sub groups of nodes that cooperate with each other, called cooperation group. We use the AF relaying protocol at the relays. The communication is done in two phases, as follows,

Phase 1

After sensing the information from its surrounding area, each sensor in the cooperation group shares this information with the nodes in its neighbor list in a TDMA manner.

Every node in the neighbor list that receives this data, stores it in its local memory.

The received signal $r_{i,j}$ at the relay node V_i , from the source node V_j , in phase 1 is,

$$r_{i,j} = \sqrt{E_{s1}}v_j\beta_{i,j} + n_{i,j}, \quad (3.7)$$

where E_{s1} is the transmitted symbol power in phase 1, v_j is the BSPK-modulated symbol sent from node V_j , and $n_{i,j}$ is the additive white Gaussian noise at node i from node j , with variance, N_0 . The data packet sent by each node in this phase is shown in Fig. 3.6(a).

Phase 2

The size of the data packets sent by a sensor is usually small and sending each packet separately to the BS requires a large number of transmissions, which increases the energy consumption. Therefore, aggregation of data is used at the intermediate nodes to reduce the control packet overhead and the number of transmissions required to send the same amount of data to the BS. The aggregated data is forwarded to the BS by using the AF protocol, in which, the relay equalizes the channel fades between the source and the relay by amplifying the received signal by a factor that is inversely proportional to the received power.

Each node V_i , combines the received information from the nodes within its cooperation group, \mathcal{V} , to form a cooperative data packet. The cooperative data packet represented by x_i at a node i , consists of a concatenation of the received and amplified packets from all the nodes in the cooperation group ($\zeta_{i,j}\hat{u}_{i,j}$, $j = 1, 2, \dots, \mathcal{G}$ and $j \neq i$) and its own information v_i . $\hat{u}_{i,j}$ is the detected signal and $\zeta_{i,j}$ is the amplification factor

at the relay node V_i with a corresponding source node V_j . The cooperative data packet is formed as,

$$x_i = \begin{cases} \zeta_{i,j} \hat{u}_{i,j} & j \neq i \\ v_i & j = i \end{cases}, \quad (3.8)$$

where

$$\zeta_{i,j} = \frac{1}{\sqrt{E_{s1} |\beta_{i,j}|^2 + N_{0,i,j}}}, \quad (3.9)$$

and $N_{0,i,j}$ is the input noise variance at the relay i from node j . The cooperative data packet sent by each node in this phase is shown in Fig. 3.6(c). In the cooperative packet, all the LCS and TOA information of the cooperation group including self-information is concatenated in sequential order. T_d contains the time spent at the relay node and Observation contains the observed alarm information by each node in the cooperation group, \mathcal{V} .

Upon its turn, every node transmits the cooperative data packet to the BS. The received signal at the BS, $y_{i,D}$, can be written as,

$$y_{i,D} = \sqrt{E_{s2}} x_i \alpha_{i,D} + n_{i,D}, \quad (3.10)$$

where $\alpha_{i,D}$ is the lognormal fading channel coefficient from node V_i to the destination D and E_{s2} is the transmitted symbol power in phase 2. $n_{i,D}$ is the additive white Gaussian noise at destination D from node i , with power spectral density, N_0 . More specifically, the received signal at the destination D can be written as,

$$y_{i,D} = \frac{\sqrt{E_{s1} E_{s2}}}{\sqrt{E_{s1} |\beta_{i,j}|^2 + N_0}} \alpha_{i,D} \beta_{i,j} v_i + n'_{i,D}, \quad (3.11)$$

where

$$n'_{i,D} = \frac{\sqrt{E_{s2}}}{\sqrt{E_{s1}|\beta_{i,j}|^2 + N_0}} \alpha_{i,D} n_{i,j} + n_{i,D}. \quad (3.12)$$

Since the noise terms $n_{i,j}$ and $n_{i,D}$ can be assumed independent, then the equivalent noise $n'_{i,D}$ is a zero-mean complex Gaussian random variable with variance given as

$$N'_0 = \left(\frac{E_{s2}|\alpha_{i,D}|^2}{E_{s1}|\beta_{i,j}|^2 + N_0} + 1 \right) N_0. \quad (3.13)$$

3.3.5 Fusion at the Base Station

The information from each cooperation group is received at the base station, decoded, and combined at the fusion center. Each packet contains its sensor ID and cooperation group ID as well as the observed information. Each node sends its own as well as the observation from all other sensors in its cooperation group to the BS in a combined packet. A majority rule decision is made on the observations after collecting the received information from each sensor in the cooperation group. This helps increase the probability of correct decision at the BS even in bad channel conditions. This is illustrated with the help of an example in Table 3.1, where j is the index of the cooperating node whose information is received from the sensor s_i . Here, O, C, W, and D represent OK, Caution, Warning, and Danger, respectively. A final result $R(j)$ is obtained based on majority rule as shown in Table 3.1. A majority vote decision, which consists of votes from sensors in the cooperation group \mathcal{V} , can be mathematically represented as follows,

$$R(j) = \arg \max_X \sum_{i=1}^{\mathcal{G}} w_i I(s_i(j) = X), \quad (3.14)$$

Table 3.1: Data Fusion at the Base Station

$j \backslash s_i$	s_1	s_2	s_3	s_4	s_5	s_6	s_7	$R(j)$
1	D	O	O	O	C	C	W	O
2	C	C	W	W	W	W	D	W
3	O	O	C	C	C	C	C	C
4	W	W	D	D	D	D	D	D
5	D	D	W	C	W	C	C	C
6	O	C	W	W	W	W	W	W
7	W	W	C	C	C	W	O	C

where $s_i(j)$ is the j th cooperative symbol received from a sensor s_i with the information X . $I(\cdot)$ is an indicator function given as, $I(x) = \begin{cases} 1 & x \text{ is true} \\ 0 & x \text{ is false} \end{cases}$. For example, in the case of alarm information, $X = \{O, C, W, D\}$. Therefore, $I(x)$ will be true if the received information $s_i(j)$ is equal to one of O, C, W, or D, otherwise it will be false. w_i is the weight associated with each sensor's information. In this work, the channels are assumed to have equivalent average magnitude, therefore the weights are set to $1/\mathcal{G}$. Note that, if the weights w_i are set to $1/\mathcal{G}$, (3.14) results in the mode of $s_1, s_2, s_3, \dots, s_{\mathcal{G}}$. In the case of a tie between observations, as in row 7 of Table 3.1, the algorithm selects the smallest of the tied value, i.e., C in this case.

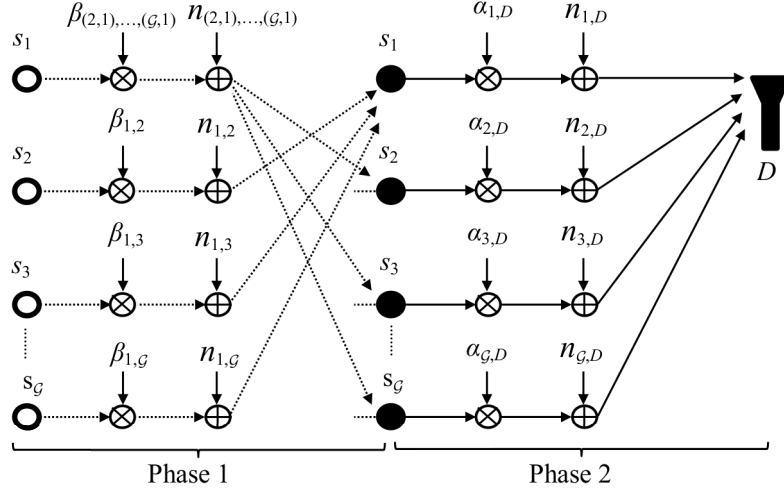


Figure 3.8: The proposed two-phase communication system. In Phase 1, sensor s_1 in the cooperation group sends its information to all other sensors during its time slot. Similarly, all the other sensors send their information to s_1 during their allocated time slots. In Phase 2, the sensors then make a cooperative packet and send it to the destination, D .

3.4 Performance Analysis

3.4.1 Symbol Error Rate

Fig. 3.8 shows the proposed dual-hop multiple-branch communication system where each relay has multiple branch inputs and a single branch output, each working in an orthogonal manner based on TDMA. AF scheme is used at the relays in order to repeat the symbols for the neighbor nodes. The resulting symbol-error rate (SER) can be approximated as stated in the following theorem.

Theorem 3.4.1. *If all of the channel links of the proposed multi-hop multi-branch*

cooperative system are known, the SER of a sensor node i at the destination D in the proposed system, can be tightly approximated as,

$$P_s(\gamma_{eq,i,D}) = F \left(1 + \frac{g_{PSK}}{N'_0 \sin^2 \theta} \left(\frac{\sigma_{i,D}^2 \prod_{j=1}^{G-1} \sigma_{i,j}^2}{\prod_{j=1}^{G-1} \sigma_{i,j}^2 + \sigma_{i,D}^2 + 1} \right) \right), \quad (3.15)$$

where $F(x(\theta)) = \frac{1}{\pi} \int_0^{(M-1)\pi/M} \frac{1}{x(\theta)} d\theta$, M is the modulation symbol size, $g_{PSK} = \sin^2(\pi/M)$, $\gamma_{eq,i,D}$ represents the instantaneous SNR per relay node at the destination, and $\sigma_{i,j}^2$, $\sigma_{i,D}^2$ are the variances of the Rayleigh fading channel coefficients $\beta_{i,j}$ and $\alpha_{i,D}$, respectively.

Proof. In order to find the SNR at the destination D , we need to calculate the signal power and noise power components at the destination. The signal power for a single link is $(\beta_{1,j}^2 \zeta_{1,j}^2) (\alpha_{1,D}^2)$. Since, each node sends independent information, we take average to approximate the received signal power for each node at the destination. The signal power received from i th relay node is given as,

$$\begin{aligned} SP_i &= [(\beta_{i,1}^2 \zeta_{i,1}^2) \times (\beta_{i,2}^2 \zeta_{i,2}^2) \times (\beta_{i,3}^2 \zeta_{i,3}^2) \times \dots \times (\beta_{i,G-1}^2 \zeta_{i,G-1}^2)] (\alpha_{i,D}^2) \\ &= \alpha_{i,D}^2 \prod_{j=1}^{G-1} \beta_{i,j}^2 \zeta_{i,j}^2. \end{aligned} \quad (3.16)$$

Similarly, the noise power for a single link is $(N_{0,1,j} \zeta_{1,j}^2) (\alpha_{1,D}^2) + N_{0,1,D}$. The total noise power at the destination can be calculated as follows,

$$\begin{aligned} NP_i &= [(N_{0,i,1} \zeta_{i,1}^2) \times (N_{0,i,2} \zeta_{i,2}^2) \times (N_{0,i,3} \zeta_{i,3}^2) \times \dots \times (N_{0,i,G-1} \zeta_{i,G-1}^2)] (\alpha_{i,D}^2) + N_{0,i,D} \\ &= N_{0,i,D} + \alpha_{i,D}^2 \prod_{j=1}^{G-1} N_{0,i,j} \zeta_{i,j}^2. \end{aligned} \quad (3.17)$$

The equivalent SNR at the destination, $\gamma_{eq,i,D}$ with respect to the relay node i can then

be calculated by dividing the signal power with noise power as follows,

$$\gamma_{eq,i,D} = \frac{\alpha_{i,D}^2 \prod_{j=1}^{\mathcal{G}-1} \beta_{i,j}^2 \zeta_{i,j}^2}{N_{0,i,D} + \alpha_{i,D}^2 \prod_{j=1}^{\mathcal{G}-1} N_{0,i,j} \zeta_{i,j}^2}. \quad (3.18)$$

Dividing the numerator and the denominator by $N_{0,i,D} \prod_{j=1}^{\mathcal{G}-1} N_{0,i,j} \zeta_{i,j}^2$, (3.18) is simplified as follows,

$$\text{Numerator} = \gamma_{i,D} \prod_{j=1}^{\mathcal{G}-1} \gamma_{i,j}, \quad (3.19)$$

$$\text{Denominator} = \frac{1}{\prod_{j=1}^{\mathcal{G}-1} N_{0,i,j} \zeta_{i,j}^2} + \frac{\alpha_{i,D}^2}{N_{0,i,D}}. \quad (3.20)$$

Putting $\zeta_{i,j} = \frac{1}{\sqrt{E_{s1}|\beta_{i,j}|^2 + N_{0,i,j}}}$ in (3.20), we get the following,

$$\text{Denominator} = \prod_{j=1}^{\mathcal{G}-1} \gamma_{i,j} + \gamma_{i,D} + 1. \quad (3.21)$$

Therefore, the equivalent SNR at the destination D with respect to a sensor node i , is given as,

$$\gamma_{eq,i,D} = \frac{\gamma_{i,D} \prod_{j=1}^{\mathcal{G}-1} \gamma_{i,j}}{\prod_{j=1}^{\mathcal{G}-1} \gamma_{i,j} + \gamma_{i,D} + 1}. \quad (3.22)$$

The SER formulation for the proposed system with M -PSK modulation, and conditioned upon known channel coefficients is given as [97],

$$\begin{aligned} P_s(\gamma_{eq,i,D}) &= \frac{1}{\pi} \int_0^{(M-1)\pi/M} e^{-\frac{g_{PSK} \gamma_{eq,i,D}}{\sin^2 \theta}} d\theta \\ &= \frac{1}{\pi} \int_0^{(M-1)\pi/M} e^{-\frac{g_{PSK}}{\sin^2 \theta} \left(\frac{\gamma_{i,D} \prod_{j=1}^{\mathcal{G}-1} \gamma_{i,j}}{\prod_{j=1}^{\mathcal{G}-1} \gamma_{i,j} + \gamma_{i,D} + 1} \right)} d\theta. \end{aligned} \quad (3.23)$$

Since, each hop in the multi-hop multi-branch communication experiences independent fading and,

$$\int_0^\infty e^{\left(-\frac{g_{PSK} E_s \mathcal{Z}}{N_0 \sin^2 \theta}\right)} p_{|h|^2}(\mathcal{Z}) d\mathcal{Z} = \frac{1}{1 + \frac{g_{PSK} E_s \sigma_h^2}{N_0 \sin^2 \theta}}, \quad (3.24)$$

where h is the corresponding fading channel coefficient [98]. Therefore, we can write

$P_s(\gamma_{eq,i,D})$ as,

$$P_s(\gamma_{eq,i,D}) = F \left(1 + \frac{g_{PSK}}{N_0' \sin^2 \theta} \left(\frac{\sigma_{i,D}^2 \prod_{j=1}^{\mathcal{G}-1} \sigma_{i,j}^2}{\prod_{j=1}^{\mathcal{G}-1} \sigma_{i,j}^2 + \sigma_{i,D}^2 + 1} \right) \right), \quad (3.25)$$

where $F(x(\theta)) = \frac{1}{\pi} \int_0^{(M-1)\pi/M} \frac{1}{x(\theta)} d\theta$. ■

Since, we use the majority voting rule in the fusion process, to decide a final outcome. Therefore, the probability of error, in the result after fusion, can be computed by using the Binomial theorem. Let, P_s , be the probability that the information sent by a sensor has error, and $l = \lceil \frac{\mathcal{G}+1}{2} \rceil$ be the minimum number of votes needed for majority, then the probability of error in the consensus is given as,

$$P_e(\mathcal{G}) = \sum_{m=l}^{\mathcal{G}} \binom{\mathcal{G}}{m} P_s^m (1 - P_s)^{\mathcal{G}-m} \quad (3.26)$$

With (3.26), we expect to obtain a diversity order of l in the final SER of the proposed system.

3.4.2 Latency and Energy Consumption

In this subsection, we aim to compare the non-cooperative and cooperative schemes in terms of latency and energy consumption of the network. For the sake of a fair

comparison, we assume a traditional dual-hop communication scheme for the non-cooperative mechanism, in which each node's data is forwarded by a relay node in the second hop towards the BS without any cooperative mechanism. Let B represent the number of bits per symbol, and the symbol duration is given by $T_s = 1/f_s$, where f_s is the symbol rate. Then, the throughput in case of non-cooperative (T_{nc}) and cooperative (T_c) dual-hop communication is given as,

$$\begin{aligned} T_{nc} &= \frac{\mathcal{G}B}{\mathcal{G}T_s + \mathcal{G}T_s} \text{ bps} \\ T_c &= \frac{\mathcal{G}B}{\mathcal{G}T_s + \mathcal{G}\mathcal{G}T_s} \text{ bps} \end{aligned}, \quad (3.27)$$

where the addition in denominator represents the time taken by two hops to transmit the symbol to BS. The additional \mathcal{G} in the denominator for T_c comes from the fact that each node relays the data of \mathcal{G} nodes in the second phase. The time taken by \mathcal{G} nodes to transmit \mathcal{G} packets to the BS in the case of non-cooperative (\mathcal{D}_{nc}) and cooperative (\mathcal{D}_c) scheme is then computed as,

$$\begin{aligned} \mathcal{D}_{nc} &= \frac{\mathcal{G} \times \text{size of data packet (bits)}}{T_{nc} \text{ (bps)}} \\ \mathcal{D}_c &= \frac{\mathcal{G} \times \text{size of data packet (bits)}}{T_c \text{ (bps)}} \end{aligned}. \quad (3.28)$$

Using $T_s = 50 \mu s$ [99], the time delay given by (3.28) is plotted in Fig. 3.9(a).

In order to compute the energy consumption, let E_t , E_i , E_r , and E_f represent the energy consumed by the transmit operation by a sensor, idle listening, reception at a sensor node/BS, and fusion operation, respectively. In the case of non-cooperative dual-hop communication, each node transmits with energy E_t in phase 1 and the other $\mathcal{G} - 1$ nodes receive this information with energy E_r . This process is repeated \mathcal{G} times. In phase 2, each node transmits with energy E_t to the BS while the other $\mathcal{G} - 1$ nodes

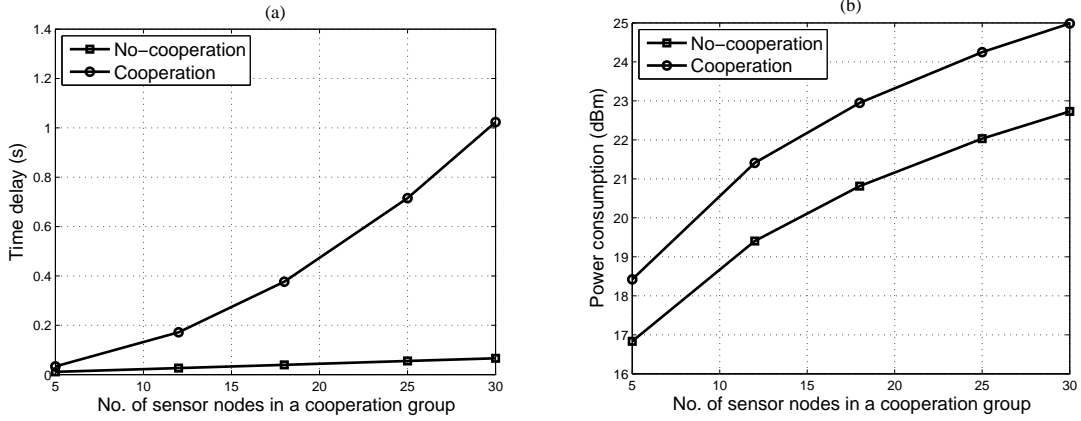


Figure 3.9: Results of (3.28), (3.29), and (3.30). (a) Time delay for packet delivery. (b) Energy consumption of the network.

remain idle, and the BS receives each node's data with energy E_r . Thus the total energy consumed (\mathcal{E}_{nc}) is given as,

$$\mathcal{E}_{nc} = \mathcal{G} (E_t + (\mathcal{G} - 1) E_r) + \mathcal{G} (E_t + (\mathcal{G} - 1) E_i + E_r). \quad (3.29)$$

In the case of the proposed cooperative dual-hop communication, the total energy consumed (\mathcal{E}_c) is given as,

$$\mathcal{E}_c = \mathcal{G} (E_t + (\mathcal{G} - 1) E_r) + \mathcal{G} (E_t + (\mathcal{G} - 1) E_i + E_r) + \mathcal{G}^2 E_f, \quad (3.30)$$

where E_f is the additional energy spent in fusion at the BS and \mathcal{G}^2 represent the number of multiply-and-accumulate operations performed to compute the fusion result for \mathcal{G} cooperative packets each containing \mathcal{G} number of observations given in (3.14).

Using $E_t = 31.6$ mW, $E_i = 2.8$ μ W, $E_r = 17.4$ mW [100], and $E_f = 13.3$ mW [101], the results of (3.29) and (3.30) are plotted in Fig. 3.9.

Fig. 3.9(a) shows that the time required transmitting a certain amount of data to

Table 3.2: FAR and PDR Comparison

Performance	[10]	[91]	[92]	[93]	[38]	This Work
Metrics						
FAR	—	—	—	3.8%	10.5%	1.8%
PDR	~70%	~73%	~84%	—	—	~86%

the BS increases in the case of our proposed cooperation scheme. But the given delay is still acceptable as it is 336 ms for $\mathcal{G} = 18$ and can go up to 957 ms for $\mathcal{G} = 30$. This amount of delay is not very critical and can be accepted in return for improved robustness and reliability. Fig. 3.9(b) shows that the cooperation mechanism increases the amount of energy consumption by about 2 dB for $\mathcal{G} = 12$ and remains below 3 dB for $\mathcal{G} = 30$. This increase in the energy consumption is easily offset by the gain in SNR which is achieved by our proposed scheme, and will be explained in Section 3.5.

3.4.3 Comparison with Related Works

The false alarm rate (FAR) and packet delivery rate (PDR) metrics are used to compare our results with some of the previous works mentioned in Section 3.1. The FAR and PDR for our work was calculated and averaged over a range of SNR (0 to 30 dB) and a total of 12,000 packets. In order to make a fair comparison, we use the PDR reported by [10] for IWSN and the PDR reported by [91], when no relay selection mechanism is used. As shown in Table 3.2, our work shows a significant improvement in the FAR as compared to [93] and [38]. The PDR of our scheme is higher than that of [92] and is significantly higher than [10] and [91]. For improving the PDR, these

Table 3.3: Simulation Parameters

Parameter	Value
Total area, P_{AREA}	$100\text{ m} \times 100\text{ m}$
No. of cooperation nodes, \mathcal{G}	12
Carrier frequency	2.4 GHz (ISM Band)
Transmit power, E_{s1}, E_{s2}	1 mW
Standard deviation, σ	7 (Indoor NLOS)
Path-loss exponent, σ	3 (Indoor NLOS)
Sensing radius of each sensor, r	18 m

works involve a significant overhead of retransmission, guide-path discovery, and relay selection mechanism, respectively. In contrast, our work does not involve guide-path discovery, relay selection, and retransmission overhead but still gives a higher PDR and very low FAR.

3.5 Simulation Results

We assume an indoor communication environment of $100\text{ m} \times 100\text{ m}$ with hard-partitioned rooms. Some machines are scattered inside this area that generate some kind of radiation information i.e., temperature. Suppose that a higher temperature at a certain location represents a fault in the operation or state of the machine at that location. We model this information over the entire area as a Gaussian random field. The field varies from high temperature to low, which generates four different kinds of alarms i.e., Danger, Warning, Caution, and OK, respectively. We assume the destination location at the edge of the area under consideration, and the nodes deployed

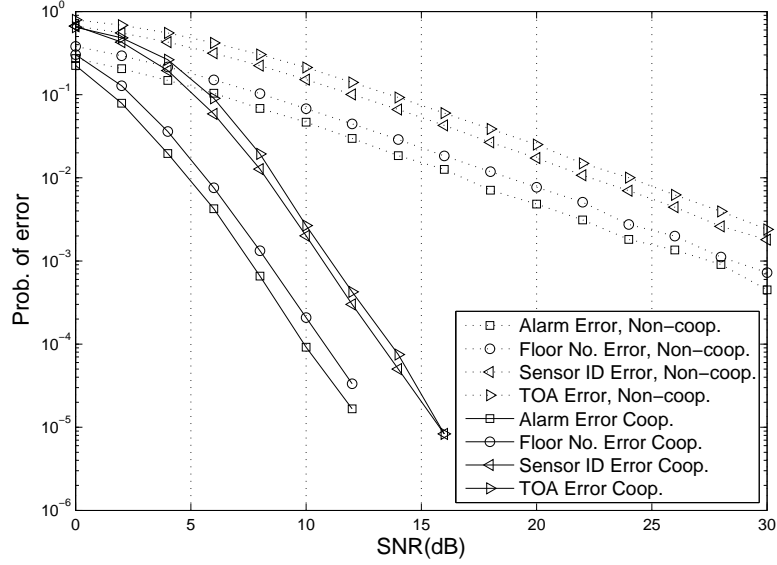


Figure 3.10: Simulation results for 12-node cooperation group, showing the probability of error in different parts of the received packet at the BS.

according to the scheme discussed in Section 3.2.1. The results are averaged over 20,000 sensing operations and compare our proposed scheme with that of a non-cooperative dual-hop communication. The simulation parameters used in this experiment are given in Table 3.3.

Fig. 3.10 shows the probability of error for the alarms generated at the BS, floor number, sensor ID, and TOA for 12-node cooperation. We can see a clear advantage by using the proposed cooperation schemes, which achieves, on average, 10^{-3} probability of error at almost 20 dB lower SNR compared with the non-cooperative scheme. By taking into account the 2 dB increase in the cooperative transmission to the BS for $\mathcal{G} = 12$, we can still get ~ 18 dB savings in the SNR as compared to the traditional dual-hop transmission without cooperation.

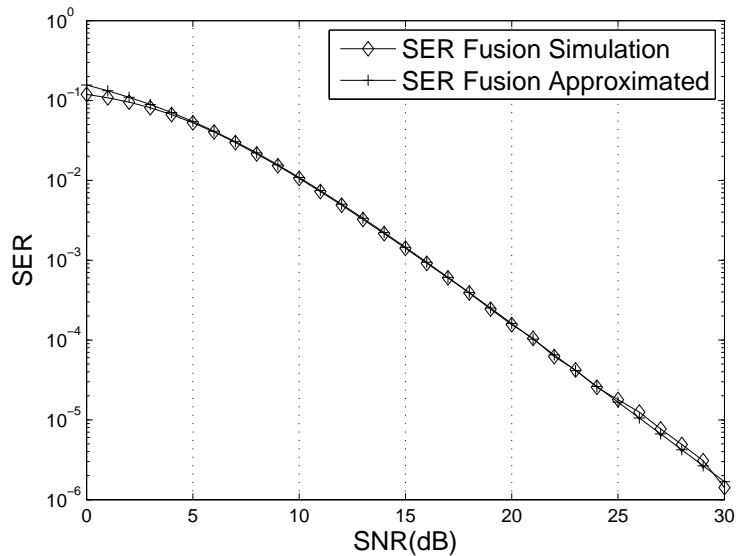


Figure 3.11: Comparison of simulation result after fusion at the BS and the approximated SER given in (3.26).

Fig. 3.11 shows the numerical result obtained in (3.26) for the SER of a cooperation group of 3 nodes, using majority vote fusion scheme at the BS compared with the simulated result. We can see that the approximated result matches that of simulation, especially at high SNR. The result also verifies that our proposed cooperation and fusion scheme is able to achieve the full diversity order of $l = 2$ here.

3.6 Conclusion

In this work, we have proposed a relay based dual-hop cooperative WSN to monitor the state of an indoor industrial environment. By applying the proposed cooperation scheme, we obtain a much better performance in terms of SER and achieve a highly accurate decision at the base station. The packet overhead and energy consumption is

reduced by combining a limited number of sensors' data into one packet for transmission. The energy saving provided by the proposed scheme is almost 18 dB, which is very significant for the harsh indoor industrial environment. The proposed cooperation protocol is robust to communication link failures and adapts to changing link conditions in the wireless channel. We also derived a closed-form solution for the SER of the proposed scheme, which verifies the diversity benefit of the scheme.

Chapter 4

Cooperative Relaying Using Cluster Heads

In Chapter 3, the proposed solution uses full repetition mechanism at the relay nodes to relay the cooperative packets to the BS. An obvious drawback of this method is increased power consumption, increased latency, and an unnecessary increase in the redundancy required for reliable transmission of information to the BS. Therefore, in this chapter, we propose a modification to the previous work by introducing cluster heads in the cooperation groups. In this way, the increase in power consumption and latency can be controlled to a certain limit, and the extra redundancy which resulted in the case of full repetition scheme is eliminated up to a desired limit.

4.1 Background and Contributions of this Work

The amount of data transmitted by the network nodes and the required processing at the receiver contributes towards the energy consumption per bit of the network. Since cooperation among nodes can lead to an increase in the data transmitted within the network, data aggregation at the intermediate nodes is an important factor of cooperative multi-hop communication system. Since all the packets are addressed to a single destination and the size of data packets is usually small, therefore, a reduction in the size of control packet overhead and the number of transmission packets, can improve the energy efficiency, and throughput, of the system [13], [102], and [103]. In

our previous work [44], we have used the concept of in-network data aggregation and cooperation to improve the reliability in the received information at the base station (BS). However, [44] uses repetition of the aggregated data transmission at every node in the cooperation group, which results in some unnecessary redundancy and thus leads to a much more reduced throughput that may be critical to the performance of the network.

In this work, we propose an improvement to our previous work [44] by using cluster heads which helps in reducing the amount of transmissions required to transmit the same information to the BS and also reduces the latency at the expense of some reduction in performance. The proposed system is a two-phase user cooperation scheme for WSNs in indoor environment that has heavy machinery and harsh wireless characteristics. In the first phase, all the sensors in a cooperation group share their information with the cluster heads, unlike [15], [56], and [64] in which the data is received at the BS in the first phase as well. In the second phase, the cooperative information is sent to the BS by a selected number of cluster head (CH) nodes, unlike [44] in which each node in the cooperation group sends the aggregated information to the BS. Also, different from the relay mechanisms in [15], [56], and [64], we use the received data at the relay without regard to it being correctly received or not. The relays only detect the received symbols and do not need to decode the symbols, rather use these symbols in the cooperation phase even if not correctly received. Also, our proposed scheme does not involve the extra overhead of retransmission in order to ensure successful packet delivery, unlike [91] and [10]. This simplifies the hardware and signal processing requirements of

the relay node. This work combines the data aggregation and cooperation mechanism to improve the reliability of the received information at the BS as well as keep the redundancy overhead to a certain limit in order to perform at a low-latency. In this work, we also propose a modification to the OOP protocol (Chapter 3) for the operation of the cooperative IWSN.

4.2 Network Design

The general network scenario remains the same as explained in Chapter 3. A floor of a factory building or area of interest is covered by N number of nodes, as shown in Fig. 3.2(b). Each node sends four types of information to the base station as shown in Fig. 3.3. All this information from each sensor is combined at the base station to arrive at a single result on the state of the area covered by those sensors. Sensor deployment is done according to the scheme in Section 3.2.1, and the indoor factory area wireless channel was explained in Section 3.2.4.

4.2.1 Organize and Operate Protocol with Cluster Heads (OOP-CH)

The network consists of cooperation groups that communicate with the destination in a dual-hop manner. Each node in a cooperation group schedules its communication link in collaboration with other nodes in the group. Every node in a group is assumed to be able to communicate with a minimum number (6 to 20) of neighbor nodes. This neighbor list is maintained by keeping the source address of these nodes which is broadcasted by using a control channel. A node will decode the information received

only from the nodes in the neighbor list and discard the rest. The cooperation groups are updated periodically depending on the application and conditions of the sensor nodes. This operation is controlled by the BS by initiating the organization operation of the network. After the organization stage, the usual sensing and reporting operations continue until the next organization process.

In the Organize and Operate Protocol with Cluster Heads (OOP-CH), described in Fig. 4.1, the BS sends an “Organize” message to all the nodes in the network, indicating to organize themselves in cooperation groups. Upon receiving this message, the nodes stop Tx/Rx operations and update their list of neighbor nodes, and then update their status to “Organized”. After all the nodes are organized in groups, the BS chooses a predefined number of CH nodes based on the received signal strength information (RSSI). Note that, since we use a majority voting-based fusion technique at the BS, therefore, a certain amount of redundancy in the data received at the BS is necessary. The minimum number of CH nodes required to perform majority vote-based fusion at the BS is 3, however, choosing 3 CH nodes does not show significant improvement in the probability of error in the received information at the BS (results not shown here). In this work, we choose the number of CH nodes to be 5 and we show with the help of simulations that this number may be good enough for cooperation groups of small to medium sizes. After CH nodes are notified, the BS then sends “Operate” message to the nodes indicating to start normal sense and transmit operations. The nodes in a cooperation group then share their sensed information with the neighboring CH nodes. After receiving messages from all the nodes in the cooperation group, each CH node

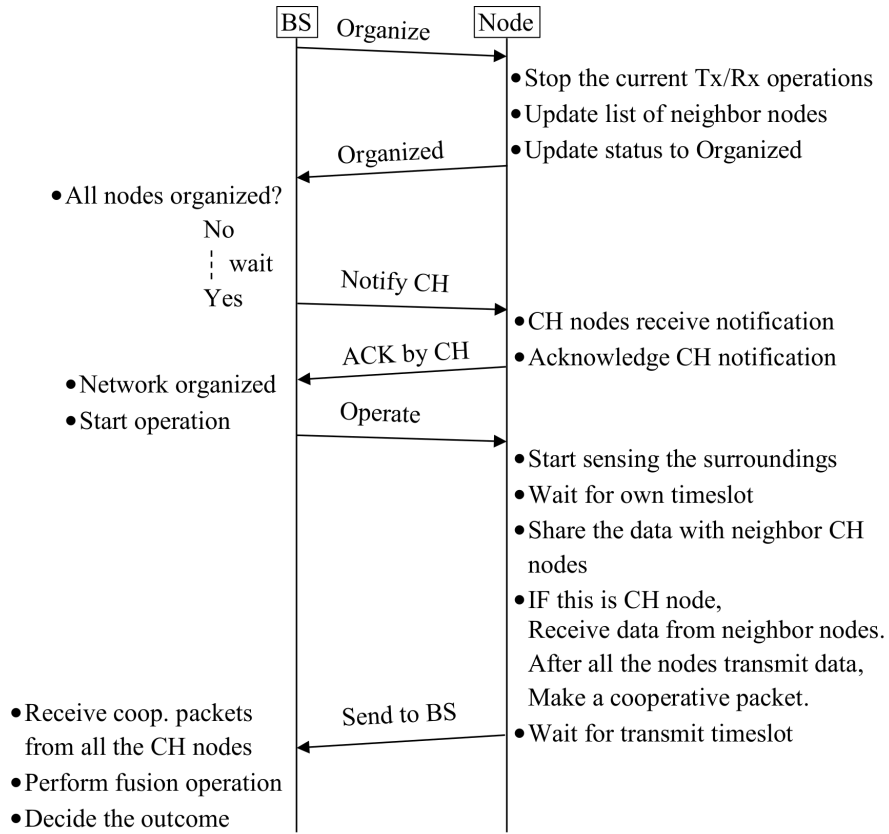


Figure 4.1: The proposed organize and operate protocol with cluster heads (OOP-CH) for WSN.

makes a cooperative data packet and transmits it to the BS in its own timeslot. The BS, upon receiving the cooperative packets from all the CH nodes in the cooperation group, performs majority voting-based fusion operation and decides the outcome of the received information from the sensor nodes.

4.2.2 Cooperative Communication

As before, the wireless nodes are organized in cooperation groups, but in this work, we choose a limited number (5) of nodes to act as cluster heads in order to perform

cooperation in transmitting the information to the BS. In this subsection, we only point out the modifications in cooperative communication to the BS from that explained in Section 3.3.4.

Phase 1

In phase 1, after sensing the information from its surrounding area, each sensor in the cooperation group shares this information with the CH nodes in its neighbor list, instead of all the nodes in the cooperation group.

Phase 2

In phase 2, each CH node makes a cooperative data packet by combining the information received from the cooperating nodes within its cooperation group, during the first phase. The amplify-and-forward (AF) relaying mechanism is used at the relays. Upon its turn, each CH node transmits the cooperative data packet to the BS in a TDMA manner.

4.2.3 Fusion at the Base Station

The information from each cooperation group is received at the base station, decoded, and combined at the fusion center. Each packet contains its sensor ID and cooperation group ID as well as the observed information. Each CH node sends its own observation as well as that from all other sensors in its cooperation group in an aggregated packet to the BS. A majority rule decision is made on the observations after collecting the received information from each CH node in the cooperation group.

This helps increase the probability of correct decision at the BS even in bad channel conditions. A majority vote decision, which consists of votes from CH nodes in the cooperation group \mathcal{V} , can be mathematically represented as follows,

$$R(j) = \arg \max_X \sum_{i=1}^{\mathcal{C}} w_i I(s_i(j) = X), \quad (4.1)$$

where $y_i(j)$ is the j th cooperative symbol received from a sensor i , w_i is the weight associated with each sensor's information, and $I(\cdot)$ is an indicator function. If the weights are set to $1/\mathcal{C}$, Eq. (4.1) gives the mode of $y_1, y_2, y_3, \dots, y_{\mathcal{C}}$. In our experiments, we set the weights w_i to $1/\mathcal{C}$ because the channels are assumed to have equivalent average magnitude and $\mathcal{C} = 5$ as the number of CH nodes is chosen to be 5.

We illustrate the fusion mechanism with the help of an example. Let O represent OK, C represent Caution, W represent Warning, and D represent Danger and j is the index of the cooperating node whose information is received from the CH node i . The fusion mechanism is shown in Table 4.1, which shows a cooperation group of 8 sensor nodes with 5 CH nodes communicating to the base station in a cooperative manner. $R(j)$ shows the final result about the sensed information by each sensor, after fusion. When there is a tie in votes, as in row 8 of Table 4.1, the algorithm selects the smallest of the tied values, i.e., O in this case.

4.3 Performance Analysis

4.3.1 Symbol Error Rate

The proposed system is a dual-hop multiple-branch communication system, as shown in Fig. 4.2. Each relay has multiple branch inputs and repeats the symbols

Table 4.1: Data Fusion at the Base Station

$j \backslash s_i$	s_i					$R(j)$
	s_1	s_2	s_3	s_4	s_5	
1	D	O	D	D	C	D
2	C	C	W	C	W	C
3	O	O	W	W	W	W
4	W	O	O	O	D	O
5	C	D	C	C	C	C
6	W	W	C	W	W	W
7	D	D	D	W	D	D
8	O	C	O	W	C	O

for its neighbor nodes, in a single branch output by using AF scheme, in an orthogonal manner based on TDMA. The resulting SER can be approximated as stated in the following theorem.

Theorem 4.3.1. *If all of the channel links of the proposed multi-hop multi-branch cooperative system are known, the SER of a sensor node i at the destination D in the proposed system, can be tightly approximated as,*

$$P_s(\gamma_{eq,i,D}) = F \left(1 + \frac{g_{PSK}}{N'_0 \sin^2 \theta} \left(\frac{\sigma_{i,D}^2 \prod_{j=1}^{C-1} \sigma_{i,j}^2}{\prod_{j=1}^{C-1} \sigma_{i,j}^2 + \sigma_{i,D}^2 + 1} \right) \right), \quad (4.2)$$

where $F(x(\theta)) = \frac{1}{\pi} \int_0^{(M-1)\pi/M} \frac{1}{x(\theta)} d\theta$, M is the modulation symbol size, $g_{PSK} = \sin^2(\pi/M)$, $\gamma_{eq,i,D}$ represents the instantaneous SNR per relay node at the destination, and $\sigma_{i,j}^2$, $\sigma_{i,D}^2$ are the variances of the Rayleigh fading channel coefficients $\beta_{i,j}$ and $\alpha_{i,D}$, respectively.

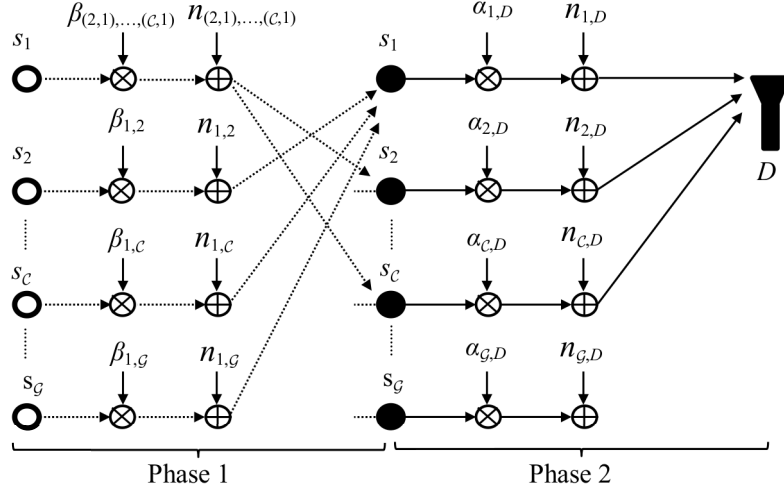


Figure 4.2: The proposed two-phase communication system. In Phase 1, sensor s_1 in the cooperation group sends its information to all CH sensors during its time slot. Similarly, all the other sensors send their information to CH sensors during their allocated time slots. In Phase 2, only the CH sensors then make a cooperative packet and send it to the destination, D .

Proof. The signal power and noise power components at the destination D , can be used to find the SNR. The signal power for a single link is $(\beta_{1,j}^2 \zeta_{1,j}^2) (\alpha_{1,D}^2)$. To approximate the received signal power, we take its average at the destination, because each node sends independent information. The signal power received from i th relay node is given as,

$$\begin{aligned} \text{SP}_i &= [(\beta_{i,1}^2 \zeta_{i,1}^2) \times (\beta_{i,2}^2 \zeta_{i,2}^2) \times (\beta_{i,3}^2 \zeta_{i,3}^2) \times \dots \times (\beta_{i,c-1}^2 \zeta_{i,c-1}^2)] (\alpha_{i,D}^2) \\ &= \alpha_{i,D}^2 \prod_{j=1}^{c-1} \beta_{i,j}^2 \zeta_{i,j}^2. \end{aligned} \quad (4.3)$$

The noise power for a single link is $(N_{0,1,j} \zeta_{1,j}^2) (\alpha_{1,D}^2) + N_{0,1,D}$. The total noise power

at the destination from i th relay node can be calculated as follows,

$$\begin{aligned} \text{NP}_i &= [(N_{0,i,1}\zeta_{i,1}^2) \times (N_{0,i,2}\zeta_{i,2}^2) \times (N_{0,i,3}\zeta_{i,3}^2) \times \dots \times (N_{0,i,C-1}\zeta_{i,C-1}^2)] (\alpha_{i,D}^2) + N_{0,i,D} \\ &= N_{0,i,D} + \alpha_{i,D}^2 \prod_{j=1}^{C-1} N_{0,i,j}\zeta_{i,j}^2. \end{aligned} \quad (4.4)$$

The equivalent SNR at the destination, $\gamma_{eq,i,D}$ with respect to the relay node i can then be calculated by dividing SP with NP. After dividing the numerator and the denominator by $N_{0,i,D} \prod_{j=1}^{C-1} N_{0,i,j}\zeta_{i,j}^2$, and putting $\zeta_{i,j} = \frac{1}{\sqrt{E_s 1|\beta_{i,j}|^2 + N_{0,i,j}}}$ in the denominator, the equivalent SNR at the destination D with respect to a sensor node i , is given as,

$$\gamma_{eq,i,D} = \frac{\gamma_{i,D} \prod_{j=1}^{C-1} \gamma_{i,j}}{\prod_{j=1}^{C-1} \gamma_{i,j} + \gamma_{i,D} + 1}. \quad (4.5)$$

The SER formulation for the proposed system with M -PSK modulation, and conditioned upon known channel coefficients is given as [97],

$$\begin{aligned} P_s(\gamma_{eq,i,D}) &= \frac{1}{\pi} \int_0^{(M-1)\pi/M} e^{-\frac{g_{PSK}\gamma_{eq,i,D}}{\sin^2\theta}} d\theta \\ &= \frac{1}{\pi} \int_0^{(M-1)\pi/M} e^{-\frac{g_{PSK}}{\sin^2\theta} \left(\frac{\gamma_{i,D} \prod_{j=1}^{C-1} \gamma_{i,j}}{\prod_{j=1}^{C-1} \gamma_{i,j} + \gamma_{i,D} + 1} \right)} d\theta. \end{aligned} \quad (4.6)$$

Since, each hop in the multi-hop multi-branch communication experiences independent fading and,

$$\int_0^\infty e^{-\frac{g_{PSK}E_s\mathcal{Z}}{N_0\sin^2\theta}} p_{|h|^2}(\mathcal{Z})d\mathcal{Z} = \frac{1}{1 + \frac{g_{PSK}E_s\sigma_h^2}{N_0\sin^2\theta}}, \quad (4.7)$$

where h is the corresponding fading channel coefficient [98]. Therefore, we can write

$P_s(\gamma_{eq,i,D})$ as,

$$P_s(\gamma_{eq,i,D}) = F \left(1 + \frac{g_{PSK}}{N_0'\sin^2\theta} \left(\frac{\sigma_{i,D}^2 \prod_{j=1}^{C-1} \sigma_{i,j}^2}{\prod_{j=1}^{C-1} \sigma_{i,j}^2 + \sigma_{i,D}^2 + 1} \right) \right), \quad (4.8)$$

where $F(x(\theta)) = \frac{1}{\pi} \int_0^{(M-1)\pi/M} \frac{1}{x(\theta)} d\theta$. ■

From (4.2), P_s is the probability of error in the information received from a sensor. The minimum number of votes needed for majority is $l = \lceil \frac{C+1}{2} \rceil$. The probability of error in the consensus can then be computed by using the Binomial theorem,

$$P_e(C) = \sum_{m=l}^C \binom{C}{m} P_s^m (1 - P_s)^{C-m} \quad (4.9)$$

Fig. 4.3 shows the numerical result obtained in (4.9) for the SER of a cooperation group of 12 nodes with 5 CH nodes, compared with the simulated result. The simulation result shows an error floor beyond the SNR of 20 dB, because a limited number of nodes are used as relay nodes. However, our approximated result can be used to predict the performance of the proposed scheme before the error floor region appears.

4.3.2 Latency and Energy Consumption

For the sake of a fair comparison between non-cooperative and cooperative systems, we assume a traditional dual-hop communication scheme for the non-cooperative mechanism. In this scheme, a relay node forwards the data from a source node in the second hop towards the BS without any cooperative mechanism. Let B represent the number of bits per symbol, and the symbol duration is given by $T_s = 1/f_s$, where f_s is the symbol rate. Then, the throughput in case of non-cooperative (T_{nc}) and cooperative

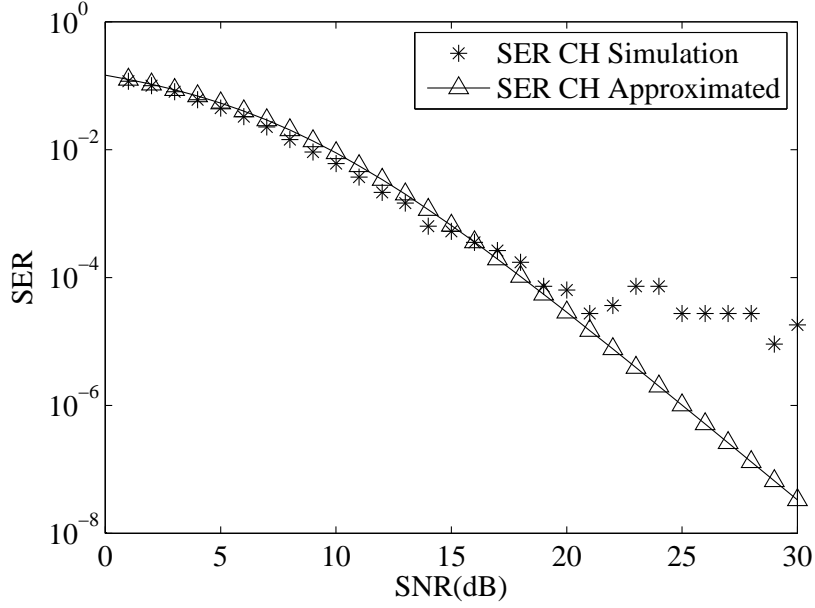


Figure 4.3: Comparison of CH simulation and the approximated result given in (4.9).

In this experiment, 5 CH nodes were chosen from a cooperation group of 12.

(T_c) dual-hop communication is given as,

$$\begin{aligned} T_{nc} &= \frac{\mathcal{G}B}{\mathcal{G}T_s + \mathcal{G}T_s} \text{ bps} \\ T_c &= \frac{\mathcal{G}B}{\mathcal{G}T_s + \mathcal{C}\mathcal{G}T_s} \text{ bps} \end{aligned}, \quad (4.10)$$

where the addition in denominator represents the time taken by two hops to transmit the symbol to BS. Since \mathcal{C} CH node relays the data of \mathcal{G} nodes in the second phase, it results in the additional \mathcal{C} in the denominator for T_c . The delay incurred in transmitting \mathcal{G} packets to the BS in the case of non-cooperative (\mathcal{D}_{nc}) and cooperative (\mathcal{D}_c) scheme is then computed as,

$$\begin{aligned} \mathcal{D}_{nc} &= \frac{\mathcal{G} \times \text{size of data packet (bits)}}{T_{nc} \text{ (bps)}} \\ \mathcal{D}_c &= \frac{\mathcal{G} \times \text{size of data packet (bits)}}{T_c \text{ (bps)}} \end{aligned}. \quad (4.11)$$

In order to compute the energy consumption, let E_t , E_i , E_r , and E_f represent the energy consumed by the transmit operation by a sensor, idle listening, reception at a sensor node/BS, and fusion operation, respectively. In the case of non-cooperative dual-hop communication, each node transmits with energy E_t in phase 1 and the other $\mathcal{G} - 1$ nodes receive this information with energy E_r . This process is repeated \mathcal{G} times. In phase 2, each node transmits with energy E_t to the BS while the other $\mathcal{G} - 1$ nodes remain idle, and the BS receives each node's data with energy E_r . Thus the total energy consumed (\mathcal{E}_{nc}) is given as,

$$\mathcal{E}_{nc} = \mathcal{G} (E_t + (\mathcal{G} - 1) E_r) + \mathcal{G} (E_t + (\mathcal{G} - 1) E_i + E_r). \quad (4.12)$$

In the case of the proposed cooperative dual-hop communication, the total energy consumed (\mathcal{E}_c) is given as,

$$\mathcal{E}_c = \mathcal{G} (E_t + (\mathcal{G} - 1) E_r) + \mathcal{C} (E_t + (\mathcal{G} - 1) E_i + E_r) + \mathcal{C}\mathcal{G}E_f, \quad (4.13)$$

where E_f is the additional energy spent in fusion at the BS and $\mathcal{C}\mathcal{G}$ represent the number of multiply-and-accumulate operations performed to compute the fusion result for \mathcal{C} cooperative packets each containing \mathcal{G} number of observations given in (4.1). Also, in the second term in (4.13), \mathcal{G} is replaced by \mathcal{C} as there are \mathcal{C} CH nodes transmitting to the BS instead of all the \mathcal{G} relay nodes.

Using $T_s = 50 \mu s$ [99], $E_t = 31.6 \text{ mW}$, $E_i = 2.8 \mu\text{W}$, $E_r = 17.4 \text{ mW}$ [100], and $E_f = 13.3 \text{ mW}$ [101], the results of (4.11), (4.12), and (4.13) are plotted in Fig. 4.4.

Fig. 4.4 shows the energy consumption and time delay results of our proposed CH cooperation scheme in comparison with the full repetition (F-Rep.) cooperation

in which each node transmits a cooperative packet in phase 2 to the BS, as in [44], and the relayed transmission in which each node's data is forwarded by a relay node towards the BS in the second hop without any cooperation mechanism. The results show that the time required transmitting a certain amount of data to the BS increases in the case of F-Rep. cooperation and CH cooperation. However, the increase in energy consumption is reduced from ~ 2 dB to ~ 0.5 dB for $\mathcal{G} = 12$ and from ~ 3 dB to ~ 0.2 dB when $\mathcal{G} = 30$, in the cases of CH cooperation and F-Rep. cooperation, respectively. Similarly, the time delay has been reduced from ~ 145 ms to ~ 53 ms for $\mathcal{G} = 12$ and from ~ 957 ms to ~ 132 ms when $\mathcal{G} = 30$, in the cases of F-Rep. cooperation and CH cooperation, respectively. This amount of delay and energy consumption is a further reduction from that reported in [44] and will be helpful in achieving the low-latency design goal of future communication systems. The increase in the energy consumption is easily offset by the gain in SNR, which is achieved by our proposed scheme, and will be shown in Section 4.4.

4.3.3 Comparison with Related Works

The false alarm rate (FAR) and packet delivery rate (PDR) metrics are used to compare our results with some of the previous works including our own [44]. The FAR and PDR for this work and in [44], were calculated and averaged over a range of SNR (0 to 30 dB) with a total of 12,000 packets. In order to make a fair comparison, we use the PDR reported by [91], when no relay selection mechanism is used, and the PDR reported by [10] for IWSN. As shown in Table 4.2, our work shows a significant

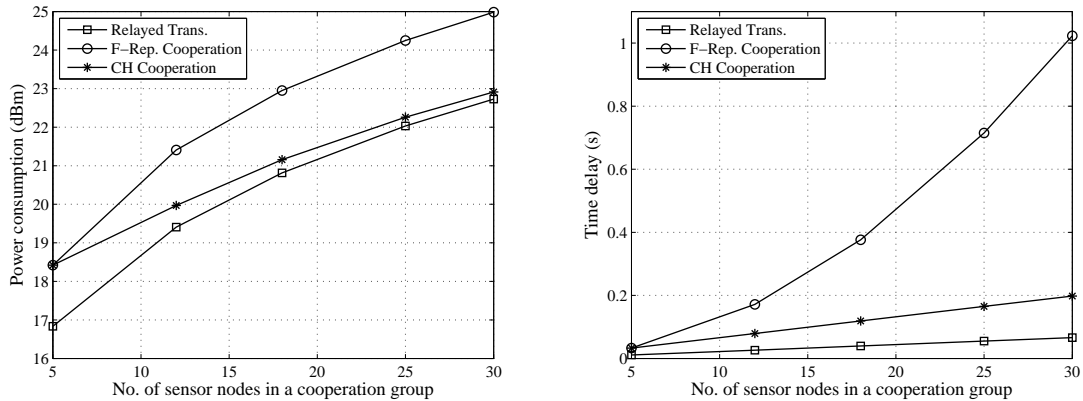


Figure 4.4: Comparison of non-cooperative and cooperative schemes in terms of power consumption and latency.

Table 4.2: FAR and PDR Comparison

Performance	[10]	[91]	[92]	[93]	[38]	[44]	This Work
Metrics							
FAR	—	—	—	3.8%	10.5%	1.8%	5.1%
PDR	~70%	~73%	~84%	—	—	~86%	~76%

improvement in the FAR as compared to [38], performs similar to [93] and shows increased FAR as compared to [44]. The PDR of our scheme is higher than that of [91] and [10] but lower than [92] and [44]. For improving the PDR, [10], [91], and [92] involve a significant overhead of retransmission, guide-path discovery, and relay selection mechanism, respectively. In contrast, our work does not involve these overheads and still gives a higher PDR and very low FAR.

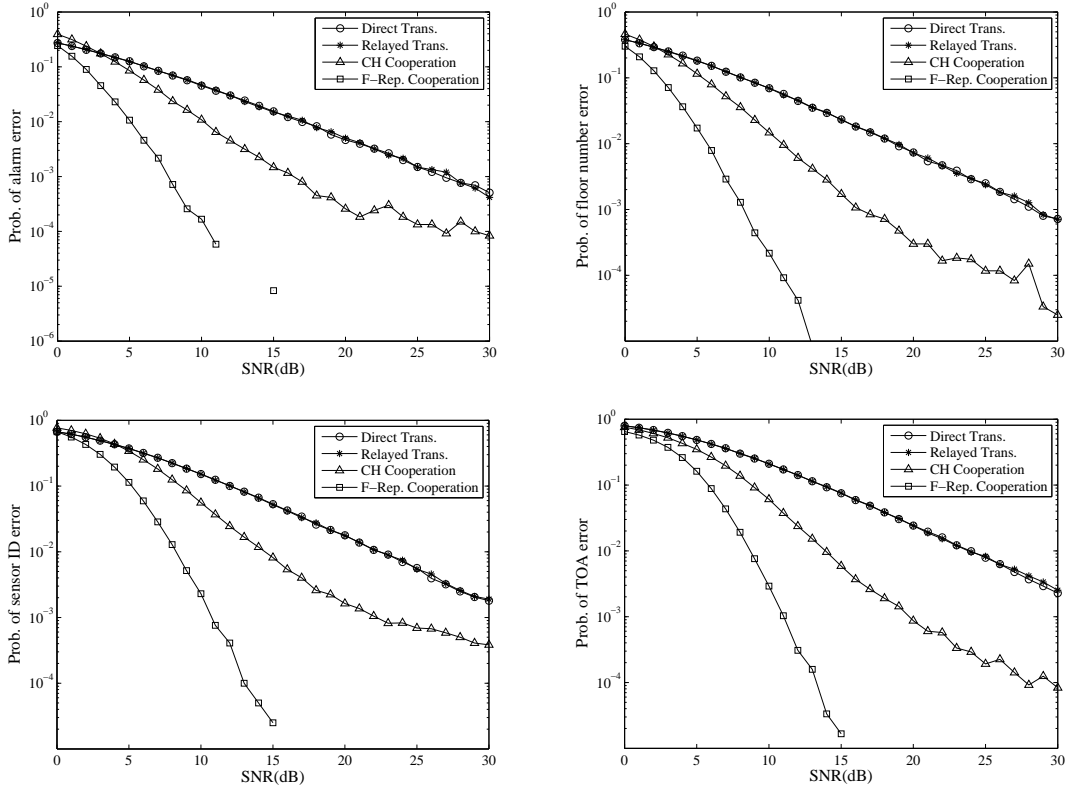


Figure 4.5: Comparison of the probability of error in the received information, between direct, relayed, F-Rep., and CH cooperation transmission.

4.4 Simulation Results

The simulation environment is similar to the one used in Section 3.5. We simulate a cooperation group of 12 nodes with 5 CH nodes, and the results are averaged over 10,000 sensing operations. The channel model parameters are taken according to the indoor factory environment wireless communication channel.

Fig. 4.5 compares the probability of error for the alarms generated at the BS, floor number, sensor ID, and TOA for non-cooperation and 12-node cooperation schemes. We can see a clear advantage by using cooperation among the group of nodes. The

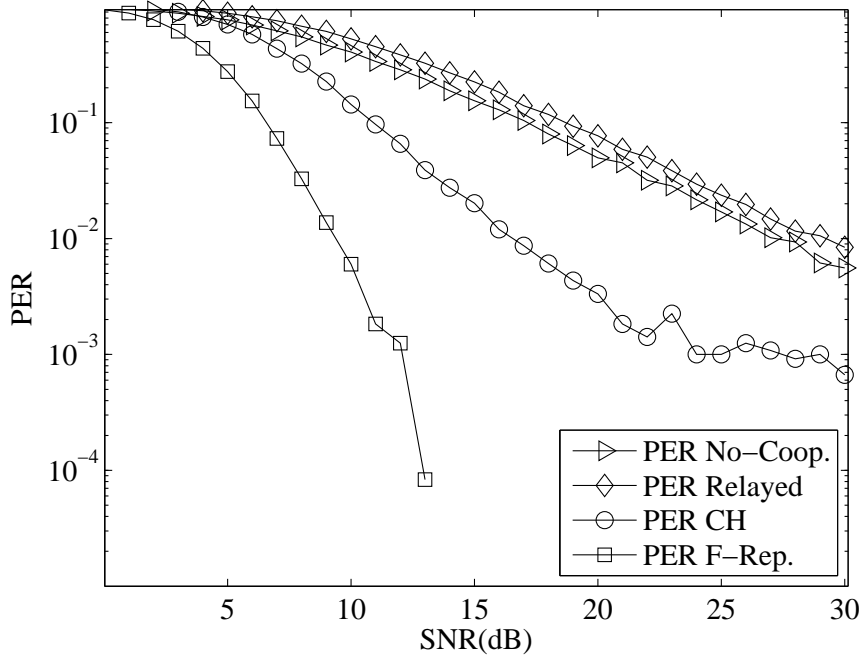


Figure 4.6: Comparison of simulated results of the proposed CH scheme, F-Rep. scheme, relayed transmission, and no cooperation scheme.

F-Rep. cooperation and CH cooperation schemes achieve, on average, 10^{-3} probability of error at almost 20 dB and 12 dB lower SNR compared with no cooperation schemes, respectively. Despite the extra energy (~ 0.5 dB) spent by the network in phase 1 transmission and in the cooperative packet transmission in phase 2, we can still get a saving of ~ 11 dB by using the proposed CH cooperation scheme. Note that this reduction in energy saving as compared to that in F-Rep. cooperation is a result of the loss in performance due to using fewer nodes to relay the cooperative packet rather than using F-Rep. cooperation, as in [44].

Fig. 4.6 compares the packet error rate (PER) of the proposed CH, F-Rep., relayed,

and no-cooperation schemes. The F-Rep. cooperation and CH cooperation schemes achieve, on average, 10^{-2} probability of error at almost 20 dB and 12 dB lower SNR compared with no cooperation scheme, respectively. This result also confirms the ~ 11 dB saving by using the proposed CH cooperation scheme. The energy savings reported in [44] are ~ 18 dB. The reduction in CH scheme is a result of the loss in performance due to using fewer nodes to relay the cooperative packet rather than using F-Rep. cooperation. Thus, the CH cooperation scheme is able to reduce the latency and energy consumption of the network at the expense of some performance benefits.

4.5 Conclusion

In this work, we have proposed a relay based cooperative WSN to monitor an indoor industrial environment. This is an improvement to our own work presented in Chapter 3. We have analyzed the SER, energy consumption, and latency of the proposed scheme. With the proposed cooperation scheme, the PER has been reduced significantly and a highly accurate decision at the base station has been achieved. The energy saving achieved is almost 11 dB, which can be very beneficial in increasing the lifetime of the sensors. The proposed cooperation scheme is able to reduce the energy consumption and latency in data transmission as compared to the F-Rep. cooperation scheme but with an increased FAR and reduced PDR.

Chapter 5

Conclusions and Future Research Directions

In this thesis, we have introduced methods to improve the reliability in transmitting information from distributed wireless sensors to a base station, in a harsh communication environment. The communication environments considered were the challenging underwater acoustic channel and the indoor industrial channel.

5.1 Summary of Contributions

Let h be the time taken by a non-cooperative sensor network in transmitting the observed information to the BS. Then the improvements and reductions in performance as a result of using our proposed cooperation and decision-making schemes are summarized in Table 5.1, in the case of 12-node cooperation. Table 5.1 shows that using our proposed cooperation and decision-making schemes, we can achieve a huge coding and diversity gain at the expense of some increased latency and a negligible increase in the energy consumption. The overall effect of our proposed schemes in terms of the battery life of a network is a significant increase in the lifetime of a network from 4 to 10 times that of a non-cooperative network used for the same purpose.

Table 5.1: Summary of Contributions

Work	Cooperation Method	Decision-Making	Coding Gain	Latency	Energy Consumption	Battery Life
[39]	Network coding (SCCNC)	Joint iterative decoding	~ 11 dB	$\sim 2h$	~ 1.6 dB increase	$\sim 6.5h$ increase
[44]	Full repetition (OOP)	Fusion (majority vote)	~ 18 dB	$\sim 6.5h$	~ 2 dB increase	$\sim 9.6h$ increase
[47], [48]	Partial repetition (OOP-CH)	Fusion (majority vote)	~ 11 dB	$\sim 3h$	~ 0.5 dB increase	$\sim 4.3h$ increase

5.2 Future Research Directions

5.2.1 Adaptive SCCNC

In the case of underwater acoustic communication, our proposed solution in [39] shows that the coding gain achieved through the joint iterative channel-network code decoding scheme helps in increasing the battery life by about $6.5h$ times that of a non-cooperative COFDM scheme. However, the delay in transmitting the same amount of information to the BS has been increased by $2h$ times. In a future work, this scheme can be modified to use a limited number of relay nodes that forward the data to the BS, or the the number of relay nodes used can be made adaptive to channel conditions. This will help reduce the latency from the current $2h$.

5.2.2 Development of MAC Protocol for Industrial Communication

In the case of indoor industrial communication, the proposed solutions in [44], [46], and [48], can be used to obtain a huge coding and diversity benefit which helps in increasing the battery life by $9.6h$ times and $4.3h$ times, respectively. However, the latency in [44] has been increased significantly. This was addressed in our modified solution for the same application in [46], and [48], where the latency has been reduced to an acceptable level but the coding gain was reduced which resulted in a reduction in the battery life improvement. As a future work, the proposed cooperation protocols in our proposed schemes can be further developed for integration in to the existing standards for indoor industrial area communication systems.

Bibliography

- [1] L. Liu, S. Zhou, and J.-H. Cui, “Prospects and problems of wireless communication for underwater sensor networks,” *Wiley Wirele. Commun. Mob. Comput. Sp. Issue on Underwater Sensor Networks*, vol. 8, no. 8, pp. 977–994, Oct. 2008.
- [2] I. F. Akyildiz, D. Pompili, and T. Melodia, “Challenges for efficient communication in underwater acoustic sensor networks,” *ACM SIGBED Rev.*, vol. 1, no. 2, pp. 3-8, Jul. 2004.
- [3] M. Stojanovic and J. Preisig, “Underwater acoustic communication channels: Propagation models and statistical characterization,” *IEEE Commun. Mag.*, vol. 47, no. 1, pp. 84-89, Jan. 2009.
- [4] I. F. Akyildiz, D. Pompili, and T. Melodia, “Underwater acoustic sensor networks: research challenges,” *Elsevier Ad Hoc Networks*, vol. 3, pp. 257-279, Mar. 2005.
- [5] D. B. Kilfoyle and A. B. Baggeroer, “The state of the art in underwater acoustic telemetry,” *IEEE Jr. Oceanic Eng.*, vol. 25, no. 1, pp. 4-27, Jan. 2000.
- [6] L. Tang, K. C. Wang, Y. Huang, and F. Gu, “Channel characterization and link quality assessment of IEEE 802.15.4-compliant radio for factory environments,” *IEEE Trans. Ind. Inf.*, vol. 3, no. 2, pp. 99-110, May 2007.
- [7] B. Silva, R. M. Fisher, A. Kumar, and G. P. Hancke, “Experimental link quality characterization of wireless sensor networks for underground monitoring,” *IEEE Trans. Ind. Inf.*, vol. 11, no. 5, pp. 1099-1110, Oct. 2015.

- [8] Y. Ai, M. Cheffena, and Q. Li, "Radio frequency measurements and capacity analysis for industrial indoor environments," *Proc. 9th Eur. Conf. Ant. and Propag. (EuCAP)*, pp. 1-5, May 2015.
- [9] L. D. Xu, W. He, and S. Li, "Internet of things in industries: a survey," *IEEE Trans. Ind. Inf.*, vol. 10, no. 4, pp. 2233-2243, Nov. 2014.
- [10] J. Niu, L. Cheng, Y. Gu, L. Shu, and S. K. Das, "R3E: Reliable reactive routing enhancement for wireless sensor networks," *IEEE Trans. Ind. Inf.*, vol. 10, no. 1, pp. 784-794, Feb. 2014.
- [11] W. L. Tan, W. C. Lau, and O. Yue, "Performance analysis of an adaptive, energy-efficient MAC protocol for wireless sensor networks," *Jr. Parallel. Distrib. Comput.*, vol. 72, no. 4, pp. 504-514, Apr. 2012.
- [12] H. S. AbdelSalam, and S. Olariu, "Toward adaptive sleep schedules for balancing energy consumption in wireless sensor networks," *IEEE Trans. Computers*, vol. 61, no. 10, pp. 1443-1458, Oct. 2012.
- [13] E. Fasolo, M. Rossi, J. Widmer, and M. Zorzi, "In-network aggregation techniques for wireless sensor networks: a survey," *IEEE Wirele. Commun.*, vol. 14, no. 2, pp. 70-87, Apr. 2007.
- [14] P. Murphy and A. Sabharwal, "Design, implemenation, and characterization of a cooperative communications system," *IEEE Trans. Veh. Tech.*, vol. 60, no. 6, pp. 2534-2544, Jul. 2011.

- [15] G. Kramer, M. Gastpar, and P. Gupta, “Cooperative strategies and capacity theorems for relay networks,” *IEEE Trans. Info. Theory*, vol. 51, no. 9, pp. 3037-3063, Sep. 2005.
- [16] L. Bai, F. Xu, R. Xu, and S. Zheng, “LDPC Application Based on CI/OFDM Underwater Acoustic Communication System,” *Int. Conf. Inf. Sc. and Eng. (ICISE)*, pp. 2641-2644, Dec. 2009.
- [17] J. Huang, S. Zhou, and P. Willett, “Nonbinary LDPC coding for multicarrier underwater acoustic communication,” *IEEE JSAC Sp. Issue on Underwater Wirel. Commun. and Net.*, vol. 26, no. 9, pp. 1684–1696, Dec. 2008.
- [18] B. Li, J. Huang, S. Zhou, K. Ball, M. Stojanovic, L. Freitag, and P. Willett, “MIMO-OFDM for high-rate underwater acoustic communications,” *IEEE Jr. Oceanic Eng.*, vol. 34, no. 4, pp. 634-644, Oct. 2009.
- [19] R. Diamant and L. Lampe, “Adaptive error-correction coding scheme for underwater acoustic communication networks,” *IEEE Jr. Oceanic Eng.*, vol. 40, no. 1, pp. 104-114, Jan. 2015.
- [20] L. Wan, H. Zhou, X. Xu, Y. Huang, S. Zhou, Z. Shi, and J.-H. Cui, “Adaptive modulation and coding for underwater acoustic OFDM,” *IEEE Jr. Oceanic Eng.*, vol. 40, no. 2, pp. 327-336, Apr. 2015.
- [21] C. Polprasert, J. A. Ritcey, and M. Stojanovic, “Capacity of OFDM systems over fading underwater acoustic channels,” *IEEE Jr. Oceanic Eng.*, vol. 36, no. 4, pp. 514-524, Oct. 2011.

- [22] K. Pelekanakis, and A. B. Baggeroer, “Exploiting space–time–frequency diversity with MIMO–OFDM for underwater acoustic communications,” *IEEE Jr. Oceanic Eng.*, vol. 36, no. 4, pp. 502-513, Oct. 2011.
- [23] Z. Wang, S. Zhou, J. Catipovic, and P. Willett, “Asynchronous multiuser reception for OFDM in underwater acoustic communications,” *IEEE Trans. Wirele. Commun.*, vol. 12, no. 3, pp. 1050-1061, Mar. 2013.
- [24] M. C. Domingo, “Overview of channel models for underwater wireless communication networks,” *Elsevier Phy. Commun.*, vol. 1, no. 3, pp. 163-182, Sept. 2008.
- [25] L. M. Brekhovskikh and Y. P. Lysanov, *Fundamentals of Ocean Acoustics*, 3rd Ed. New York: Springer-Verlag, 2003.
- [26] Y. M. Khattabi and M. M. Matalgah, ”Performance analysis of multiple-relay AF cooperative systems over Rayleigh time-selective fading channels with imperfect channel estimation,” *IEEE Trans. Veh. Tech.*, vol. 65, no. 1, pp. 427- 434, Jan. 2016.
- [27] J. Rebelatto, B. Uchoa-Filho, Y. Li, and B. Vucetic, “Multiuser cooperative diversity through network coding based on classical coding theory,” *IEEE Trans. Sig. Process.*, vol. 60, no. 2, pp. 916–926, Feb. 2012.
- [28] B. Chen, L. Tong, and P. K. Varshney, “Channel-aware distributed detection in wireless sensor networks,” *IEEE Signal Process. Mag.*, vol. 23, no. 4, pp. 16–26, Jul. 2006.

- [29] A. G. Dimakis, S. Kar, J. M. F. Moura, M. G. Rabbat, and A. Scaglione, “Gossip algorithms for distributed signal processing,” *Proc. IEEE*, vol. 98, no. 11, pp. 1847–1864, Nov. 2010.
- [30] J. Manyika and H. Durrant-Whyte, *Data Fusion and Sensor Management: A Decentralized Information-Theoretic Approach*, Prentice Hall, Upper Saddle River, NJ, USA, 1995.
- [31] A. Jara, D. Genoud, and Y. Bocchi, “Sensors data fusion for smart cities with knime: A real experience in the smartsantander testbed,” *2014 IEEE World Forum on Internet of Things (WF-IoT)*, pp. 173–174, March 2014.
- [32] S. M. Javadi, and A. Peiravi, “Fusion of weighted decisions in wireless sensor networks,” *IET Wirele. Sensor Syst.*, vol. 5, no. 2, pp. 97-105, 2015.
- [33] A. Argyriou, and O. Alay, “Distributed Estimation in Wireless Sensor Networks With an Interference Canceling Fusion Center,” *IEEE Trans. Wirele. Commun.*, vol. 15, no. 3, pp. 2205-2214, Mar. 2016.
- [34] D. Ayllon, H. A. Sanchez-Hevia, R. Gil-Pita, M. U. Manso, and M. R. Zurera, “Indoor Blind Localization of Smartphones by Means of Sensor Data Fusion,” *IEEE Trans. Instr. Mea.*, vol. 65, no. 4, pp. 783-794, Apr. 2016.
- [35] C. Habib, A. Makhoul, R. Darazi, and C. Salim, “Self-Adaptive Data Collection and Fusion for Health Monitoring Based on Body Sensor Networks,” *IEEE Trans. Ind. Inf.*, vol. 12, no. 6, pp. 2342-2352, Dec. 2016.

- [36] P. R. Rossi, D. Ciuonzo, K. Kansanen, and T. Ekman, "Performance Analysis of Energy Detection for MIMO Decision Fusion in Wireless Sensor Networks Over Arbitrary Fading Channels," *IEEE Trans. Wirele. Commun.*, vol. 15, no. 11, pp. 7794-7806, Nov. 2016.
- [37] Z. Xing, and Y. Xia, "Distributed Federated Kalman Filter Fusion Over Multi-Sensor Unreliable Networked Systems," *IEEE Trans. Circ. Sys.-1 Reg. Pap.*, vol. 63, no. 10, pp. 1714-1725, Oct. 2016.
- [38] O. Kreibich, J. Neuzil, and R. Smid, "Quality-based multiple-sensor fusion in an industrial wireless sensor network for MCM," *IEEE Trans. Ind. Elect.*, vol. 61, no. 9, pp. 4903-4911, Sep. 2014.
- [39] © 2016 IEEE. Reprinted, with permission, from Zafar Iqbal and Heung-No Lee, "Spatially concatenated channel-network code for underwater wireless sensor networks," *IEEE Trans. Commun.*, vol. 64, no. 9, pp. 3901-3914, Sep. 2016.
- [40] Heung-No Lee, and Zafar Iqbal, "Sensing data processing apparatus and data processing method," *Korean Patent*, Application number: 10-2016-0066621, May 30, 2016.
- [41] Zafar Iqbal and Heung-No Lee, "Deployment strategy analysis for underwater cooperative wireless sensor networks," *6th Int. Conf. on ICT Convergence (ICTC)*, South Korea, Oct. 2015.

- [42] Zafar Iqbal and Heung-No Lee, "Underwater acoustic channel model and variations due to changes in node and buoy positions," *5th Pacific Rim Underwater Acoustics Conference*, Russia, Sep. 2015.
- [43] Zafar Iqbal, Hyeonh-Won Jeon, and Heung-No Lee, "A realistic channel model for OFDM based underwater acoustic communications," *2012 Korea Inf. and Commun. Society Summer Conference*, South Korea, Jun. 2012.
- [44] © 2016 IEEE. Reprinted, with permission, from Zafar Iqbal, Kiseon Kim, and Heung-No Lee, "A cooperative wireless sensor network for indoor industrial monitoring," *IEEE Trans. Ind. Inf.*, vol. 13, no. 2, pp. 482-491, Apr. 2017.
- [45] Heung-No Lee, and Zafar Iqbal, "Data processing apparatus and method for wireless sensor network," *Korean Patent*, Application number: 10-2016-0066625, May 30, 2016.
- [46] Zafar Iqbal and Heung-No Lee, "A self-organizing wireless sensor network for industrial monitoring," *31st Int. Conf. on Circuits/Systems, Computers, and Communications (ITC-CSCC 2016)*, Okinawa, Japan, pp. 351-354, Jul. 10-13, 2016.
- [47] Zafar Iqbal and Heung-No Lee, "Performance analysis of a clustered cooperative WSN for indoor communication," *Submitted to IEEE Access*, Apr. 2017.
- [48] © 2017 IEEE. Reprinted, with permission, from Zafar Iqbal and Heung-No Lee, "Low-latency and high-reliability cooperative WSN

- for indoor industrial monitoring,” *IEEE 85th Vehicular Tech. Conf.*, Sydney, Australia, Jun. 4-7, 2017.
- [49] R. Ahlswede, N. Cai, S.-Y. R. Li, and R. W. Yeung, “Network information flow,” *IEEE Trans. Inf. Theory*, vol. 46, no. 4, pp. 1204-1216, Jul. 2000.
- [50] S.-Y. R. Li, R. W. Yeung, and N. Cai, “Linear network coding,” *IEEE Trans. Inf. Theory*, vol. 49, no. 2, pp. 371-381, Feb. 2003.
- [51] B. Zhao and M. Valenti, “Distributed turbo coded diversity for relay channel,” *Electronics Letters*, vol. 39, no. 10, pp. 786–787, May 2003.
- [52] A. Chakrabarti, A. de Baynast, A. Sabharwal, and B. Aazhang, “Low density parity check codes for the relay channel,” *IEEE Jr. Sel. Areas Commun.*, vol. 25, no. 2, pp. 280–291, Feb. 2007.
- [53] J. Yuan, Z. Chen, Y. Li, and L. Chu, “Distributed space-time trellis codes for a cooperative system,” *IEEE Trans. Wirele. Commun.*, vol. 8, no. 10, pp. 4897–4905, Oct. 2009.
- [54] Z. Wang, J. Huang, S. Zhou, and Z. Wang, “Iterative receiver processing for OFDM modulated physical-layer network coding in underwater acoustic channels,” *IEEE Trans. Commun.*, vol. 61, no. 2, pp. 541-553, Feb. 2013.
- [55] Y. Chen, Z. Wang, L. Wan, H. Zhou, S. Zhou, and X. Xu, “OFDM-modulated dynamic coded cooperation in underwater acoustic channels,” *IEEE Jr. Oceanic Eng.*, vol. 40, no. 1, pp. 159-168, Jan. 2015.

- [56] J. N. Laneman and G. W. Wornell, "Distributed space-time-coded protocols for exploiting cooperative diversity in wireless networks," *IEEE Trans. Info. Theory*, vol. 49, no. 10, pp. 2415- 2425, Oct. 2003.
- [57] Y. Li, and X. -G. Xia, "A family of distributed space-time trellis codes with asynchronous cooperative diversity," *IEEE Trans. Commun.*, vol. 55, no. 4, pp. 790-800, Apr. 2007.
- [58] C. Li, G. Yue, M. A. Khojastepour, X. Wang, and M. Madihian, "LDPC-coded cooperative relay systems: performance analysis and code design," *IEEE Trans. Commun.*, vol. 56, no. 3, pp. 485-496, Mar. 2008.
- [59] D. E. Lucani, M. Medard, and M. Stojanovic, "Underwater acoustic networks: channel models and network coding based lower bound to transmission power for multicast," *IEEE Jr. Sel. Areas Commun.*, vol. 26, no. 9, pp. 1708-1719, Dec. 2008.
- [60] M. Elfituri, W. Hamouda, and A. Ghrayeb, "A convolutional-based distributed coded cooperation scheme for relay channels," *IEEE Trans. Veh. Tech.*, vol. 58, no. 2, pp. 655-669, Feb. 2009.
- [61] Z. Guo, B. Wang, P. Xie, W. Zeng, and J. -H. Cui, "Efficient error recovery with network coding in underwater sensor networks," *Elsevier Ad Hoc Networks*, vol. 7, no. 4, pp. 791-802, Jun. 2009.
- [62] T. E. Hunter and A. Nosratinia, "Diversity through coded cooperation," *IEEE Trans. Wirele. Commun.*, vol. 5, no. 2, pp. 283-289, Feb. 2006.

- [63] S. Schwandter, A. G. Amat, G. Matz, “Spatially-coupled LDPC codes for decode-and-forward relaying of two correlated sources over the BEC,” *IEEE Trans. Commun.*, vol. 62, no. 4, pp. 1324-1337, Apr. 2014.
- [64] X. Bao and J. Li, “Adaptive network coded cooperation (ANCC) for wireless relay networks: matching code-on-graph with network-on-graph,” *IEEE Trans. Wirele. Commun.*, vol. 7, no. 2, pp. 574-583, Feb. 2008.
- [65] Z. Ding, K. Leung, D. Goeckel, and D. Towsley, “A relay assisted cooperative transmission protocol for wireless multiple access systems,” *IEEE Trans. Commun.*, vol. 58, no. 8, pp. 2425–2435, Aug. 2010.
- [66] J. Rebelatto, B. Uchoa-Filho, Y. Li, and B. Vucetic, “Multiuser cooperative diversity through network coding based on classical coding theory,” *IEEE Trans. Sig. Process.*, vol. 60, no. 2, pp. 916–926, Feb. 2012.
- [67] A. M. Jalil, and A. Ghrayeb, “Distributed channel coding for underwater acoustic cooperative networks,” *IEEE Trans. Commun.*, vol. 62, no. 3, pp. 848-856, Mar. 2014.
- [68] D. Pompili, T. Melodia, and I. F. Akyildiz, “Three-dimensional and two-dimensional deployment analysis for underwater acoustic sensor networks,” *Elsevier Ad Hoc Networks*, vol. 7, no. 4, pp. 778-790, Jun. 2009.
- [69] F. Xue, and P. R. Kumar, “The number of neighbors needed for connectivity of wireless networks,” *Springer-Verlag Jr. Wirele. Net.*, vol. 10, no. 2, pp. 169-181, Mar. 2004.

- [70] H.-W. Jeon, S.-J. Lee, and H.-N. Lee, "LDPC coded OFDM system design and performance verification on a realistic underwater acoustic channel model," *Mil. Commun. Conf., MILCOM 2011*, pp. 2200-2204, Nov. 2011.
- [71] A. G. Zajic, "Statistical modeling of MIMO mobile-to-mobile underwater channels," *IEEE Trans. Veh. Tech.*, vol. 60, no. 4, pp. 1337-1351, May 2011.
- [72] M. Chitre, "A high-frequency warm shallow water acoustic communications channel model and measurements," *Jr. Acous. Soc. Amer.*, vol. 122, no. 5, pp. 2580-2586, Nov. 2007.
- [73] M. Stojanovic, "Underwater acoustic communications: design considerations on the physical layer," *Ann. Conf. Wirele. on Demand Net. Sys. Serv. (WONS 2008)*, pp. 1-10, Jan. 2008.
- [74] M. Stojanovic, 1999. "Underwater Acoustic Communication," *Wiley Encyc. of Electr. and Electron. Eng.*, vol. 22, pp. 688-698, 1999.
- [75] K. V. Mackenzie, "Nine-term equation for sound speed in the oceans," *Jr. Acoustical Soc. America*, vol. 70, no. 3, pp. 807-812, Sep. 1981.
- [76] F. J. Millero, C. T. Chen, A. Bradshaw, and K. Schleicher, "A new high pressure equation of state for seawater," *Elsevier Deep Sea Research Part A*, vol. 27, no. 3-4, pp. 255-264, Apr. 1980.

- [77] P. Qarabaqi and M. Stojanovic, "Modeling the large scale transmission loss in underwater acoustic channels," *Ann. Allerton Conf. Commun., Cont., Comp.*, pp. 445-452, Sept. 2011.
- [78] W.-B. Yang and T. C. Yang, "High-frequency channel characterization for M-ary frequency-shift-keying underwater acoustic communications," *Jr. Acous. Soc. Amer.*, vol. 120, no. 5, pp. 2615-2626, Nov. 2006.
- [79] A. Radosevic, J. G. Proakis, and M. Stojanovic, "Statistical characterization and capacity of shallow water acoustic channels," *OCEANS 2009 – EUROPE*, pp. 1-8, May 2009.
- [80] M. Evans, N. Hastings, and B. Peacock, *Statistical Distributions*, Hoboken, NJ: Wiley-Interscience, 2000.
- [81] R. Coates, *Underwater Acoustic Systems*, New York: Wiley, 1989.
- [82] R. G. Gallager, *Low-Density Parity-Check Codes*, M.I.T. Press, 1963.
- [83] B. Sklar, *Digital Communications: Fundamentals and Applications*, 2nd Ed., Prentice Hall, 2001.
- [84] D. J. C. MacKay, "Good error-correcting codes based on very sparse matrices," *IEEE Trans. Inf. Theory*, vol. 45, no. 2, pp. 399-431, Mar. 1999.
- [85] S. ten Brink, "Convergence behavior of iteratively decoded parallel concatenated codes," *IEEE Trans. Commun.*, vol. 49, no. 10, pp. 1727-1737, Oct. 2001.

- [86] LinkQuest Inc., *LinkQuest Underwater Acoustic Modems, UWM2000 Specifications*, accessed on Sep. 27, 2013. [Online]. Available: <http://www.linkquest.com/html/uwm2000.htm>.
- [87] EvoLogics GmbH., *Underwater Acoustic Modems, S2CR Acoustic Modem*, accessed on Sep. 27, 2013. [Online]. Available: http://www.evologics.de/en/products/acoustics/s2cr_18_34.html.
- [88] T. Mohsenin, D. N. Truong, and B. M. Baas, "A low-complexity message-passing algorithm for reduced routing congestion in LDPC decoders," *IEEE Trans. Circ. Sys. I: Regular Papers*, vol. 57, no. 5, pp. 1048–1061, May 2010.
- [89] A. J. Blanksby and C. J. Howland, "A 690-mW 1-Gb/s 1024-b, rate-1/2 low-density parity-check code decoder," *IEEE Jr. Solid-State Circ.*, vol. 37, no. 3, pp. 404–412, Mar. 2002.
- [90] M. M. Mansour and N. R. Shanbhag, "A 640-Mb/s 2048-bit programmable LDPC decoder chip," *IEEE Jr. Solid-State Circ.*, vol. 41, no. 3, pp. 684–698, Mar. 2006.
- [91] N. Marchenko, T. Andre, G. Brandner, W. Masood, and C. Bettstetter, "An experimental study of selective cooperative relaying in industrial wireless sensor networks," *IEEE Trans. Ind. Inf.*, vol. 10, no. 3, pp. 1806–1816, Aug. 2014.
- [92] A. Ulusoy, O. Gurbuz, and A. Onat, "Wireless model-based predictive networked control system over cooperative wireless network," *IEEE Trans. Ind. Inf.*, vol. 7, no. 1, pp. 41–51, Feb. 2011.

- [93] J. Neuzil, O. Kreibich, and R. Smid, “A distributed fault detection system based on IWSN for machine condition monitoring,” *IEEE Trans. Ind. Inf.*, vol. 10, no. 2, pp. 1118-1123. May 2014.
- [94] R. Williams, *The Geometrical Foundation of Natural Structure: A Source Book of Design*. Dover Pub. Inc., New York, pp. 51-52, 1979.
- [95] N. Xu, S. Rangwala, K. K. Chintalapudi, D. Ganesan, A. Broad, R. Govindan, and D. Estrin, “A wireless sensor network for structural monitoring,” *2nd ACM Int. Conf. Emb. Net. Sen. Sys. (SenSys’04)*, Nov. 2004.
- [96] P. Huang, L. Xiao, S. Soltani, M. W. Mutka, and N. Xi, “The evolution of MAC protocols in wireless sensor networks: a survey,” *IEEE Commun. Surv. Tuto.*, vol. 15, no. 1, pp. 101-120, 2013.
- [97] M. K. Simon, and M.-S. Alouini, *Digital communication over fading channels*, 2nd Ed. Wiley-Interscience, NJ, 2005.
- [98] K. J. R. Liu, A. K. Sadek, W. Su, and A. Kwasinski, *Cooperative Communication and Networking*, Cambridge University Press, 2009.
- [99] IEEE 802.15.4-2011, “Part 15.4: Low-rate wireless personal area networks (LR-WPANs),” *IEEE-SA Standards Board*, Jun. 2011.
- [100] Silicon Labs, *EFR32 Flex Gecko Proprietary Wireless SoC*, accessed, Jun. 2016. [Online]. Available: www.silabs.com.

- [101] K.-Y. Wu, C.-Y. Liang, K.-K. Yu, and S.-R. Kuang, “Multi-mode floating-point multiply-add fused unit for trading accuracy with power consumption,” *IEEE/ACS Int. Conf. Comp. Inf. Sci.*, pp.429-435, Jun. 2013.
- [102] P. Jesus, C. Baquero, and P. S. Almeida, “A survey of distributed data aggregation algorithms” *IEEE Commun. Surv. Tuto.*, vol. 17, no. 1, pp. 381-404, Mar. 2015.
- [103] H. Harb, A. Makhoul, R. Tawil, and A. Jaber, “Energy-efficient data aggregation and transfer in periodic sensor networks,” *IET Wirele. Sensor Syst.*, vol. 4, no. 4, pp. 149-158, Dec. 2014.

Acknowledgements

There has been contributions from many people in my life to this research work and writing my thesis. Without their help and support it would have been impossible to go through this period of time successfully.

First of all, I would like to express my sincere gratitude and thanks to my supervisor, Prof. Heung-No Lee, for his guidance and training in developing my research skills and analytical thinking. My thesis review committee members, Prof. Kim Kiseon (GIST), Prof. Hyuk Lim (GIST), Prof. Jungwoo Lee (SNU), and Prof. Jalel Ben-Othman (Univ. Paris 13), for their time and valuable comments on this work. I would also like to mention my M.S. supervisor, Prof. Saeid Nooshabadi, for his guidance and motivation that helped me achieve a Ph.D. Finally, I want to say thanks to my colleagues and seniors in the INFONET Lab, Hwanchul Jang, Jintaek Seong, Wonngbi Lee, Younghak Shin, Seungchan Lee, Sangjun Park, M. Asif Raza, Jungmin Ryu, Hyeong-Won Jeon, Jusung Kang, Jehyuk Jang, M. Yaseen, Pavel Ni, Haeong Choi, Jaewon Bang, Hyeonjun Han, Cheolsun Kim, Rohit Thakur, and Jeong Park, for their support and discussions during this research work.

Fun times are as important as the research, and I would like to say thanks to my friends and colleagues, Riaz Uddin, Sajid Hussain, M. Waleed, Bilal Ahmed, Saad Khan, Zia Ur Rehman, M. Ijaz Anwar, G. H. Qasim, and others for helping provide the little joys of life that helped me go through this phase happily.

And the most important of all is my family who have supported me during these times in every possible way. I would like to say hearty thanks to my parents for their

encouragement and prayers, my wife Nosheen Mahmood, for her love and sacrifice of many beautiful moments. Without her support, it would have been impossible to achieve this goal. And finally, my little joy, Bahram Khan, whose presence has given us moments that filled all this time with happy memories.

Curriculum Vitae

Name : Zafar Iqbal
Birth Date : Feb 17, 1981
Birth Place : Totalai, Buner, Khyber Pakhtunkhwa, Paksitan
Permanent Address : Vill. and P.O Totalai, Tehsil Khudukhel, Distt. Buner, KP, Pakistan

Education

2012.09–2017.08 **Ph.D.** Electrical Engineering and Computer Science, Gwangju Institute of Science and Technology (GIST), Gwangju, South Korea.
2008.09–2010.08 **M.S.** Information and Mechatronics, Gwangju Institute of Science and Technology (GIST), Gwangju, South Korea.
2001.01–2005.01 **B.S.** Computer Engineering, COMSATS Institute of Information Technology (CIIT), Islamabad, Pakistan.

Work Experience

2011.12–present **Research Assistant**, GIST, Gwangju, South Korea.
2011.02–2011.07 **R&D Engineer**, Vieworks Co. Ltd., Seongnam, South Korea.
2008.09–2011.01 **Research Assistant**, GIST, Gwangju, South Korea.
2005.10–2008.03 **Telecom Engineer**, ZTE Corporation, Shanghai, China.
2005.03–2005.10 **HW Design Engineer**, RWR Pvt. Ltd., Islamabad, Pakistan.

Achievements and Awards

1. Received the distinction of Silver Medal in the graduating class of B.S. Computer Engineering at CIIT.
2. Received the award of Korea IT Industry Promotion Agency scholarship for M.S. study at GIST.
3. Received the award of Korean Government Scholarship for Ph.D. study at GIST.

4. Received the Brain Korea 21 (BK21) scholarship during Ph.D. at GIST.
5. Received the Best Employee of the month and year awards several times at ZTE Corporation.

Publications

SCI Journals:

1. **Zafar Iqbal**, and Heung-No Lee, "Performance analysis of a clustered cooperative WSN for indoor communication," *Submitted to IEEE Access*, Apr. 2017.
2. **Zafar Iqbal**, K. S. Kim, and H.-N. Lee, "A cooperative wireless sensor network for indoor industrial monitoring," *IEEE Transactions on Industrial Informatics*, vol. 13, no. 2, pp. 482-491, Apr. 2017.
3. **Zafar Iqbal**, and H.-N. Lee, "Spatially concatenated channel-network code for underwater wireless sensor networks," *IEEE Transactions on Communications*, vol. 64, no. 9, pp. 3901-3914, Sep. 2016.
4. **Zafar Iqbal**, S. Nooshabadi, and H.-N. Lee, "Analysis and design of coding and interleaving in a MIMO-OFDM communication system," *IEEE Transactions on Consumer Electronics*, vol. 58, no. 3, pp. 758-766, Aug. 2012.

Conferences:

1. **Zafar Iqbal**, and H.-N. Lee, "Low-latency and high-reliability cooperative WSN for indoor industrial monitoring," *IEEE 85th Vehicular Tech. Conf. (IEEE VTC-Spring)*, Sydney, Australia, Jun. 4-7, 2017.
2. **Zafar Iqbal**, and H.-N. Lee, "Dual-hop cooperation protocol for spectrum sensing in cognitive radio networks," *16th Int. Conf. on Electron. Inf. and Commun. (ICEIC 2017)*, pp. 409-410, Phuket, Thailand, Jan. 11-14, 2017.
3. **Zafar Iqbal**, and H.-N. Lee, "A self-organizing wireless sensor network for industrial monitoring," *31st Int. Conf. on Circuits/Systems, Computers, and Commun. (ITC-CSCC 2016)*, Okinawa, Japan, pp. 351-354, Jul. 2016.
4. **Zafar Iqbal**, and H.-N. Lee, "Underwater acoustic channel model and variations due to changes in node and buoy positions," *5th Pacific Rim Underwater Acoustics Conference (PRUAC)*, Russia, Sep. 2015.
5. **Zafar Iqbal**, and H.-N. Lee, "Deployment strategy analysis for underwater cooperative wireless sensor networks," *6th Int. Conf. on ICT Convergence (ICTC)*, South Korea, Oct. 2015.
6. Muhammad A. Raza, **Zafar Iqbal**, Seungchan Lee, Haeung Choi, and Heung-No Lee, "Issues and Resolution Efforts Pertaining to TV Whitespace Usage", *2014 Korea Inf. and Commun. Society Winter Conference*, pp.77-79, Jan 22-24, 2014.

7. **Zafar Iqbal**, S. Nooshabadi, and H.-N. Lee, "Efficient interleaver design for MIMO-OFDM based communication systems on FPGA," *16th IEEE Int. Sym. on Consumer Electronics (ISCE)*, USA, Jun. 2012.
8. **Zafar Iqbal**, H.-W. Jeon, and H.-N. Lee, "A realistic channel model for OFDM based underwater acoustic communications," *2012 Korea Inf. and Commun. Society Summer Conference*, South Korea, Jun. 2012.
9. **Zafar Iqbal**, and S. Nooshabadi, "Effects of channel coding and interleaving in MIMO-OFDM systems," *IEEE 54th Int. Midwest Sym. on Circuits and Systems*, South Korea, Aug. 2011.

Patents:

1. Heung-No Lee, and **Zafar Iqbal**, "Data processing apparatus and method for wireless sensor network," *Korean Patent*, Application number: 10-2016-0066625, May 30, 2016.
2. Heung-No Lee, and **Zafar Iqbal**, "Sensing data processing apparatus and data processing method," *Korean Patent*, Application number: 10-2016-0066621, May 30, 2016.